

2

AD-A243 730



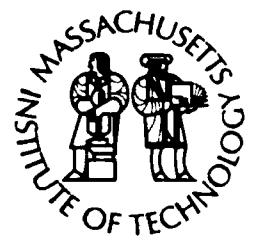
WHOI-91-29

DTIC
UNCLASSIFIED

Woods Hole Oceanographic Institution Massachusetts Institute of Technology



Joint Program
in Oceanography
and
Oceanographic
Engineering



DOCTORAL DISSERTATION

Upper Ocean Dynamics during the LOTUS and
TROPIC HEAT Experiments

by

Rebecca R. Schudlich

September 1991

91-18780



Woods Hole
Institution
Dedicated

WHOI-91-29

Upper Ocean Dynamics during the LOTUS and
TROPIC HEAT Experiments

by

Rebecca R. Schudlich

Woods Hole Oceanographic Institution
Woods Hole, Massachusetts 02543

and

The Massachusetts Institute of Technology
Cambridge, Massachusetts 02139

September 1991

DOCTORAL DISSERTATION

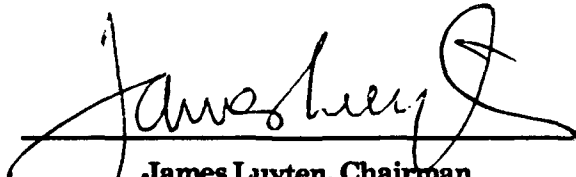
Funding was provided by the Office of Naval Research under Grant No. N00014-89-J-1053.

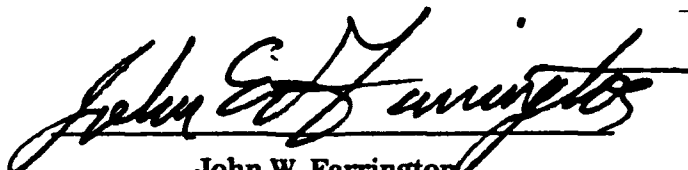
Reproduction in whole or in part is permitted for any purpose of the
United States Government. This thesis should be cited as: Rebecca R. Schudlich, 1991.
Ph.D. Thesis. MIT/WHOI, WHOI-91-29.



Approved for publication; distribution unlimited.

Approved for Distribution:


James Luyten, Chairman
Department of Physical Oceanography


John W. Farrington
Dean of Graduate Studies

Accession For	
NTIS GRA&I	<input checked="" type="checkbox"/>
DTIC Tab	<input type="checkbox"/>
Unannounced	<input type="checkbox"/>
Justification	
By	
Distribution/	
Availability Codes	
Dist	Special
A-1	

UPPER OCEAN DYNAMICS DURING
THE LOTUS AND TROPIC HEAT EXPERIMENTS

by

Rebecca R. Schudlich

B.S. Atmospheric and Oceanic Science, University of Michigan, 1983
M.S. Oceanic Science, University of Michigan, 1985

submitted in partial fulfillment of the
requirements for the degree of

DOCTOR OF PHILOSOPHY

at the

MASSACHUSETTS INSTITUTE OF TECHNOLOGY

and the

WOODS HOLE OCEANOGRAPHIC INSTITUTION

September 1991

© Rebecca R. Schudlich 1991

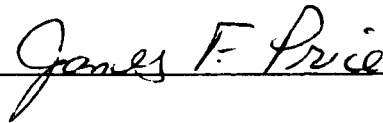
The author hereby grants to MIT and WHOI permission to reproduce
and distribute copies of this thesis document in whole or in part.

Signature of Author



Joint Program in Oceanography,
Massachusetts Institute of Technology/
Woods Hole Oceanographic Institution
September 4, 1991

Certified by



James F. Price
Thesis Supervisor

Accepted by



Lawrence J. Pratt
Chairman, Joint Committee for Physical Oceanography,
Massachusetts Institute of Technology/
Woods Hole Oceanographic Institution

Upper Ocean Dynamics during the LOTUS and TROPIC HEAT Experiments

by

Rebecca R. Schudlich

Submitted to the Massachusetts Institute of Technology
and the Woods Hole Oceanographic Institution
Joint Program in Physical Oceanography
on September 4, 1991, in partial fulfillment of the
requirements for the degree of Doctor of Philosophy

ABSTRACT

This thesis examines the effect of mean large-scale currents on the vertical structure of the upper ocean during two recent observational programs: the Long Term Upper Ocean Study (LOTUS) and the TROPIC HEAT experiments. The LOTUS experiment took place in the northwest Atlantic Ocean, a mid-latitude region away from strong mean currents, and extended over one entire seasonal cycle. The TROPIC HEAT experiments took place in the central equatorial Pacific Ocean during two 12-day periods in 1984 and 1987, at opposite extremes of the seasonal cycle. We use observations from these field experiments as well as one-dimensional numerical models of the upper ocean to analyze the dynamics of the vertical structure of the upper ocean at the equator and in mid-latitudes. Due to the different nature of the observations, we focus on the long term mean structure of the upper ocean in the LOTUS observations (Chapters 2 and 3), and on the diurnal cycle in the equatorial upper ocean in our analysis of the TROPIC HEAT observations (Chapters 4 and 5).

In the LOTUS observations, we find that the observed current is coherent with the wind over low frequencies (greater than an inertial period). Using a wind-relative averaging method we find good agreement with Ekman transport throughout the first summer and winter of the LOTUS experiment, with the exception of a downwind component in the wintertime. The mean current spiral is flat compared to the classic Ekman spiral, in that it rotates less with depth than does the Ekman spiral. The mean current has an e-folding depth scale of 12 m in the summer and 25 m in the winter.

Diurnal cycling is the dominant variability in the summer and determines the vertical structure of the spiral. In the winter, diurnal cycling is almost non-existent due to greatly reduced solar insolation. There is a persistent downwind shear in the upper 15 m during the winter which may be partially due to a bias induced by surface wave motion but which is also consistent with a logarithmic boundary layer.

The Price et al. (1986) model is reasonably successful in simulating the current structure during the summer, capturing both the mean and the diurnal variation. The model is less successful in the winter, though it does capture the overall depth scale of the current spiral.

In our analysis of the TROPIC HEAT observations, we extend the Price et al. (1986) model to the equatorial upper ocean. The model is initialized with the stratification and shear of the Equatorial Undercurrent (EUC), and is driven with heating and wind stress. A surface mixed layer is determined by bulk stability requirements, and a transition layer below the mixed layer is simulated by requiring that the gradient Richardson number be no

less than 1/4. A principal result is that the nighttime phase of the diurnal cycle is strongly affected by the EUC, resulting in deep mixing and large dissipation at night consistent with observations of the equatorial upper ocean during TROPIC HEAT. Other features of the equatorial circulation (upwelling and the zonal pressure gradient) are of little direct importance to the diurnal cycle.

The daytime (heating) phase of the simulated diurnal cycle is unaffected by equatorial circulation and is very similar to its mid-latitude counterpart. Solar heating produces a stably stratified surface layer roughly 10 m thick within which there is little, $O(3 \times 10^{-8} \text{ W kg}^{-1})$, turbulent dissipation. The diurnal stratification, though small compared to the EUC, is sufficient to insulate the EUC from wind stress during the day. For the typical range of conditions at the equator, diurnal warming of the sea surface is 0.2-0.5°C, and the diurnal variation of surface current (diurnal jet) is 0.1-0.2 m s⁻¹, consistent with observations.

The nighttime (cooling) phase of the simulated diurnal cycle is quite different from that seen at mid-latitudes. As cooling removes the warm, stable surface layer, the wind stress can work directly against the shear of the EUC. This produces a transition layer that can reach to 80 m depth, or nearly to the core of the EUC. Within this layer the turbulent dissipation is quite large, $O(2 \times 10^{-7} \text{ W kg}^{-1})$. Thus, the simulated dissipation has a diurnal range of more than a factor of five, as observed in the 1984 TROPIC HEAT experiment, though the diurnal cycle of stratification and current are fairly modest.

Dissipation estimated from the model is due to wind working directly against EUC, and is similar to observed values of dissipation in both magnitude and depth range. Overall dissipation values in the model are set by the strength of the wind stress rather than the structure of the EUC, and rise approximately like u_*^3 for a given Undercurrent. This suggests that the lower values of dissipation observed in the 1987 TROPIC HEAT experiment were due to the lower wind stress values rather than the relatively weak Undercurrent.

The main findings of this thesis are: 1) When the diurnal cycle in solar heating is strong, it determines the local vertical structure of the upper ocean (in both the LOTUS and TROPIC HEAT observations). The Price et al. (1986) model and its extension to the equator simulate the upper ocean fairly well when the diurnal cycle is strong. Under these conditions it is necessary to make measurements very near the surface (< 10 m depth) to fully resolve the wind-driven flow. 2) When surface waves are strong, surface-moored measurements of current may have a significant wave bias. To accurately estimate this bias, simultaneous measurements of current, current meter motion, and surface waves are needed. 3) Mean currents strongly amplify the nighttime phase of the diurnal cycle in the equatorial upper ocean, and therefore alter the mean structure of the equatorial upper ocean.

Thesis Supervisor: Dr. James F. Price
Title: Associate Scientist, Woods Hole Oceanographic Institution

ACKNOWLEDGEMENTS

I would like to thank my advisor, Jim Price, for years of patience and support through the ups and downs of graduate school, and for forcing me to answer (or at least think about) the hard questions. I also would like to thank Harry Bryden, Bob Weller, John Toole, Paola Rizzoli, and Nelson Hogg for their thoughtful comments and for the time they spent in my committee meetings and reviewing my thesis. Bob Weller, Mindy Hall, Harry Bryden and John Toole provided me with opportunities to go to sea several times during graduate school, which I enjoyed and appreciated very much. Nancy Pennington was very helpful in answering my questions about the LOTUS observations years after the experiment was completed. Jim Moum provided me with data from the 1987 TROPIC HEAT experiment prior to its publication. I collaborated extensively with Markku Santala in my estimates of the wave bias.

I would also like to thank John Farrington, Dean of Graduate Studies at WHOI, and Beverly Kozol-Tattlebaum, Pam Phillips, and Michael Vidaurri of the Earth, Atmospheric, and Planetary Sciences Department at MIT, who made it possible for me to work at MIT when Hurricane Bob left WHOI without power the week before my defense.

I want to thank all my friends and fellow students whose support and fun-loving-ness have made the Joint Program an incredible learning and growing experience for me. In particular, LuAnne Thompson, Molly Baringer, Kurt Polzin, Cecilie Mauritzen, Kirby Olson, and Susan Wijffels have all been great friends. For helping me stay in sound body and mind while in graduate school I am indebted to Heather Shepley and Saralee Perel. Finally, I want to thank David Parnes for putting up with me and waiting for me while I finished my dissertation, and for helping me to keep it all in perspective.

The Office of Naval Research supported this work under contract N00014-89-J-1053.

CONTENTS

Abstract	3
Acknowledgements	5
Chapter 1. Introduction	
1.1 Introduction and scope of thesis	9
1.2 Mid-latitude upper ocean dynamics	10
1.3 Equatorial upper ocean dynamics	17
1.4 Structure of thesis	21
Chapter 2. Observations of the Ekman Balance in Summer Conditions	
2.1 Overview of the LOTUS experiment	23
2.2 The wind-relative averaging method	30
2.3 Applying the wind-relative average method to the LOTUS 3 data	34
2.4 Summertime mean current spiral and transport	36
2.5 Diurnal variability during LOTUS 3	46
2.6 Numerical simulation of the mean current	53
2.7 Summary and conclusions	55
Chapter 3. Observations of the Ekman Balance in Winter Conditions	
3.1 Applying the wind-relative average method to the LOTUS 4 data	57
3.2 Wintertime mean current spiral and transport	61
3.3 Numerical simulation of the mean current	66
3.4 The near-surface downwind shear	73
3.5 Conclusions and comparison of summer and winter	81
Chapter 4. A Model of the Equatorial Upper Ocean	
4.1 Introduction	83
4.2 A simple model of the equatorial upper ocean	83
4.3 The diurnal cycle in the equatorial upper ocean model	89
4.4 Parameter dependence of the diurnal cycle at the equator	95
4.5 Summary and concluding remarks	111

Chapter 5. Tropic Heat Case Studies	
5.1 Motivation for the Tropic Heat experiment	113
5.2 Estimating dissipation from the equatorial upper ocean model	118
5.3 Tropic Heat 1984 simulation	119
5.4 Tropic Heat 1987 simulations	130
5.5 Dependence of turbulent dissipation on surface heating, wind stress, and the equatorial undercurrent	136
5.6 Conclusions and summary	141
Chapter 6. Summary and Conclusions	
6.1 Summary of the thesis	143
6.2 Conclusions	147
References	149
Biographical Note	155

Chapter 1

Introduction

1.1. INTRODUCTION AND SCOPE OF THESIS

The circulation of the world's oceans is ultimately driven at the surface by wind stress and by buoyancy forcing due to heating, cooling, evaporation and precipitation. This forcing is absorbed within a surface layer that is often nearly vertically uniform in density and current due to turbulent mixing, and is therefore commonly referred to as the ocean surface "mixed layer". The thickness of the uniform mixed layer can range from almost vanishing during periods of strong heating and light winds to several hundred meters under the most severe conditions of intense cooling and high winds. However, the direct effect of surface forcing is not limited to the mixed layer, but extends into the stratified region below the mixed layer that blends smoothly into the ocean interior. The entire region that is directly forced at the surface might thus be more properly thought of as the upper ocean, rather than simply the uniform mixed layer.

This dissertation examines the vertical structure of the upper ocean in two places; the mid-latitudes and at the equator. High quality data from two recent field experiments are available to analyze the upper ocean's vertical structure under very different conditions. We use field observations from the Long Term Upper Ocean Study (LOTUS) in the North Atlantic ocean to study the mid-latitude upper ocean structure throughout a seasonal cycle in a region away from strong mean currents. Observations from the TROPIC HEAT experiments in the equatorial Pacific ocean are used to examine the effect of the strong equatorial circulation on the upper ocean. We also use one-dimensional numerical models of the mid-latitude and equatorial upper ocean to interpret these observations. We

concentrate on the long-term mean current structure in our analysis of the mid-latitude LOTUS observations, while our analysis of the equatorial upper ocean emphasizes the interaction between the diurnal cycle and the equatorial undercurrent.

In this chapter, observations and models of the upper ocean are reviewed as a context for the analysis of mid-latitude and equatorial upper ocean observations and simulations presented in the following chapters. First, we briefly present Ekman's theory for upper ocean currents and the subsequent modifications to this theory. We review recent observational attempts to verify the Ekman relation. The mid-latitude upper ocean model of Price, Weller and Pinkel (1986) is presented as an alternative explanation for the vertical structure of the upper ocean. Then we briefly describe the dynamical differences between the equatorial and mid-latitude upper ocean. We present recent observations of the equatorial upper ocean, and then review modelling studies of the equatorial upper ocean. Finally, we outline the central questions and the structure of the dissertation.

1.2. MID-LATITUDE UPPER OCEAN DYNAMICS

In 1905, Ekman provided the field of physical oceanography with its first theoretical description of ocean currents. He deduced an explanation for wind-driven flow in the surface layer of the ocean (Ekman, 1905). Assuming a dominant balance between wind stress and the Coriolis force (except at the equator, where the Coriolis force vanishes), flow in the upper ocean satisfies the Ekman balance,

$$\int_0^{\delta} u \, dz = \tau_s / \rho f, \quad (1.1)$$

where δ is the depth over which wind stress τ_s is distributed in the upper ocean, u is the current in the direction 90° to the right of the wind, and f is the Coriolis parameter. Ekman originally solved this problem assuming a constant viscosity. The resulting current profile

$$[u, v] = V_0 \exp(-z/D) [\cos(\pi/4 - z/D), \sin(\pi/4 - z/D)] \quad (1.2)$$

spirals clockwise with depth (in the Northern Hemisphere), and the surface current $V_0 = \tau_s / \rho(Af)^{1/2}$ is 45° to the right of the wind. For a given vertical viscosity A , the depth scale of the Ekman current spiral is $D = (2A/f)^{1/2}$, and A is then the only unknown in this relation. To obtain a realistic depth scale (of order 10-100 m) for the current spiral, Ekman had to assume a vertical viscosity that was much larger than the molecular viscosity of water. He assumed that turbulence caused the downward mixing of wind stress and was analogous to molecular diffusion, but more intense, and termed this larger viscosity the turbulent eddy viscosity. Eddy viscosities are then functions of the flow, not simply functions of the fluid as molecular viscosities are.

Other workers have developed Ekman's theory further. Huang (1979) reviews "turbulent Ekman theories" which allow the eddy viscosity to vary with time and depth. These theories result in spirals with a somewhat different structure, but there has been no agreement on how the eddy viscosity depends on depth (Price et al., 1987). The vertical structure of wind-driven currents in the upper ocean thus remains an open question.

1.2.1 Observations of the mid-latitude upper ocean

Since Ekman's work, many attempts have been made to verify the theoretical Ekman transport and spiral with observations. There is a great deal of indirect evidence for the validity of the Ekman transport relation, including the anticyclonic circulation of subtropical

gyres that results from Ekman pumping. However, estimates of the wind-driven transport in the upper ocean usually differ from the Ekman transport by as much as a factor of two (Price et al., 1986, Richman et al., 1987). Several studies have also shown that, to some extent, upper ocean currents have the spiral structure predicted by Ekman (Hunkins, 1966; Gonella, 1972; Weller, 1981; Price et al., 1986; Richman et al., 1987; Wijffels and Bryden, 1991). However, a classic Ekman current spiral has never been observed, a fact that even Ekman acknowledged before his death (Pond and Pickard, 1983).

Attempts to verify the Ekman relation with observations have been frustrated by lack of lengthy data sets that sample the upper ocean with sufficient vertical resolution. The upper ocean is a difficult place to make measurements, and the presence of surface waves provides a very challenging environment for the survival of instruments. The large orbital velocities of surface waves also introduce a bias in vane-and-rotor current meters (such as vector-averaging current meters); the rotors tend to accelerate faster than they decelerate and thus overestimate the current in the direction of the phase speed of the surface waves. This problem has only been resolved in the last decade with the development of the vector-measuring current meter (Weller and Davis, 1980).

A further obstacle to the observation of wind-driven upper ocean currents is that the locally-forced wind-driven flow is obscured by both local and global phenomena. These include energetic eddies, internal waves, tides, and the general circulation. Currents due to these motions have amplitudes several times larger than wind-driven Ekman flow, and it is very difficult to separate these motions from the wind-driven velocity. A standard approach in analyzing upper ocean currents has therefore been to subtract a "deep" velocity in order to isolate the locally wind-driven flow. More recently, simultaneous long-line measurements of hydrography and continuous measurements of currents by Acoustic Doppler techniques have allowed direct estimation of the geostrophic current. The calculated geostrophic

current can then be subtracted from the total measured current to yield an estimate of the wind-driven current; this approach has led to somewhat improved agreement between Ekman transport and observations (Chereskin and Roemmich, 1991; Wijffels and Bryden, 1991).

Despite the observational obstacles, there have been many recent observations of Ekman-like current spirals in the upper ocean. Richman et al. (1986) found a general right-ward turning of the current with depth, though with a large component of shear in the downwind direction near the surface that showed no turning. Weller (1981), Price et al. (1986), and Wijffels and Bryden (1991) have all observed right-ward turning mean current spirals whose amplitudes decay smoothly with depth, but whose rotation with depth is much "flatter" than an Ekman spiral, in that the observed current rotates less with depth than predicted by Ekman's theory.

Price et al. (1986) suggested an alternative explanation for the observed vertical structure. They suggested that stratification, which is not included in Ekman's theory, plays a crucial role within the upper ocean by limiting the amount of shear that can be sustained by a flow before it becomes unstable. Low stratification in the surface mixed layer creates a slab-like layer of low shear near the surface, and regions of high shear occur at some depth from the surface where the stratification increases. Furthermore, they found that the flatness of the mean current spiral was a direct result of the diurnal cycle of stratification. The depth of the well-mixed layer varies throughout the day due to the variation of solar heating, and results in an average current profile that is sheared. The smooth decay of current with depth predicted by Ekman theory is thus modified by the diurnal variation of stratification.

1.2.2 A simple model of the mid-latitude upper ocean

The upper ocean model presented by Price et al. (1986) includes the effect of diurnal stratification, and has been very successful at producing realistic profiles of both instantaneous and mean currents. We use this model throughout this thesis, both in its original form and in a form modified for the equator. The model is briefly summarized here in its original mid-latitude form.

The Price et al. (1986) model is like several other models of the upper ocean (such as Pollard et al., 1973, and Davis et al., 1981) in that it relies on shear stability requirements to determine the vertical profiles of current and density in the upper ocean. The model simulates the upper ocean with one-dimensional budgets for momentum, temperature, and salinity,

$$u_t - fv = - \frac{1}{\rho_o} \tau_x^z \quad (1.3a)$$

$$v_t + fu = - \frac{1}{\rho_o} \tau_y^z \quad (1.3b)$$

$$T_t = \frac{1}{\rho_o c_p} I_z - \frac{1}{\rho_o c_p} F_z \quad (1.3c)$$

$$S_t = - E_z \quad (1.3d)$$

where the flux profiles of momentum, heat, and salinity (τ_z , F_z , and E_z) are determined by the mixing criteria described below. I_z is the vertical penetration of solar insolation; c_p is the specific heat of seawater. Density is calculated using a linearized equation of state,

$$\rho = \rho_o (1 + \alpha(T-T_o) + \beta(S-S_o)) \quad (1.4)$$

where α and β are linear coefficients of thermal and haline expansion.

The model is forced at the surface by momentum and buoyancy fluxes due to wind stress, evaporation, precipitation, solar heating, and cooling which are assumed to be known: $\tau(0) = \tau_s$, the surface wind stress; $F(0) = Q$, the air-sea heat flux, positive downward; and $E(0) = S(E - P)$, the freshwater flux times the surface salinity.

Vertical mixing occurs until three stability conditions are satisfied:

$$\rho_z \geq 0 \quad (1.5a)$$

$$Ri_{bulk} = - \frac{g}{\rho_o} \frac{\Delta\rho h}{(\Delta u)^2} \geq 0.65 \quad (1.5b)$$

$$Ri_{gradient} = - \frac{g}{\rho_o} \frac{\rho_z}{u_z^2} \geq \frac{1}{4} \quad (1.5c)$$

where h is the mixed layer depth and Δ is the difference in density or current across the base of the mixed layer (before 1.5c is applied). This mixing produces the vertical distributions of the momentum and heat fluxes, $\tau(z)$ and $F(z)$. The first two criteria (1.5a, 1.5b) simulate convection and entrainment, respectively, and produce a slab-like surface mixed layer of depth h (Figure 1.1). The last criterion (1.5c) simulates shear flow instability and produces a sheared transition layer between the mixed layer and the fluid below. The shear flow stability criterion acts to smooth out the sharp jump in velocity and density that would otherwise occur at the base of the mixed layer by extending mixing below the well-mixed layer into a "transition layer" of depth d (see Figure 1.1). In this respect, the model more accurately simulates the vertical profiles observed in the upper ocean.

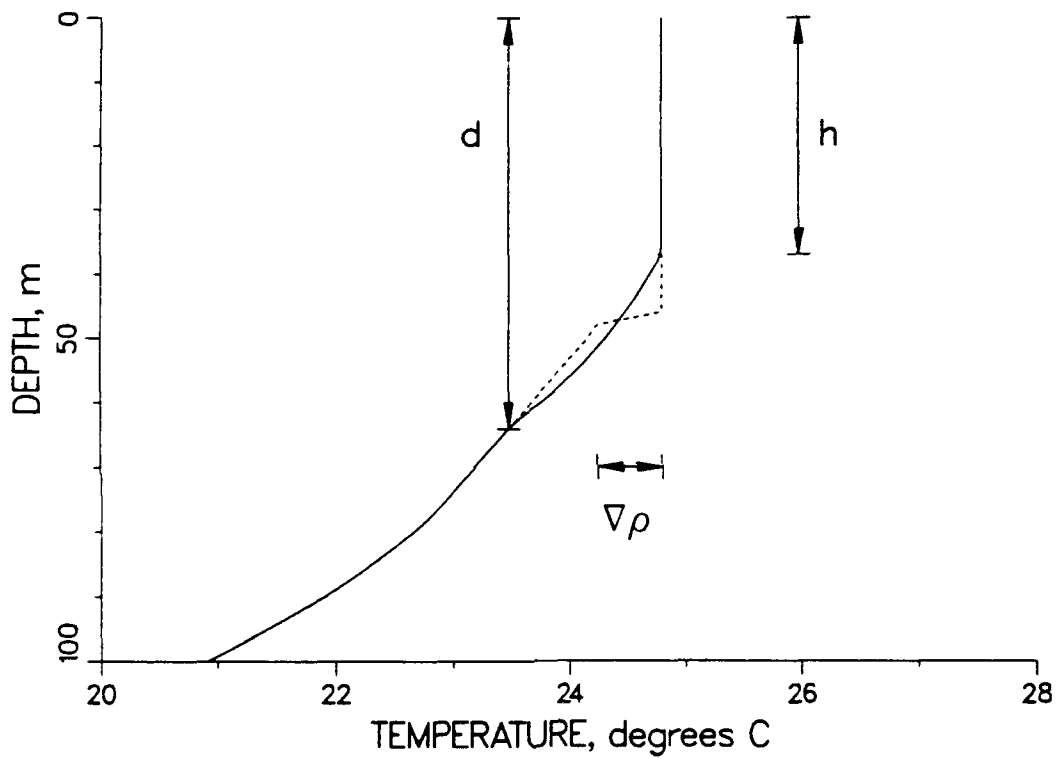


FIGURE 1.1. The sequence of the Price et al. (1986) model's mixing scheme. The dashed line shows a temperature profile at an intermediate stage in the mixing scheme, after the convection and entrainment criteria (1.5a, 1.5b) have been applied, producing a slab-like mixed layer with a jump, Δ , at its base. The solid line shows the final temperature profile, after shear flow stability (1.5c) has been achieved, and the resulting final mixed layer depth, h , and transition layer depth, d . The thickness of the transition layer is the difference between d and h .

1.3 EQUATORIAL UPPER OCEAN DYNAMICS

Several physical processes unique to the equator make the equatorial upper ocean very different from the mid-latitude upper ocean. Because the Coriolis force vanishes at the equator, the principal force balance in the equatorial upper ocean is between the zonal pressure gradient and the zonal wind stress. Bryden and Brady (1985) have shown this balance to be almost exact in the top 150 m, and McCreary (1981) found that the principal balancing force for the zonal pressure gradient, which drives the Equatorial Undercurrent, is the vertical turbulent viscosity (i.e. its distribution of the wind stress). Wind stress is vertically distributed in the upper ocean by turbulent mixing; the depth it reaches is determined by the stability of the water column, which in turn is determined by the stratification and shear. At the equator the vertical distribution of wind stress determines which modes of equatorial Kelvin and Rossby waves are forced, and governs the response of the zonal pressure gradient and the Equatorial Undercurrent to changes in the wind stress. The vertical profile of wind stress at the equator is an important aspect of the large-scale equatorial circulation, and is not well known or understood.

The thermal structure of the equatorial upper ocean is also radically different than at mid-latitudes. The vanishing Coriolis force at the equator results in strong upwelling of $O(3 \text{ m day}^{-1})$ driven by Ekman divergence in the surface waters and geostrophic convergence deeper in the water column (Wyrki, 1981, Halpern et al., 1989). This strong upwelling causes the main thermocline to be rather near the surface, intensifying the stratification and vertical shear in the equatorial upper ocean as well as providing intense cooling from below for the upper ocean. At the surface, there is a very large diurnal cycle in solar heating which, according to the mid-latitude results discussed above, should drive a surface-trapped diurnal warming and diurnal jet in the equatorial upper ocean during the

heating phase of the cycle. Furthermore it is possible that the vertical penetration of the diurnal layer is amplified because the flow on which it is imposed is near instability.

1.3.1 Observations of the equatorial upper ocean

Recent upper ocean measurements made during the TROPIC HEAT program (Niiler, 1987) revealed a large diurnal cycle in turbulent dissipation at the equator (Gregg et al., 1985; Moum and Caldwell, 1985; Peters et al., 1988; Moum et al., 1989), indicating a very strong daily variation in mixing at the equator that was previously unknown. During the day, when strong solar heating stabilizes the upper 10-20 m, little turbulent dissipation is observed; what dissipation existed is limited to depths less than about 10 m. During the night, as cooling and wind-mixing erase the daytime warming, dissipation becomes of order 10^{-7} W kg⁻¹, indicative of vigorous mixing, down to depths of 80 m, more than twice the depth of the surface mixed layer. In contrast, observations from the upper ocean at mid-latitudes show that the high values of dissipation associated with turbulent mixing penetrate only about 10 m below the mixed layer at night even when the mixed layer is very deep, O(100 m) (Shay and Gregg, 1986; Lombardo and Gregg, 1989; Price et al., 1986; see Figure 1.2). In the mid-latitude upper ocean, dissipation is also generally much less intense for similar wind and surface heating/cooling conditions.

The TROPIC HEAT observations raise the questions: what processes cause the pronounced diurnal cycle of mixing on the equator, and how is the equatorial upper ocean different from mid-latitudes? Since the only forcing that has a persistent night to day difference during TROPIC HEAT is the solar insolation (Moum and Caldwell, 1985), the diurnal cycle in dissipation presumably must be forced by the surface heat flux. The question is, what physical mechanism transfers momentum from the surface to cause the deep turbulence signal? Is it mixed layer convection or internal waves radiated from the

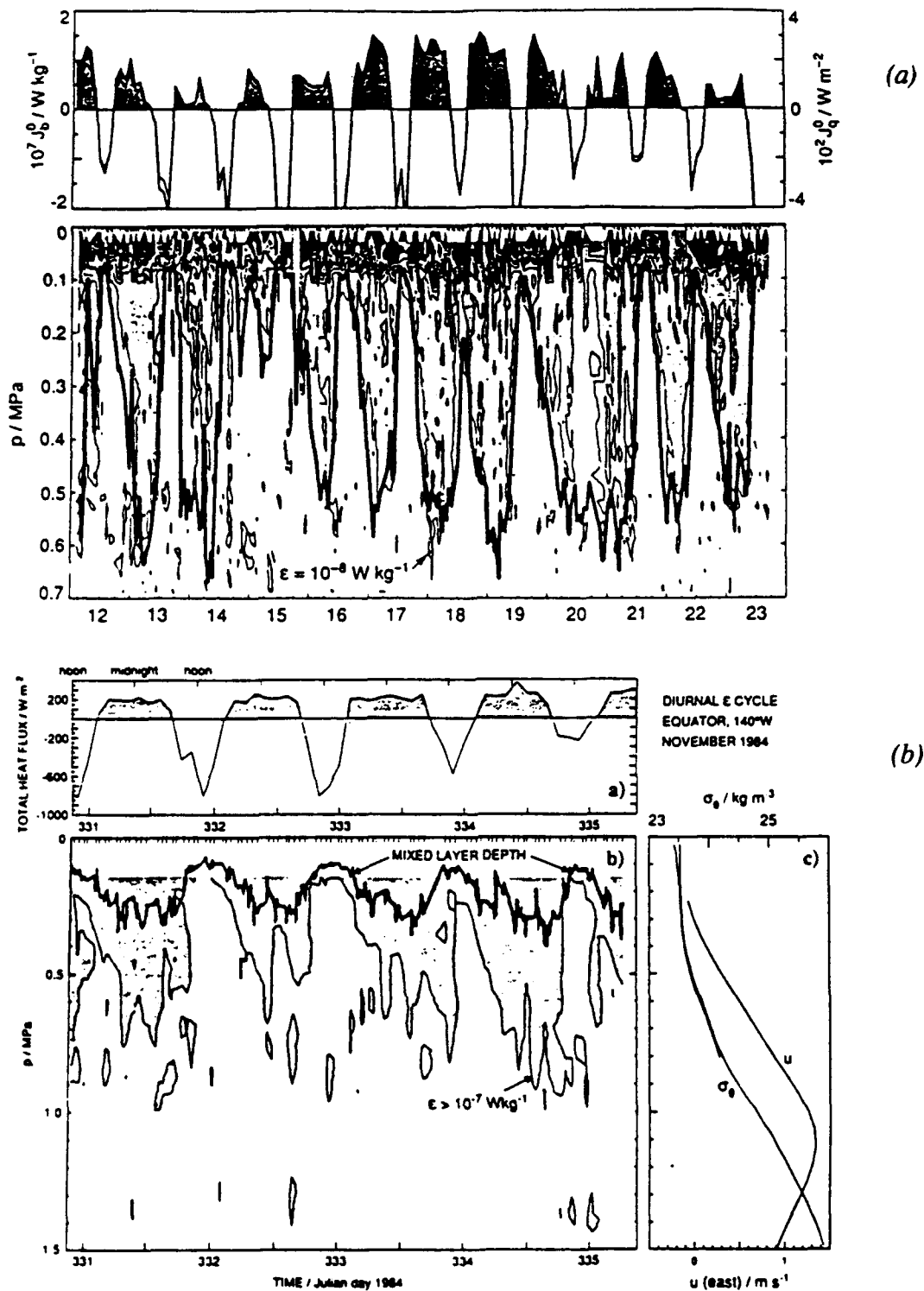


FIGURE 1.2. (a) Diurnal mixing cycle observed during PATCHEX in October 1986, from Lombardo and Gregg (1989). The mean stratification was very low, and the mixing ended within a few meters of the base of the mixed layer (solid line). (b) Deep diurnal mixing cycle observed during the 1984 TROPIC HEAT experiment, from Peters et al. (1987). Although the mixed layer only went to 30 m at night, bursts of intense mixing penetrated as deep as 90 m. Below the mixed layer the water column was well stratified but had high shear, produced by the Equatorial Undercurrent, which had maximum speed at 110 m.

mixed layer, or something else? Since the turbulent dissipation varies diurnally at depths greater than the penetration of the diurnal mixed layer, turbulent mixing appears to be caused by a process other than simple mixed layer physics (Moum and Caldwell, 1985, Moum et al., 1989, Peters et al., 1988). Our hypothesis is that the essential difference between the equator and most mid-latitude regions is the presence of the Equatorial Undercurrent (EUC), which provides a strong and persistent vertical shear within the upper 100 m of the ocean.

1.3.2 Review of modelling studies of the equatorial upper ocean

Throughout the 1980's a series of modelling studies illustrated the important role of the upper ocean mixed layer in the equatorial circulation. Large-scale modelling of the equatorial and tropical ocean had been ongoing for some time, motivated by the need to predict El Niño processes. The importance of surface wind-forcing of the equatorial circulation was appreciated in that wind pulses are known to precede and perhaps initiate El Niño events by sending a downwelling (warming) Kelvin wave eastward, but the role of surface heating has been generally unexplored because it is assumed to be insignificant relative to the large horizontal and vertical heat fluxes of the Equatorial Undercurrent system.

In one of the first models designed to understand tropical and equatorial mixed layers, Hughes (1980) predicted a simple balance between local wind and heating, modified by upwelling, resulting in a mixed layer depth equivalent to the Monin-Obukov length scale. This simple 1-1/2 layer model did not include an undercurrent (and therefore no horizontal advection), and was limited by a simple parameterization of entrainment into a quiescent lower layer. More realistic models with mixed layer physics incorporated into primitive

equation models of the large-scale equatorial circulation showed that without a mean surface heating, the Equatorial Undercurrent is wiped out by a westward wind stress (the prevailing direction) in a matter of days (Pacanowski and Philander, 1981). This result was confirmed by Schopf and Cane (1983).

The role of diurnal variations in surface heating was explored by Kraus (1987). Using a transient mixed layer model (Stull and Kraus, 1987) that included a representation of the mean Undercurrent, he showed that turbulent mixing occurs well below the truly well-mixed layer at the equator. Though this model did not show the extreme diurnal variation in turbulent mixing observed during the TROPIC HEAT experiment, it showed that surface-driven mixing in the upper ocean does interact significantly with the equatorial undercurrent. We believe the deep penetration of mixing in the equatorial upper ocean may be at least partially due to interaction between the strong diurnal heating cycle and high shear of the Equatorial Undercurrent.

1.4. STRUCTURE OF THESIS

The main goal of this work is to examine the vertical structure of the upper ocean 1) in a mid-latitude region, away from strong mean currents, and 2) at the equator, where strong and persistent mean circulation exists. To do so, we have analyzed observations from two very different observational programs: the LOTUS moored current meter array that spanned two years, and the TROPIC HEAT field experiments that provided ship-based measurements over two 12-day periods at opposite extremes of the seasonal cycle. In this thesis we address several specific questions. Can we observe the structure of an Ekman layer in a high-quality data set of long duration? Does the Price et al. (1986) model provide an explanation of the observed vertical structure of currents that make up the Ekman transport? Does the mean current structure vary with seasonal changes in the strength of

the diurnal heating cycle? How does the vertical structure of the upper ocean change at the equator in the presence of strong mean currents? Can we explain the recent observations of an intense diurnal cycle in mixing at the equator?

In Chapters 2 and 3 we describe our attempts to isolate the Ekman flow from the total observed current using observations from the LOTUS experiment, and examine the structure of the mean wind-driven current that makes up the Ekman transport. We assess the effect of diurnal and seasonal stratification over a summer and winter of the LOTUS experiment using the Price et al. (1986) model of the upper ocean. In Chapter 4 we extend the Price et al. (1986) model to the equatorial upper ocean and assess the effects of the Equatorial Undercurrent on upper ocean dynamics at the equator. In Chapter 5 we compare our equatorial model results to observations from the TROPIC HEAT experiments. Finally, in Chapter 6 we summarize our results.

Chapter 2

Observations of the Ekman Balance in Summer Conditions

In the following two chapters, we describe the mean balances and structure of the upper ocean currents observed during the Long Term Upper Ocean Study (LOTUS) experiment. Measurements of near-surface currents and meteorology were made over a period of two years during this experiment. However, during the second year of LOTUS several instruments failed relatively early on, so this part of the dataset was not used in our analysis effort. To separate out seasonal effects in our analysis, the data from the first year of LOTUS were separated into two separate pieces, one predominantly summer and the other predominantly winter.

This chapter describes observations from the first summer of the LOTUS experiment, as reported in part by Price et al. (1987). First, an overview of the LOTUS experiment is given in Section 2.1. In Section 2.2 we explain the method used to extract the wind-driven current from the observations. Section 2.3 describes how the method was applied to observations. The resulting mean current spiral and transport and the sensitivity of the results to reference level, length of averaging time, and total record length are described in Section 2.4. In Section 2.5 diurnal variability of the mean current spiral is discussed. A concluding summary is given in Section 2.6. Observations from the following winter of the LOTUS experiment are presented in Chapter 3.

2.1 OVERVIEW OF THE LOTUS EXPERIMENT

The Long Term Upper Ocean Study was planned in 1979 when it was realized that short, one- to two-month upper ocean experiments, such as the JASIN experiment, could not give

long-term statistics (Briscoe and Weller, 1984) or address seasonal changes in the upper ocean. The LOTUS experiment was therefore planned to provide continuous measurements of the upper ocean over a period of two years. The first LOTUS moorings were set in May 1982 at the old Woods Hole Site L near 34°N, 70°W (Figure 2.1). This site is in the Sargasso Sea, well south of the mean axis of the Gulf Stream, and far from any significant topography.

The LOTUS mooring array was designed to measure surface meteorology and ocean currents and temperature over the full water column. A surface-moored 3.5-m discus buoy provided a platform for meteorological measurements as well as current and temperature measurements in the upper 300 m (Figure 2.2). Surface mooring 767 (designated LOTUS 3; LOTUS 1 and 2 were earlier tests) was replaced by 770 (LOTUS 4) in October 1982, and the entire array was replaced in April 1983 (LOTUS 5). Three subsurface moorings were also set to sample the horizontal variability.

Meteorological measurements were made with a vector averaging wind recorder (VAWR), and surface fluxes were estimated with conventional bulk formulae (Large and Pond, 1981). Currents and temperature in the upper 100 m were measured primarily with vector-measuring current meters (VMCMs), which are designed to resolve the relatively weak mean currents in the upper ocean in the presence of the large and rapidly oscillating orbital velocities associated with surface waves (Weller and Davis, 1980). Below 100 m, as well as at a few shallower depths, the current was measured primarily with vector-averaging current meters (VACMs) and Aanderaa current meters, see Figure 2.2.

During the LOTUS experiment, the stratification in the upper ocean varied on seasonal and diurnal time scales (Figure 2.3). The seasonal cycle of the net heat flux creates a seasonal thermocline in the summertime, and the surface temperature warms by about 10°C in this

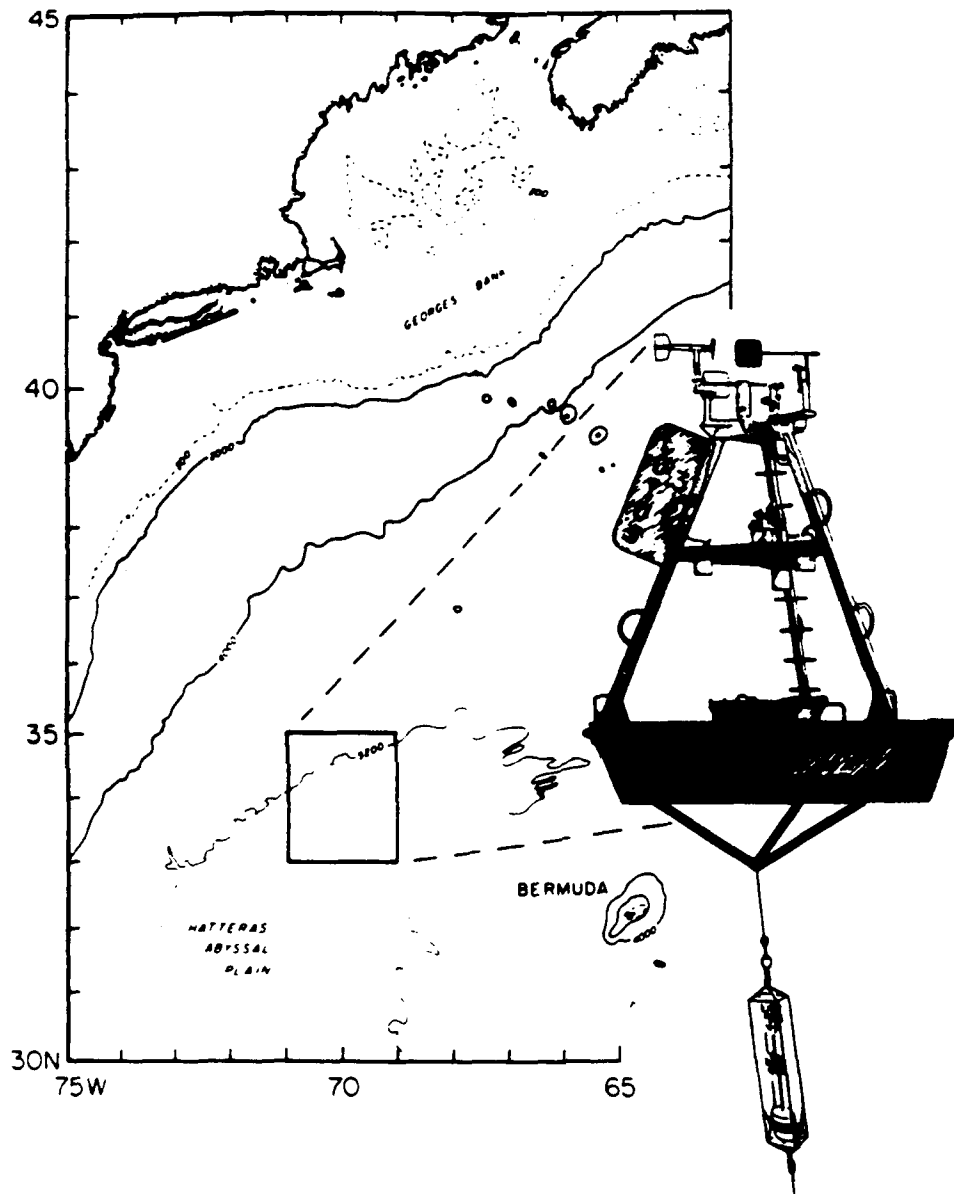


FIGURE 2.1. The location of the Long Term Upper Ocean Study area.

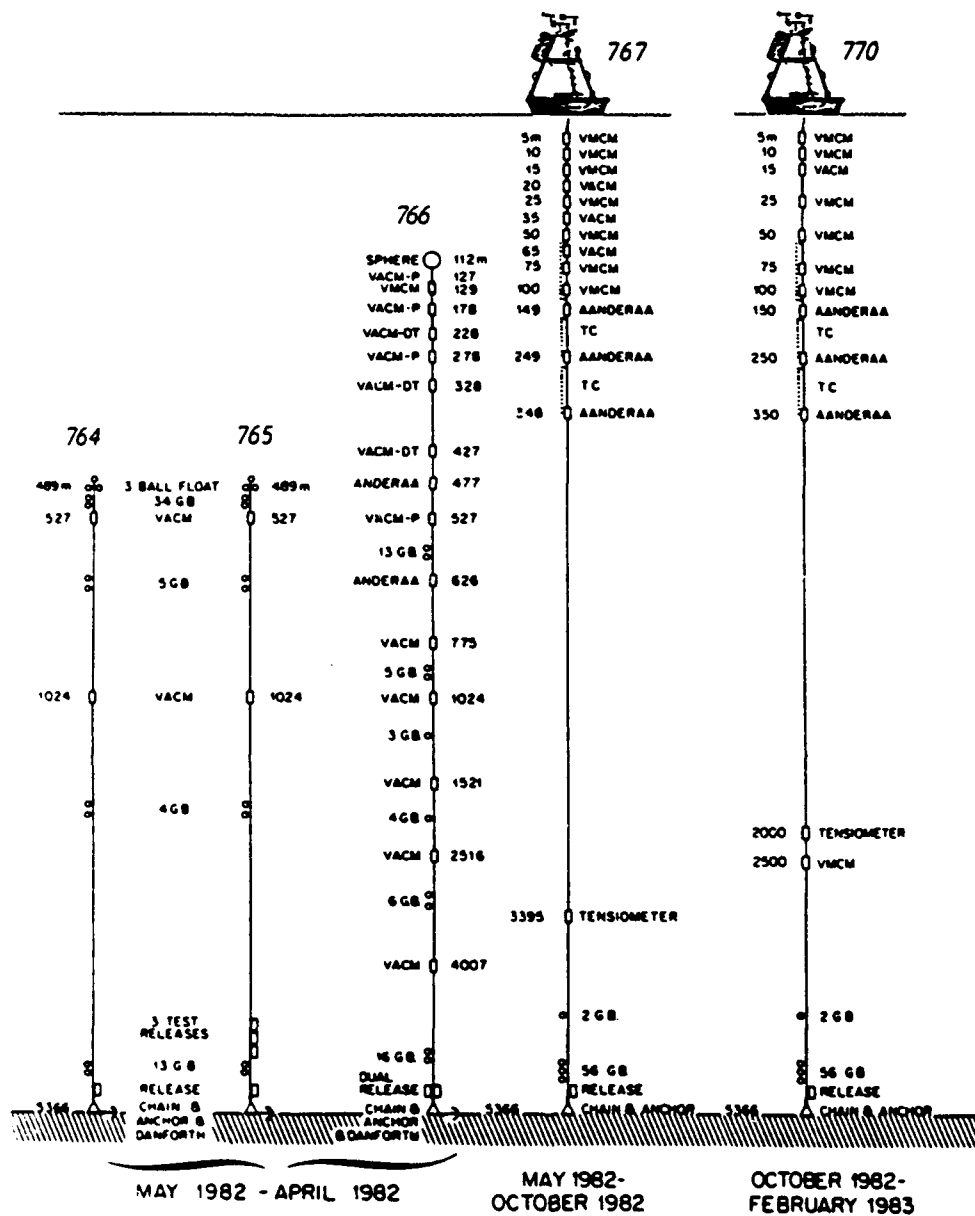


FIGURE 2.2. Diagrams of the five LOTUS moorings at sea for the first year of the experiment. Surface moorings 767 and 770 provided most of the data included in this study.

region (Bowers et al., 1986). The diurnal cycle of solar heating similarly causes the formation of diurnal stratification during the daytime which has surface amplitudes of 0.3° to 2.0°C in the summertime (Stramma et al., 1986). The LOTUS 3 period was primarily during the summer, from May 14 to October 31, 1982, spanning 170 days. Meteorological conditions were dominated by fair summer weather typical of the subtropics. Strong solar heating together with light winds caused significant diurnal warming of the sea surface on many days (Stramma et al., 1986; Bowers et al., 1986), and formed a seasonal thermocline that just began to erode at the end of LOTUS 3 (Figure 2.3). The seasonal thermocline continued to erode throughout the LOTUS 4 period (Figure 2.3). This period ran from October 31, 1982 to February 19, 1983, spanning 109 days, and was dominated by wintertime weather conditions with even more cloudiness than typical for the region (Deser et al., 1983). Net cooling at the ocean surface and strong winds combined to suppress the amplitude of the diurnal cycle and caused the deep convection that forms the 18° water mass in the North Atlantic (Worthington, 1959).

The most dominant feature of the LOTUS current measurements throughout the first year are the energetic events (Figure 2.4) that sometimes extend as deep as 4000 m, involving more than 3/4 of the water column (the total water depth at the site is approximately 5300 m). Some of these events were Gulf Stream rings and some appeared to be anticyclonic eddies (Briscoe and Weller, 1984). The rms speed of these motions was 25 cm s⁻¹ (Briscoe and Weller, 1984), about five times as large as the wind-driven surface currents, presenting a signal-to-"noise" problem that we discuss in more detail below and in the next section.

The eddy motions that dominate the observations are fairly barotropic in the upper ocean (Figure 2.4). If we reference currents to a depth of O(100 m) we can see that at low frequencies (greater than an inertial period) the upper ocean currents are coherent with the

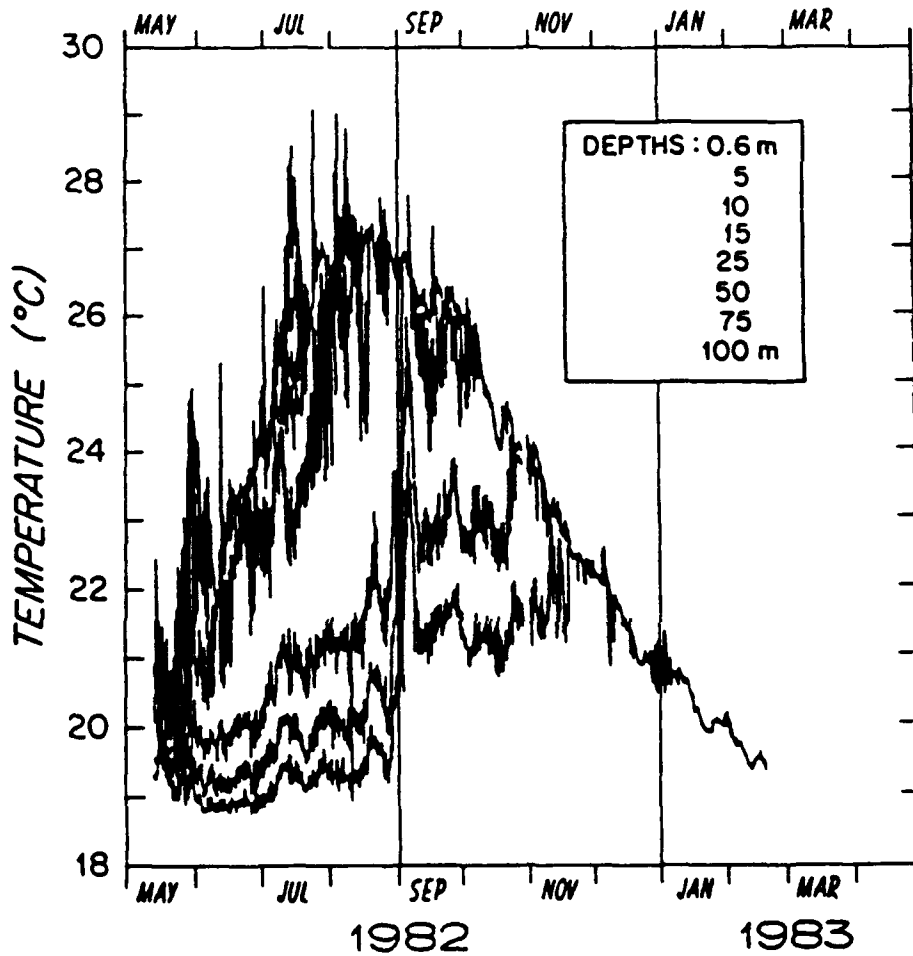


FIGURE 2.3. Temperature at eight fixed depths in the upper 100 m during the first year of the LOTUS experiment, from Briscoe and Weller (1984). Data points are at four-hour intervals. Spikes in the shallowest record are due to diurnal warming during periods of low wind. The seasonal cycle is clear, showing the mixed layer deepening to below 100 m in late November.

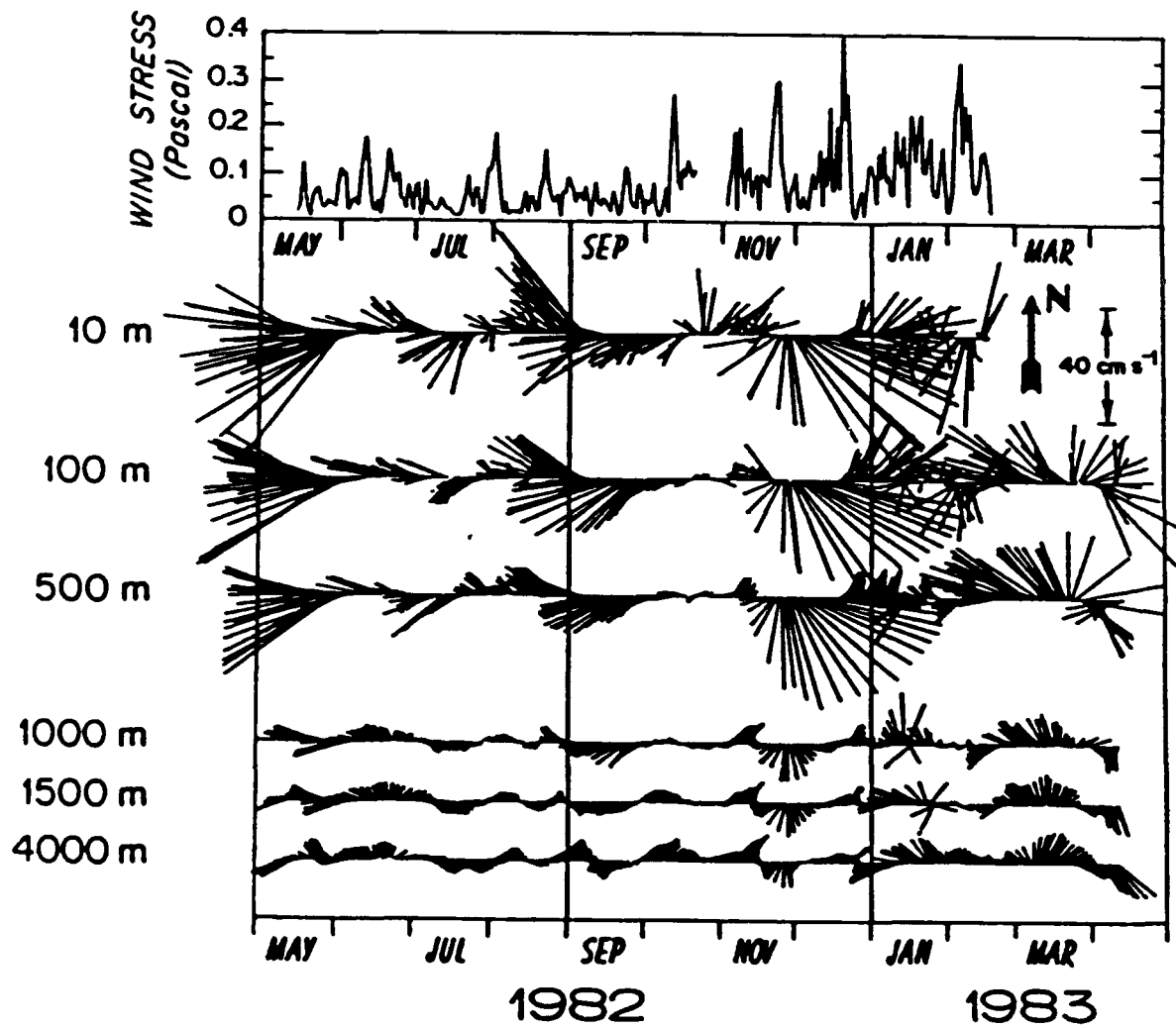


FIGURE 2.4. Wind stress magnitude and current vectors from the first year of the LOTUS experiment, taken from Briscoe and Weller (1984). Each current vector is an average over one day. Energetic mesoscale motions dominate the observed currents and are often coherent through the entire water column.

wind direction. Figures 2.5 and 2.6 show the clockwise coherence and phase spectra between wind stress and the current at 10 m for the LOTUS 3 and 4 periods, respectively. At frequencies below about 0.02 cph the current at 10 m is to the right of the wind, consistent with Ekman's theory (1.2).

2.2 THE WIND-RELATIVE AVERAGING METHOD

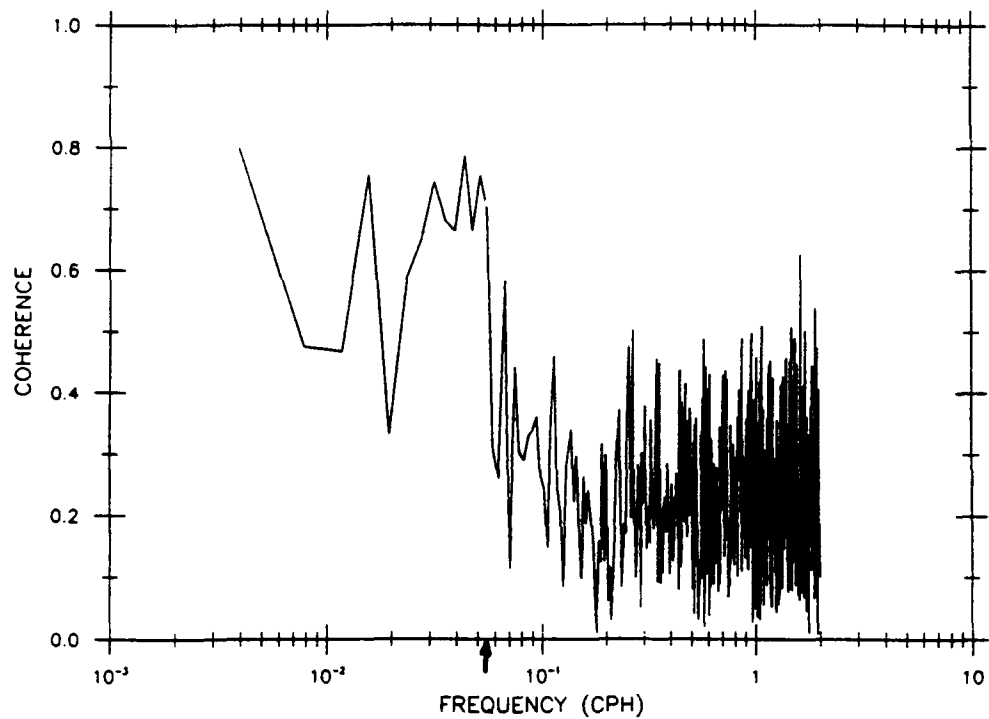
Our goal in analyzing the LOTUS data was to take advantage of the long time series to see if a long term Ekman balance existed,

$$\int_0^z [u, v] dz = \left[\frac{\tau'}{\rho f}, \frac{-\tau'}{\rho f} \right] \quad (2.1)$$

where z , is the depth below which the wind-driven current vanishes, τ' is oriented north, along the positive y-axis, and u is 90° to the right of τ' , along the positive x-axis.

To overcome the signal-to-noise ratio problem, a series of steps were taken to extract the wind-driven current from the total measured current. This is the "coherent ensemble average" method described by Price et al. (1987), but we repeat it here for completeness.

The first step is to reference the currents to a depth below the wind-driven layer to isolate the wind-driven flow from the total current, $v_{wind-driven}(z) = v(z) - v(z_r)$. Recent studies have shown that even very small amounts of stratification associated with diurnal warming can limit the penetration of wind stress into the water column (Price et al., 1986). Upper ocean models have successfully simulated the wind-driven current by assuming that it is trapped in a mixed layer. The goal, then, is to choose a reference level somewhere below the mixed layer depth.



LOTUS 3 U10 TAU CW

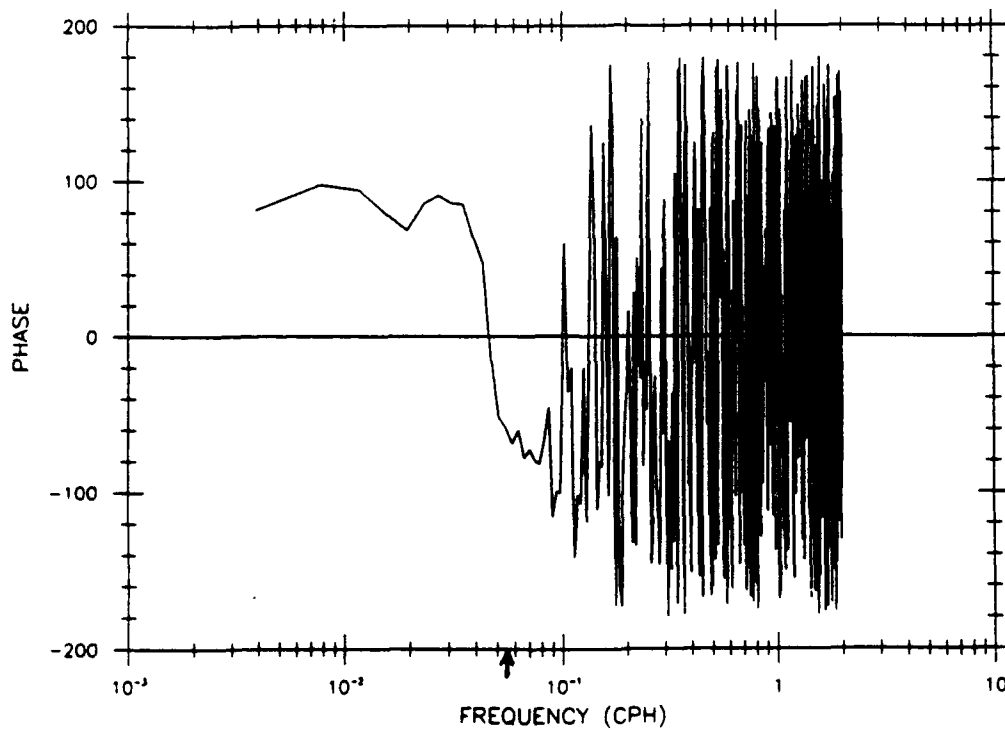
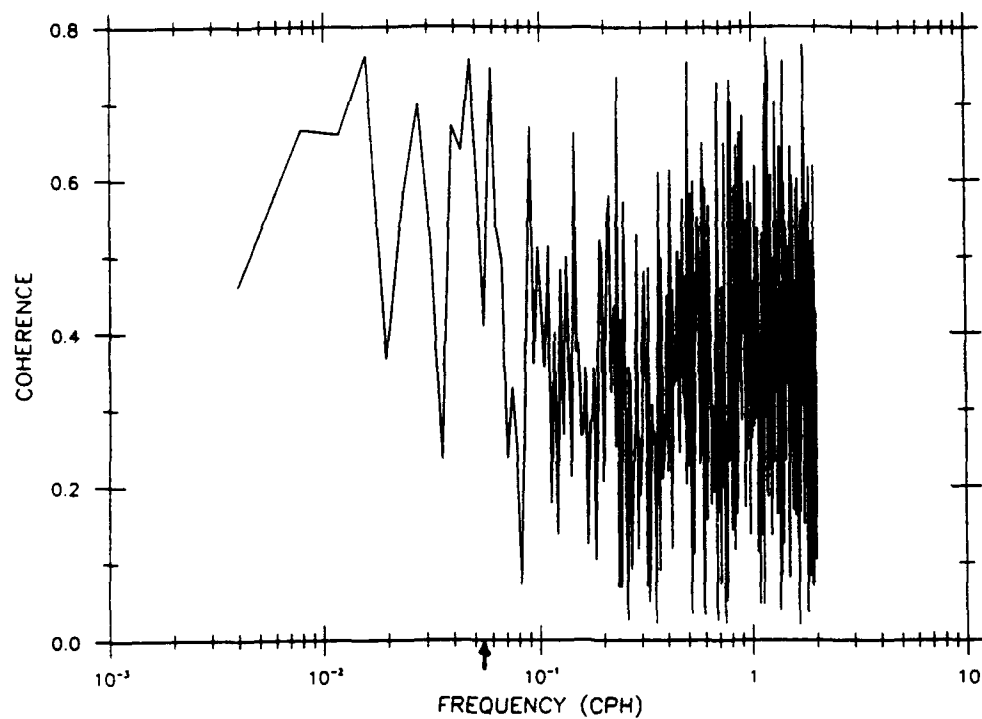


FIGURE 2.5. Coherence and phase (in degrees) of the clockwise cross-spectrum between wind stress and 10-m current observed during the LOTUS 3 period. The current at 50 m has been subtracted away from the 10-m current; this choice of a reference level is discussed in Section 2.3.1. The arrow indicates the diurnal-inertial frequency (they are nearly identical at this latitude, 34°N).



LOTUS 4 U10 TAU CW

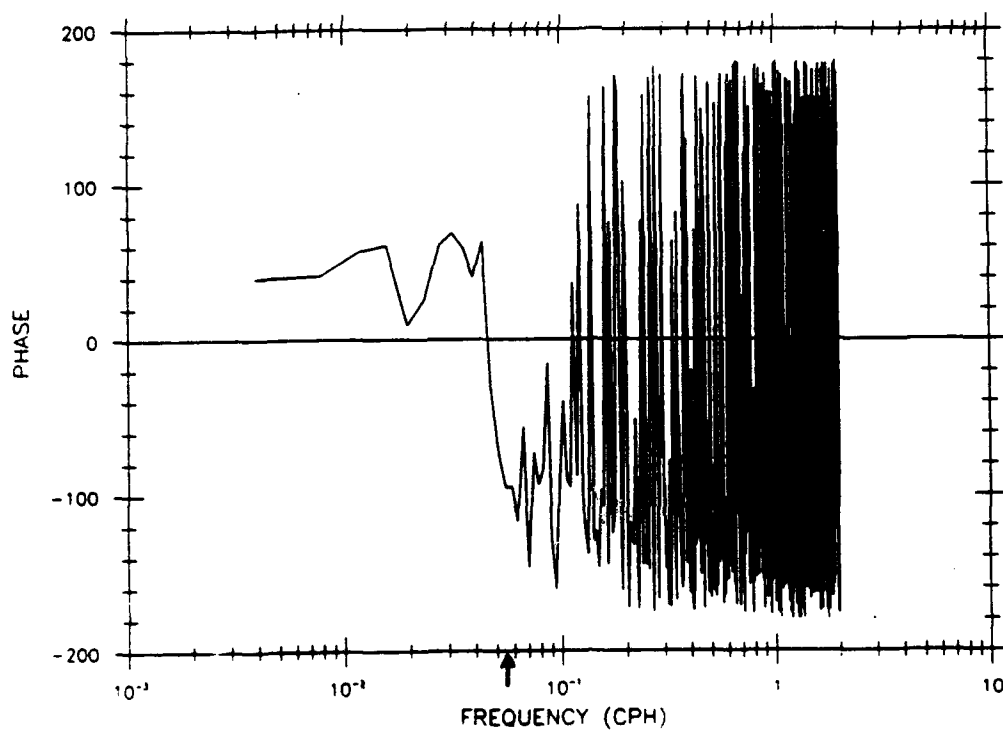


FIGURE 2.6. Coherence and phase (in degrees) of the clockwise cross-spectrum between wind stress and 10-m current observed during the LOTUS 4 period. In this case the current at 129 m has been subtracted away from the 10-m current; this choice of a reference level is discussed in Chapter 3 in Section 3.1.1. The arrow indicates the diurnal-inertial frequency (they are nearly identical at this latitude, 34°N).

The next step is to look at the currents in a wind-relative coordinate system. To do this, wind stress and ocean currents are first vector-averaged over one day, and then rotated into a crosswind, downwind coordinate system to enhance the wind-driven signal. By doing so, the average wind stress is increased by about a factor of 4, to 0.068 Pa in LOTUS 3, whereas the simple time mean wind stress is 0.015 Pa, and to 0.147 Pa in LOTUS 4, versus the simple time mean of 0.04 Pa. This coordinate system essentially follows the low frequency variations in the wind direction, and therefore serves to isolate the wind-driven current.

Finally, the individual, wind-relative daily averages of the current are ensemble-averaged together to form the long-term mean. A daily average was chosen in order to eliminate both the diurnal cycle and the inertial motions (the inertial period at this latitude is approximately 21 hours). The mean current profile is then integrated using a simple trapezoidal method to obtain estimates of the volume transport. The final mean current is then interpreted as if the wind had blown in a constant direction during the observation period.

An alternate way to describe the wind-relative averaging method was pointed out by Weller et al. (1991). The wind-relative average is equivalent to performing a regression between the current and a unit vector pointing in the direction of the wind (Weller et al., 1991). The 24-hour boxcar average is equivalent to a 48-hour low-pass filter, and thus eliminates both diurnal and inertial motions at this latitude. The wind-relative average is therefore simply an alternative way to obtain the mean, low frequency structure of the current relative to the wind that was shown in the cross spectra in Figures 2.5 and 2.6.

2.3 APPLYING THE WIND-RELATIVE AVERAGE

2.3.1. Choice of reference level

The first issue in applying this method to observations is choosing an appropriate reference level. This, of course, is limited by the vertical spacing of the instruments. Furthermore, we chose to use only VMCM-measured currents whenever possible in order to best resolve the wind-driven current. VMCMs were positioned at depths of 5, 10, 15, 25, 50, 75 and 100 m during LOTUS 3. We have estimated the mixed layer depth during the LOTUS 3 period using a temperature difference of 0.05°C from the surface (Figure 2.7). Based on these estimates, we chose a reference depth of 50 m for the LOTUS 3 data. This reference depth was below the mixed layer throughout the deployment and within the seasonal thermocline for all but the last few days of the LOTUS 3 record. A similar reference level was chosen by Weller (1981) for upper ocean current observations in the Pacific under relatively calm conditions. Most of the baroclinic structure of the eddy motions during the LOTUS experiment is in the main thermocline, between 500-1000 m (Lippert and Briscoe, 1990), so a reference level shallower than the main thermocline does not include a large amount of geostrophic shear. The sensitivity of the results to the choice of a reference level is examined in Section 2.4.4.

2.3.2. Data quality

The next step is to form individual daily averages of upper ocean currents relative to the wind-direction and then average over the record. However, as with all field observations, and particularly a long experiment like LOTUS, instrument failures and other events inevitably occur and affect the quality and availability of the data.

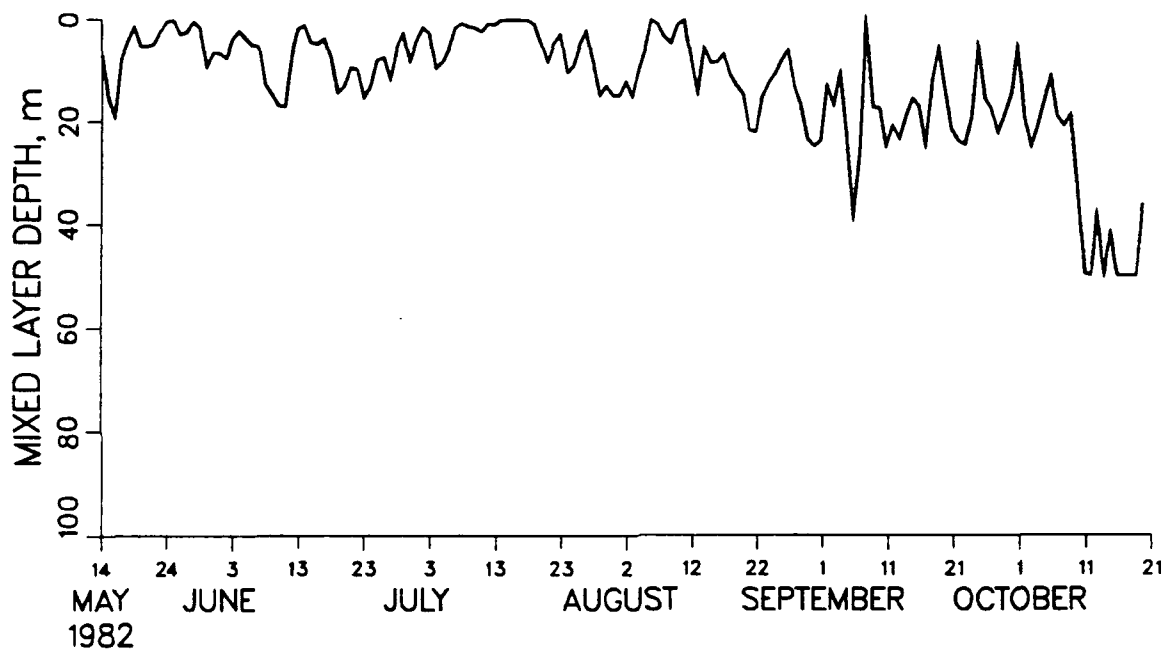


FIGURE 2.7. Mixed layer depth during the LOTUS 3 period estimated at 15-minute intervals using a temperature difference of 0.05°C from the surface, then averaged over one day. The mixed layer remains above 50 m throughout this period with the exception of the last few days.

The vector-averaging wind recorder on mooring 767 failed on October 21, after 160 days of the LOTUS 3 period. Since nearly all of our calculations are tied to wind stress measurements, we simply truncated all the other records to 160 days also. Eleven days later, the surface mooring was replaced with mooring 770, and the LOTUS 4 period began.

Also, a garbage bag (apparently dumped from a passing ship) caught in the rotor of the VMCM at 15 m depth on mooring 767 midway through the LOTUS 3 period. Surprisingly, it came free of the instrument after 11 days without damaging the rotor and the VMCM functioned normally after that. We therefore excluded the 11 "garbage days" of current measurements at the 15 m VMCM from our calculations but otherwise treated it normally. The mean current at 15 m depth is thus a 149-day average.

Finally, the VMCM at 5 m depth on mooring 767 failed after 86 days. After determining that the mean meteorological fluxes over the first 86 days were almost identical to the means over the full 160 days, and numerical simulations gave nearly identical results over these two periods (Price et al., 1987), we chose not to truncate the other records to this length. The mean current at 5 m depth for LOTUS 3 is thus an 86-day average, while at all the other depths (except 15 m, as discussed above) it is a 160-day average.

2.4 SUMMERTIME MEAN CURRENT SPIRAL AND TRANSPORT

2.4.1. *Mean spiral and transport*

The mean current at the four VMCM depths above 50 m and the resulting transport are shown in Figure 2.8. Numerical values for the mean velocity at each depth and their

uncertainties (standard errors) are listed in Table 2.1. The mean currents at 15 m and above are fairly well defined, but the 25 m value is not distinguishable from zero.

The mean current spiral is strongly surface trapped during the LOTUS 3 period, as described in detail by Price et al. (1987). The current decays rapidly with depth, and e-folds over about a 12 m scale. The current at 5 m has an amplitude of about 4 cm s^{-1} , and is about 78° to the right of the wind. The current rotates only about 20° over the e-folding depth and thus is 'flat' compared to the classic Ekman spiral, which predicts a rotation of about 60° over the e-folding depth (see 1.2). Relatively flat spirals have also been seen in other observations of the mean wind-driven current (Price et al., 1986; Weller, 1981). This flatness can also be expressed in terms of the eddy viscosity, which is estimated to be $60 \times 10^{-4} \text{ m}^2 \text{ s}^{-1}$ based on the e-folding of the current's amplitude, and $540 \times 10^{-4} \text{ m}^2 \text{ s}^{-1}$ based on the current's rotation (Price et al., 1987).

The volume transport between 50 m and the surface is quite close (within about 10%) to the theoretical Ekman transport both in magnitude and direction (see Figure 2.8 and Table 2.2). Previous estimates of wind-driven transport have typically found transports that are significantly different than the Ekman transport (e.g. Davis et al., 1981; Price et al., 1986).

2.4.2. Sensitivity to wind-rotation

In these observations, looking at the currents in a wind-relative frame is crucial. For comparison, we show the mean current spiral and transport during the LOTUS 3 period when the simple time mean is taken *without* rotating into a wind relative frame (Figure 2.9). Note that the agreement with Ekman transport is no better than previous estimates, despite the long data set. The average wind stress is significantly less than the rotated average (0.015 Pa vs. 0.068 Pa), as noted earlier. In fact, the success of this

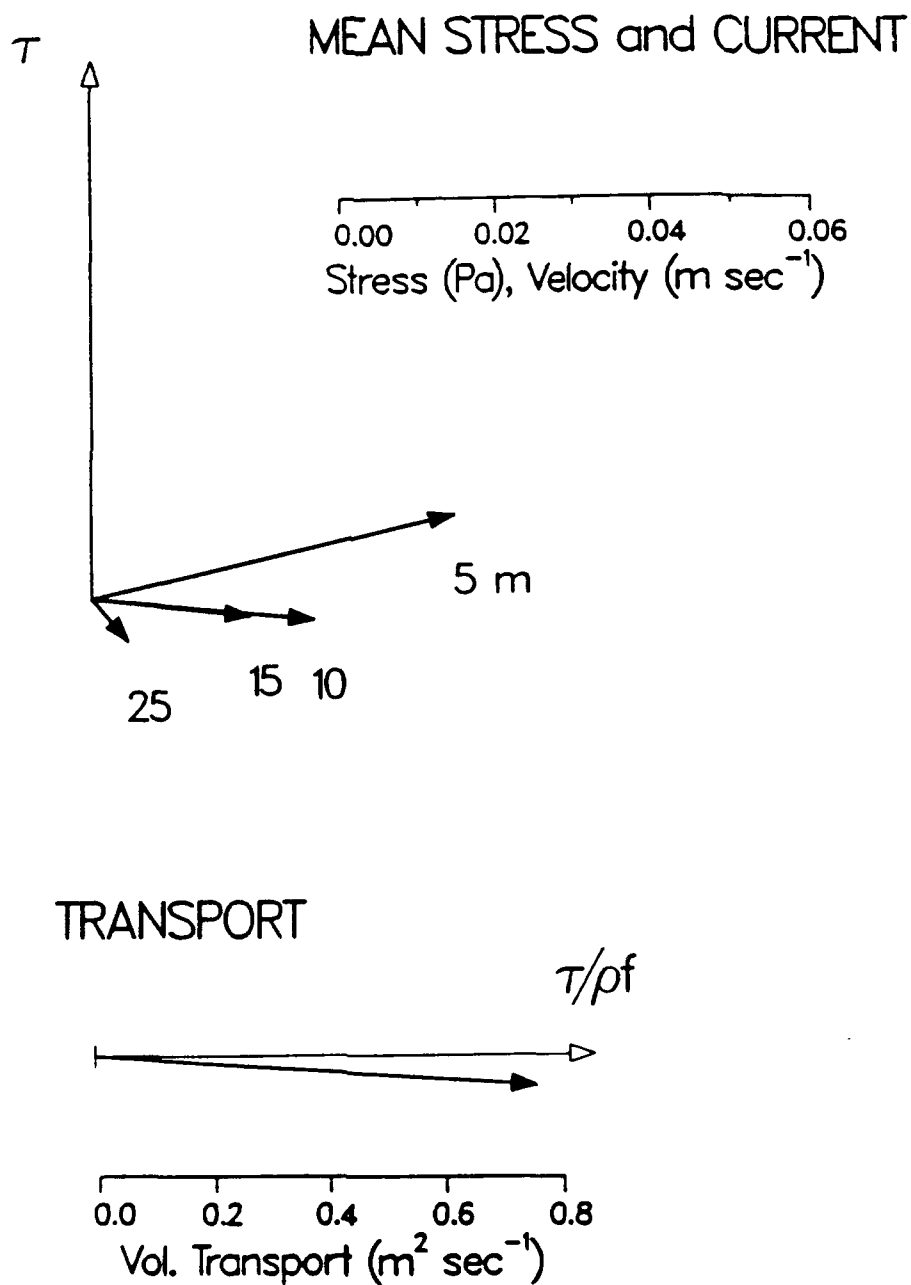


FIGURE 2.8. Wind-coherent mean wind stress, current spiral and transport relative to 50 m from the LOTUS 3 observations. The wind stress vector is arbitrarily pointed up, or "north", and is shown with an open arrowhead; current vectors are shown with solid arrowheads. Numbers at the ends of the current vectors are the depth in meters. The theoretical Ekman volume transport equal to $\tau/\rho f$ is shown with an open arrowhead, and the observed transport relative to 50 m is shown with a solid arrowhead. Uncertainties are given in Tables 2.1 and 2.2. As described in the text, the 5-m current is an 86-day average, the 15 m current is a 149-day average, and 10 and 25 m currents are 160-day averages.

TABLE 2.1.

Mean current and uncertainties during the LOTUS 3 period. Uncertainties on the data are statistical standard errors; 90% confidence limits are larger by a factor of 1.7, and 95% confidence limits are larger by a factor of 2.0. Calculating the standard error requires an estimate of the integral time scale, which we estimated from the data using a standard statistical definition (Bevington, 1969). The integral time scale for the daily values was 1.5 days, and so the number of effective degrees of freedom used to estimate the standard error for the 160-day record was taken to be $160 / (2 \times 1.5) = 53$.

DEPTH (m)	CROSSWIND CURRENT (cm s ⁻¹)	DOWNWIND CURRENT (cm s ⁻¹)
5	4.6 ± 1.2	1.0 ± 0.7
10	2.8 ± 0.7	-0.3 ± 0.4
15	2.0 ± 0.7	-0.2 ± 0.5
25	0.4 ± 0.4	-0.5 ± 0.4
50*		
75	0.6 ± 0.3	-0.2 ± 0.4
100	1.1 ± 0.6	-0.7 ± 0.6

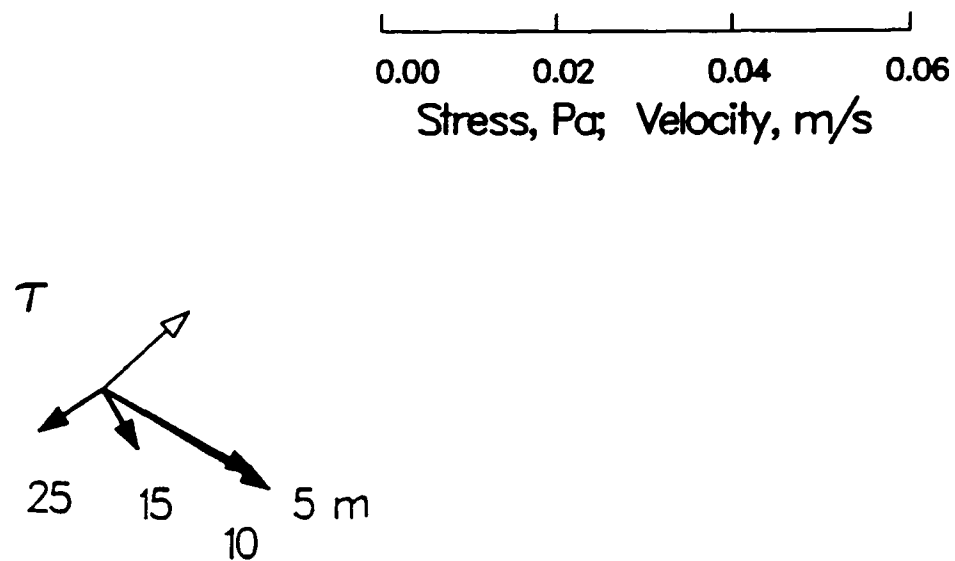
* The 50-m depth was chosen as the reference level, where the simple time-mean current was 18.1 cm s⁻¹ westward and 0.7 cm s⁻¹ northward.

TABLE 2.2.

Mean transport and errors during LOTUS 3. The Ekman transport was computed using the mean wind stress magnitude of 0.068 Pa, which is presumed to be uncertain to 20% because of uncertainty inherent in the bulk aerodynamic method (Large and Pond, 1981).

	CROSSWIND TRANSPORT (m ² s ⁻¹)	DOWNWIND TRANSPORT (m ² s ⁻¹)
OBSERVED	0.72 ± 0.19	-0.05 ± 0.14
EKMAN	0.82 ± 20%	0

MEAN STRESS and CURRENT



TRANSPORT

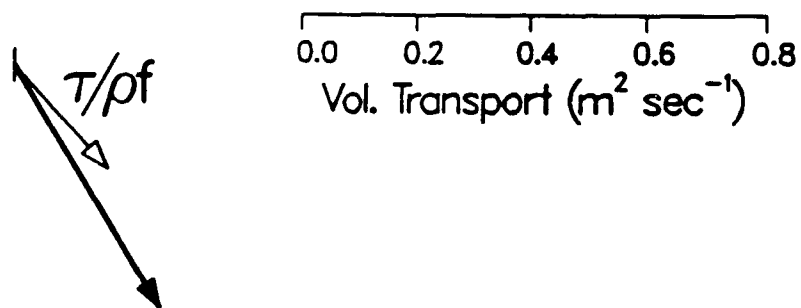


FIGURE 2.9. Simple time mean of wind stress and currents and the resulting transport relative to 50 m in a geographic E, N coordinate system. The wind stress and the theoretical Ekman transport are shown with open arrowheads; the observed currents and transport relative to 50 m are shown with solid arrowheads. Numbers at the ends of the current vectors are the depth in meters. Notice that the average wind stress is significantly reduced from the wind-coherent averaging method and agreement with Ekman transport is poor.

method in the LOTUS observations is probably improved because the wind is quite variable, and the wind variability is at a higher frequency than the mesoscale current eddies. The wind-relative average therefore successfully reduces the non-wind-driven part of the current and does not bias in a mean current, as it might in a region with steady winds (such as the trade winds) and large mean currents.

2.4.3. Sensitivity to averaging period

The choice of a daily averaging period is somewhat arbitrary and a similar ensemble average formed with individual averages over either two days or an inertial period are not significantly different (Figure 2.10). This is consistent with the stable phase relationship between the wind stress and the 10-m current shown in Figure 2.5.

2.4.4. Sensitivity to reference level

While the structure of the current spiral is relatively insensitive to the choice of reference level, the integrated volume transport does depend on it. We were fortunate that the current meter spacing on the LOTUS 3 mooring was such that observations were made at a reference depth of 50 m that was appropriate for our calculations. Had we referenced the velocities to the current measured at 25 m (the next shallowest VMCM) we would not have captured the full wind-driven current, and the observed transport is only about 3/4 of the Ekman transport (see Table 2.3). Referencing currents to either of the next VMCMs deeper than 50 m includes too much of the non-wind-driven current and the observed volume transport then begins to depart from the Ekman volume transport (Table 2.3).

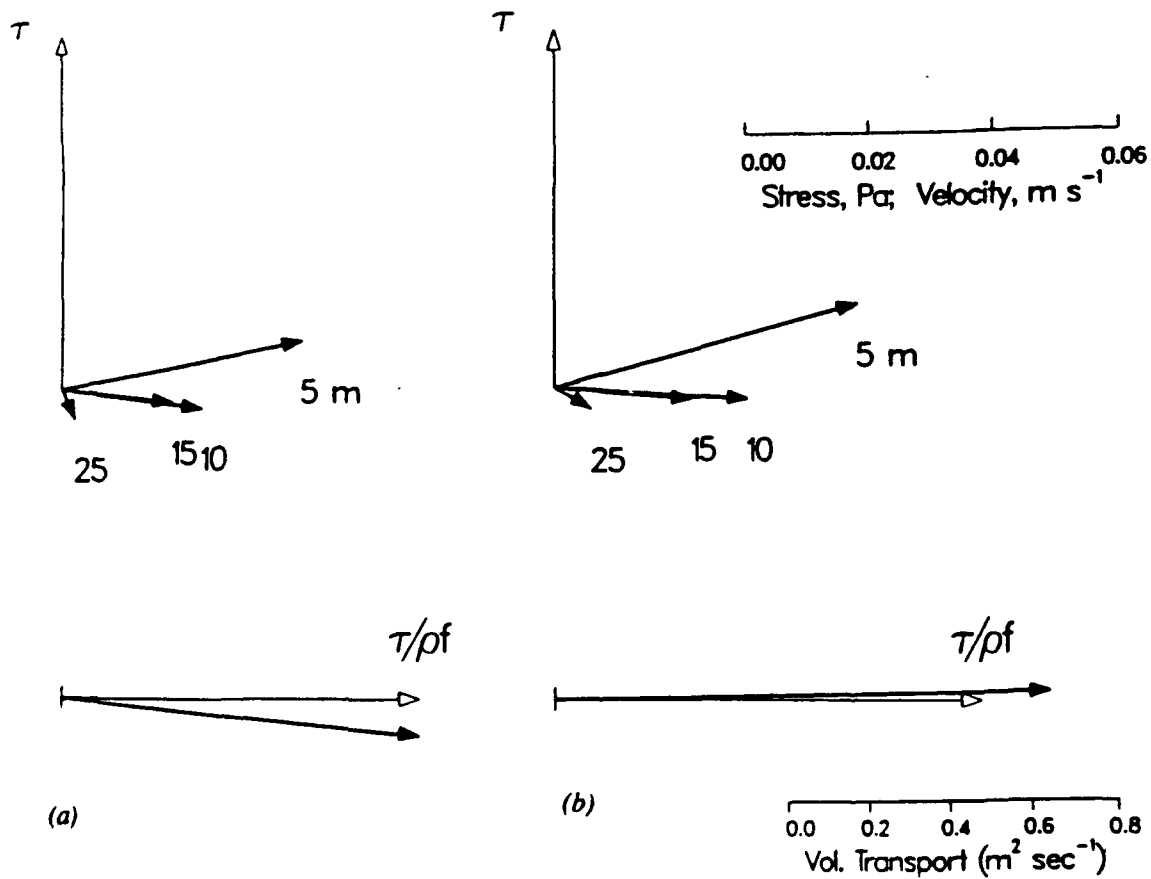


FIGURE 2.10. Wind-coherent mean spiral and transport formed with individual averages over a) 2 days, and b) 1 inertial period. The basic structure of the spiral and the volume transport are not significantly different from each other or from the mean formed with individual averages over one day (see Figure 2.8).

TABLE 2.3.
Observed transport during LOTUS 3 for different reference levels. The Ekman transport is $0.82 \text{ m}^2\text{s}^{-1}$.

REFERENCE LEVEL (m)	CROSSWIND TRANSPORT (m^2s^{-1})	DOWNWIND TRANSPORT (m^2s^{-1})
15	0.30	0.08
25	0.59	0.19
50	0.72	-0.05
75	0.34	0.06
100	-0.10	0.47

2.4.5. Sensitivity to total record length

The mean observed current and transport represent long-term averages over much variation. Figure 2.11 shows the scatter of daily estimates of observed transport relative to the daily Ekman transport. Our calculations suggest that the average crosswind component of observed transport begins to stabilize to a value near the Ekman transport after about 60 days (Figure 2.12). Similarly, the downwind component of observed transport begins to stabilize near zero after about 60 days (Figure 2.12) and remains within a few percent of this throughout the remainder of the LOTUS 3 period.

LOTUS 3 and EKMAN TRANSPORT

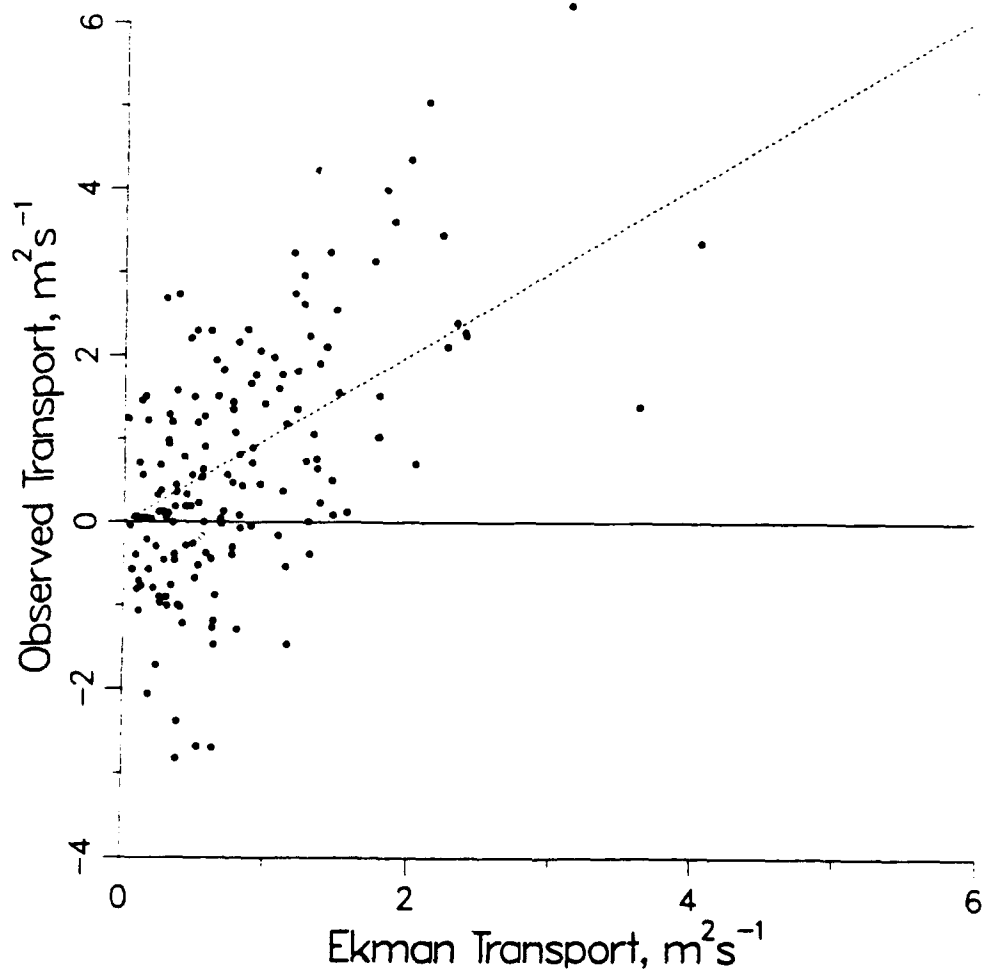


FIGURE 2.11. Crosswind component of observed transport relative to 50 m vs. the theoretical Ekman transport. Each point represents a daily average. The dashed line has a slope of one; if all days had exact agreement with Ekman transport, all the points would lie along this line.

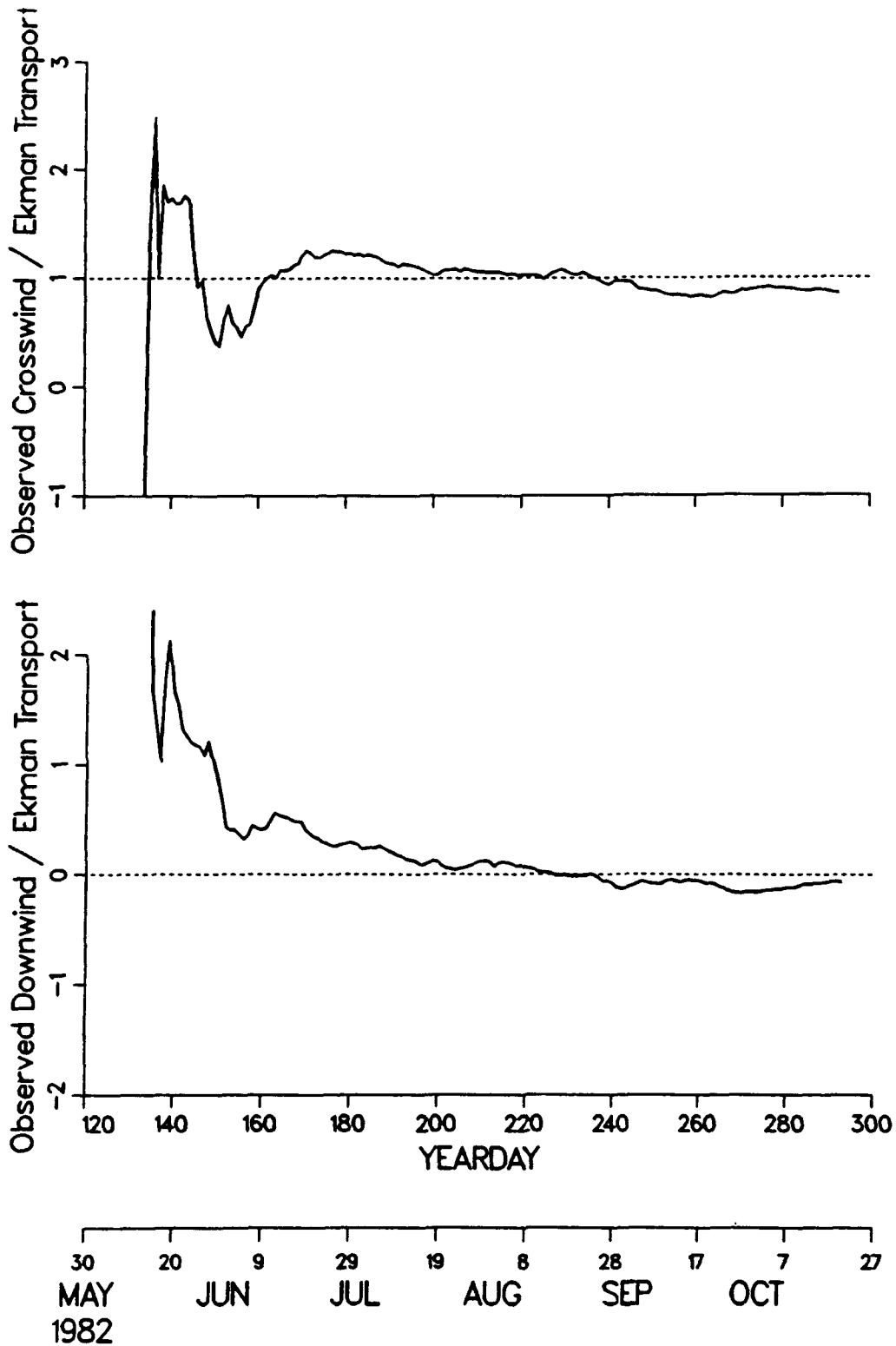


FIGURE 2.12. (a) Running average of the crosswind component of observed transport scaled by the Ekman transport. A ratio near one is attained after about 60 days. (b) Running average of the downwind component of observed transport scaled by the Ekman transport. A value near zero is attained after about 60 days.

2.5. DIURNAL VARIABILITY DURING LOTUS 3

2.5.1. *Diurnal variability of current spiral and transport*

As described in Price et al. (1987), there is a large diurnal variability in the wind-driven current. The diurnal variability cannot be seen in the ensemble average over the whole data set, but can be seen by forming separate ensemble averages over the daytime, 8 to 20 Local Solar Time (LST), and the nighttime, 20 to 8 LST (Figure 2.13). This clearly shows the large diurnal cycle in the current. The amplitude of the surface current is greatly increased in the daytime when increased current shear can be supported by the stable stratification of the diurnal thermal cycle. The shear is much reduced at night when cooling by heat loss allows wind-mixing to deepen the mixed layer well below its midday value.

The complete diurnal cycle of the current can be seen by similarly ensemble-averaging the 5-m current over 4-hour intervals throughout the day. The inertial period is just under one day at this latitude (34°N), and the diurnal cycle of the current therefore looks very similar to an inertial oscillation (Figure 2.14). During mid-afternoon when the mixed layer is shallowest the current reaches its maximum value. The diurnal cycle of the current extends all the way through the upper 50 m, as can be seen in the integrated volume transport (Figure 2.15), and further demonstrates how the diurnal thermal cycle affects the wind-driven current.

The diurnal variability in the wind-driven current is important in understanding the surface-trapping of the current. Price et al. (1987) showed that modelling the upper ocean as a uniformly accelerated "slab" layer whose depth varies throughout the day results in a mean current that is surface-trapped in the same way as the observed mean current. Wijffels and

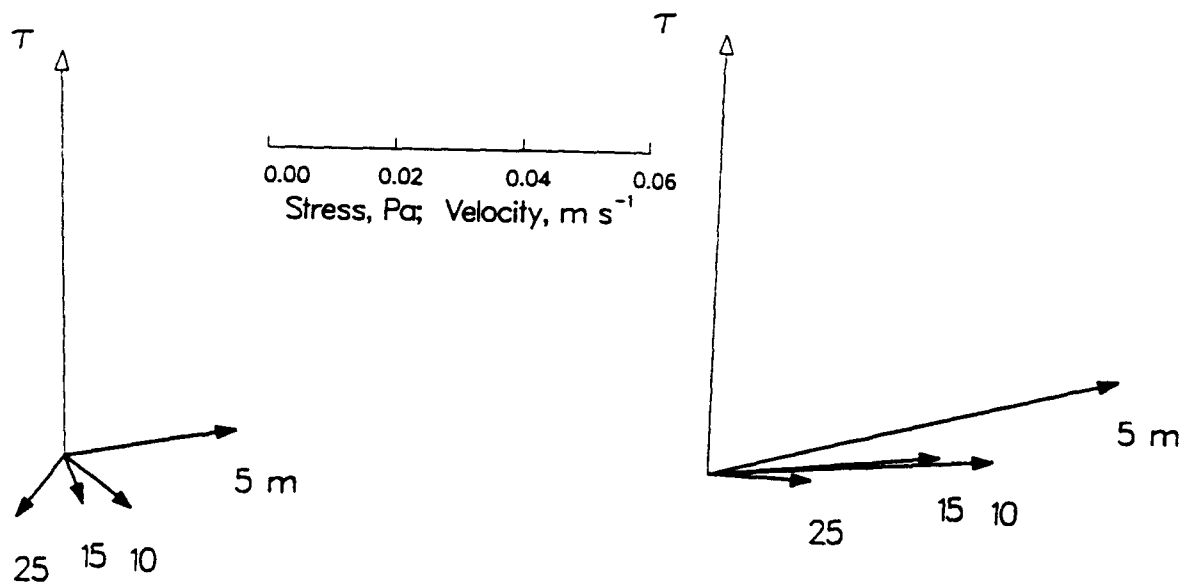


FIGURE 2.13. Diurnal cycle of the wind stress and mean current spiral (relative to 50 m). On the left is the mean current during the nighttime hours (20 to 8 LST) of the LOTUS 3 data and on the right is the mean current during the daytime hours (8 to 20 LST). Note that there is little diurnal variation in the wind stress.

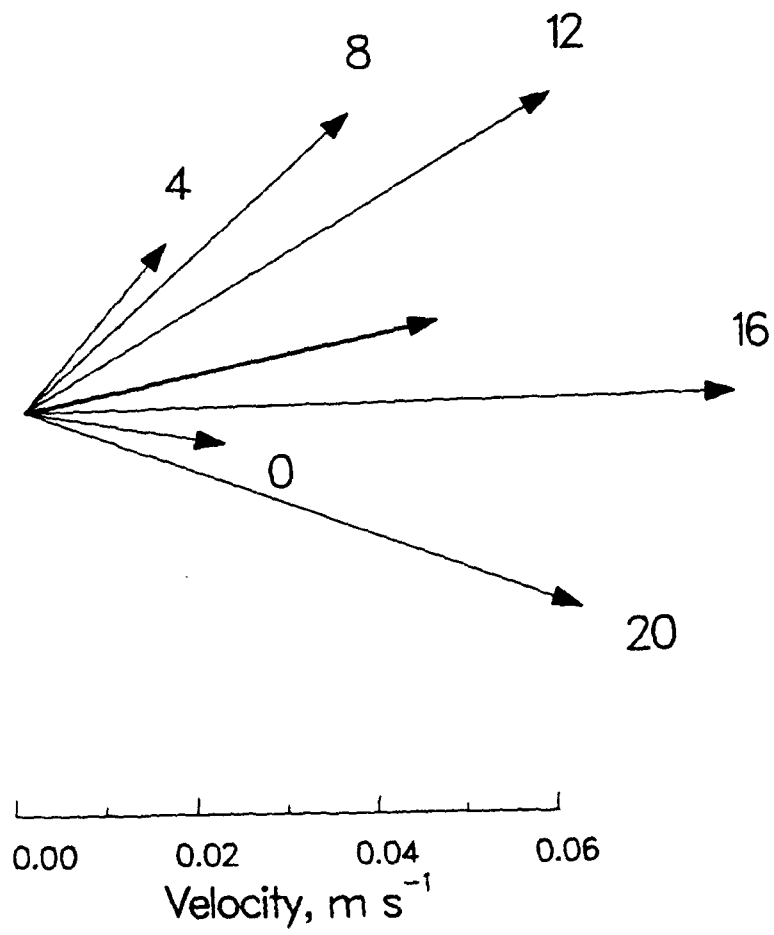


FIGURE 2.14. Diurnal cycle of the observed 5 m current (relative to 50 m). Numbers at the end of the current vectors are the hour of day, LST. The heavy vector in the middle is the mean value. The current is greatest in mid-afternoon when the mixed layer is shallowest and smallest at night when the mixed layer is deepest.

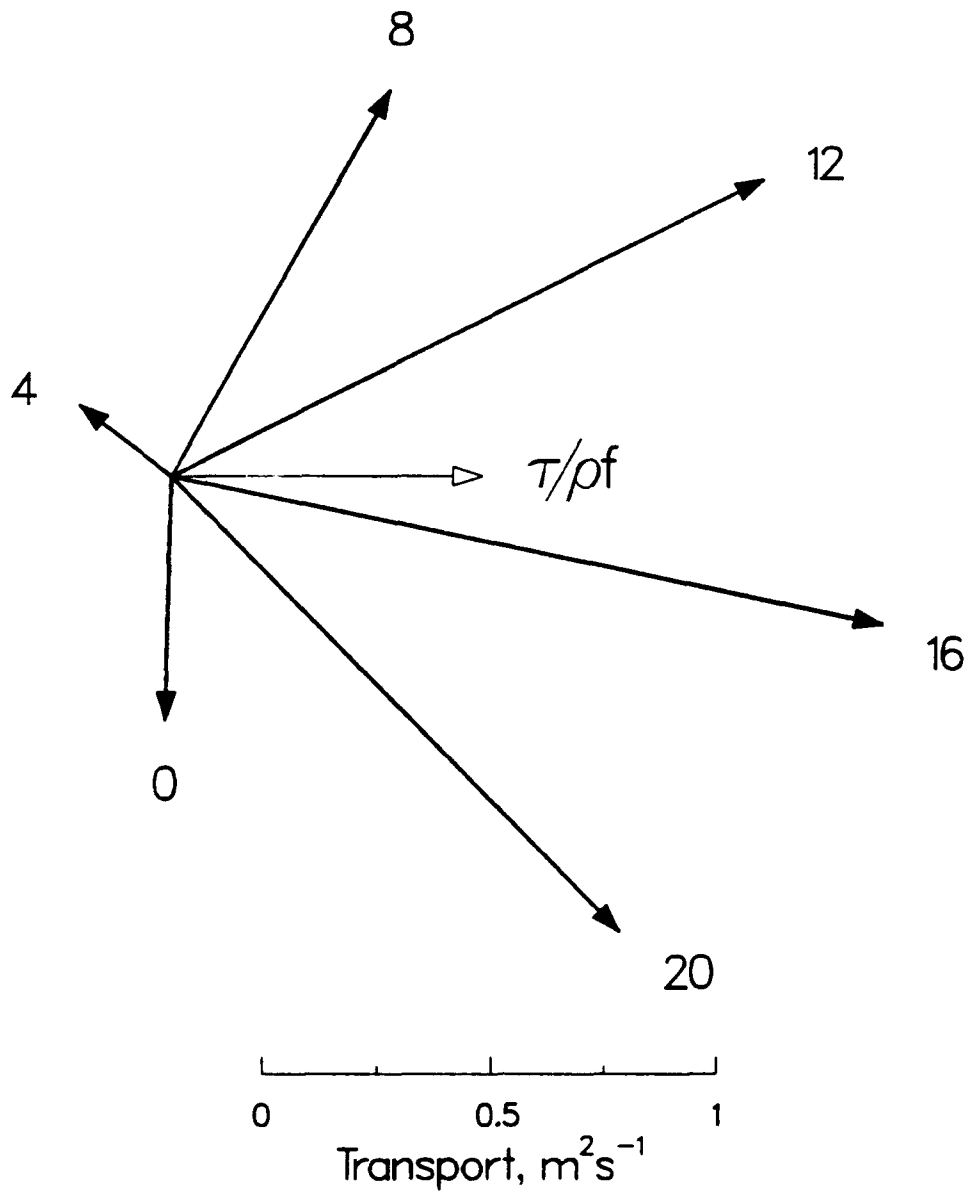


FIGURE 2.15. Diurnal cycle of the observed transport relative to 50 m. Numbers at the end of the vectors are the hour of day, LST. The light vector in the middle is the mean Ekman transport. The diurnal cycle of transport reflects the strong diurnal cycle of the currents in the upper 50 m.

Bryden (1991) have also seen uniform currents within the mixed layer after removing the geostrophic portion of the current from the total current.

2.5.2. Mean momentum balance and its diurnal variability

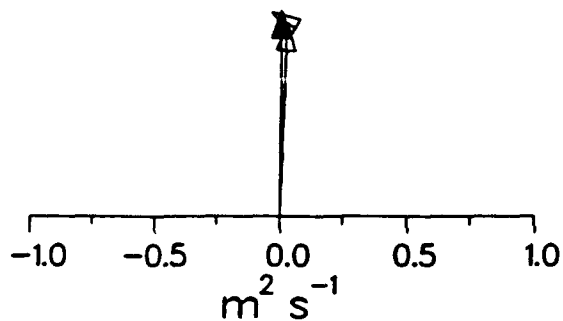
The good agreement we have found with the simple Ekman momentum balance gives us the opportunity to calculate meaningful estimates of the stress divergence in the upper ocean. Based on the simple momentum balance

$$\frac{\partial v}{\partial t} + fu = \frac{1}{\rho} \frac{\partial \tau}{\partial z} \quad (2.2)$$

the stress divergence can then be estimated from the observed mean current and acceleration. The acceleration term is calculated as the net change in velocity at each VMCM depth over each daily average, then rotated relative to the wind direction and averaged over the whole record. The Coriolis term is calculated simply as the observed mean current at each depth multiplied by the Coriolis parameter. The accuracy of this estimate of the stress divergence can be independently checked by integrating the terms on the left hand side of (2.2) and comparing their vector sum to the observed surface wind stress, τ . This comparison is essentially a check of the force balance between the Coriolis force, wind stress, and local acceleration. If the balance is exact, then the vector sum of the acceleration and the Coriolis force should equal the wind stress.

The results of this calculation reveal a mean stress divergence that decays monotonically with depth (Figure 2.16). There is significant wind stress penetration to about 15 m. The vertical structure of the stress divergence mirrors the structure of the mean current (see Figure 2.8), reflecting once more that the mean current is in Ekman balance,

FORCE BALANCE



STRESS DIVERGENCE

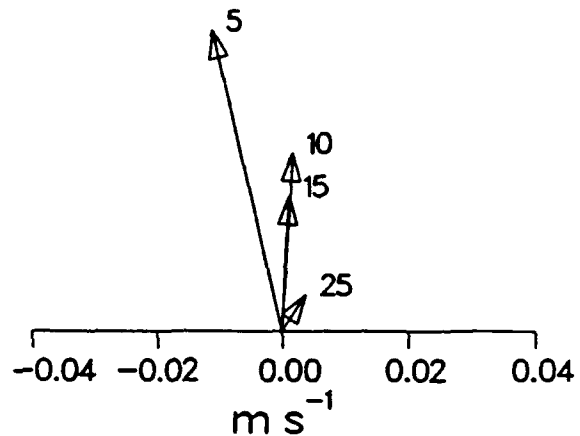


FIGURE 2.16. Mean force balance and stress divergence. The mean wind direction is "up". The estimated mean stress divergence, calculated from the observed current as described in the text, is shown on the right. Number at the tips of the vectors indicate the depth in meters. The mean wind stress vector is shown on the left with a solid arrowhead. The Coriolis force vector has an open arrowhead and is plotted with the same origin as the wind stress; the acceleration vector is also shown with an open arrowhead but is plotted with its tail at the tip of the Coriolis vector. The small net acceleration reflects the close agreement with the Ekman balance in the LOTUS 3 observations. The nearly exact force balance confirms that the estimated stress divergence is robust.

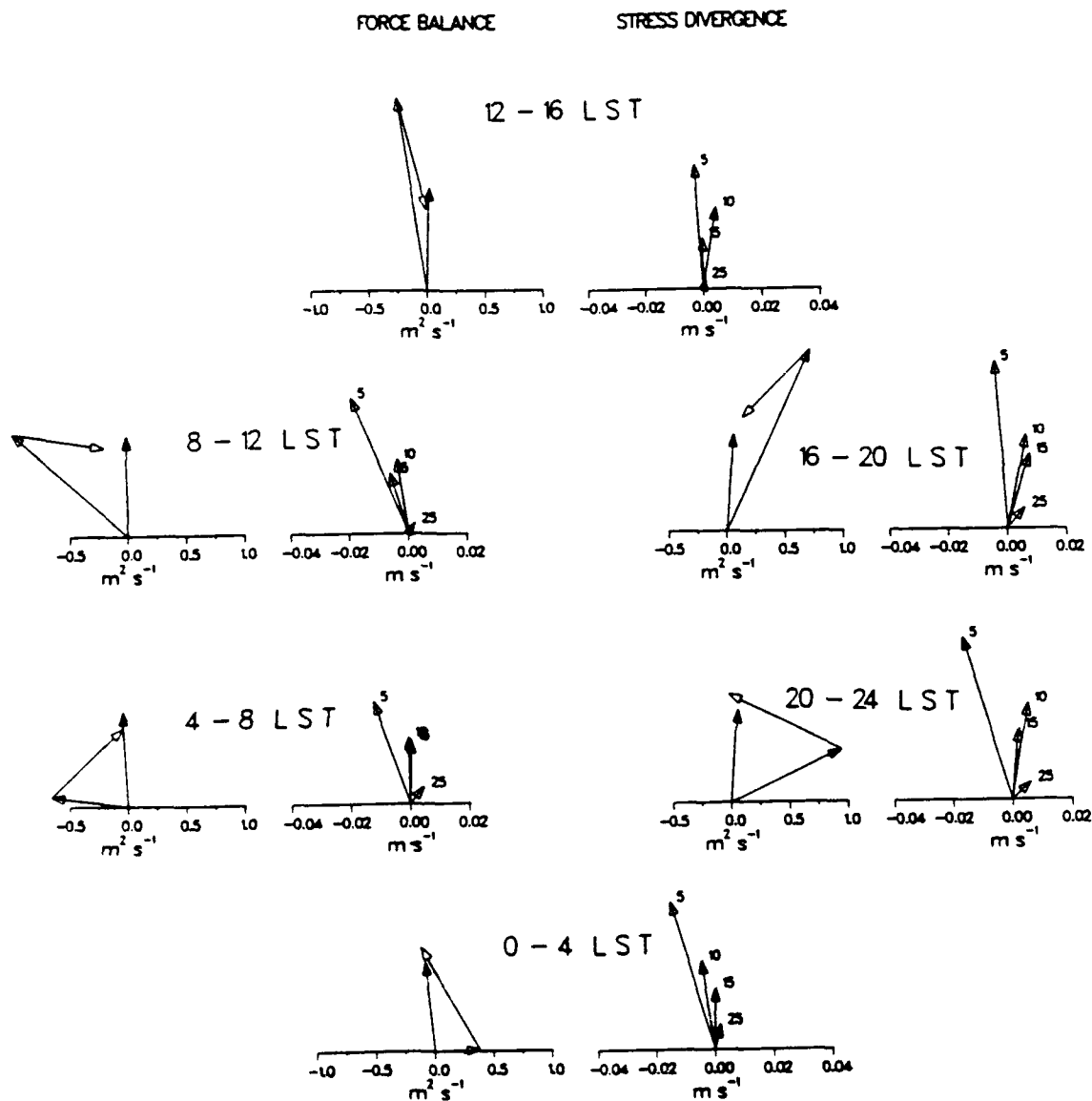


FIGURE 2.17. The diurnal progression of the force balance and stress divergence. The mean wind direction is "up". Numbers at the tips of the stress divergence vectors indicate the depth in meters. In the force balance plots, the wind stress vectors are shown with a solid arrowhead, the Coriolis force vector is shown with an open arrowhead and is plotted with the same origin as the wind stress. The acceleration vector is also shown with an open arrowhead but is plotted with its tail at the tip of the Coriolis vector, showing how the acceleration turns this vector throughout the 4-hour interval.

as does the fact that the net acceleration is very small (Figure 2.16). The mean force balance is almost exact (Figure 2.16), and confirms that this estimate of the stress divergence is robust.

We can see the diurnal progression of the force balance that drives the diurnal cycle of the mean current if we split the calculated momentum balance into four-hour intervals throughout the day and then average over the entire record (just as we did to show the diurnal variation of the mean current). The wind stress vector has very little diurnal variation (Figure 2.17) and remains almost constant. The stress divergence also has little diurnal variation. The force balance is surprisingly close to being exact throughout the day, despite a very large diurnal variation as the current rotates through its diurnal oscillation.

2.6 NUMERICAL SIMULATION OF THE MEAN CURRENT AND ITS DIURNAL VARIABILITY

The structure of the observed mean current and its diurnal variability can be successfully modelled using the simple one-dimensional model of Price et al. (1986). This model includes the important effect of diurnal stratification on upper ocean currents. The LOTUS 3 period was simulated using an observed initial stratification and integrating the model over 160 days with observed wind stress and surface heat fluxes. The simulated current was then averaged relative to the wind direction as described in Section 2.2 (though it is not necessary to subtract a reference current because there is no geostrophic flow in the model).

The simulated mean current is quite similar to the observed mean spiral, e-folding over a depth of about 12 m (Figure 2.18). The overall shape and diurnal variation of the mean current are also reproduced quite well by the model, suggesting that the model

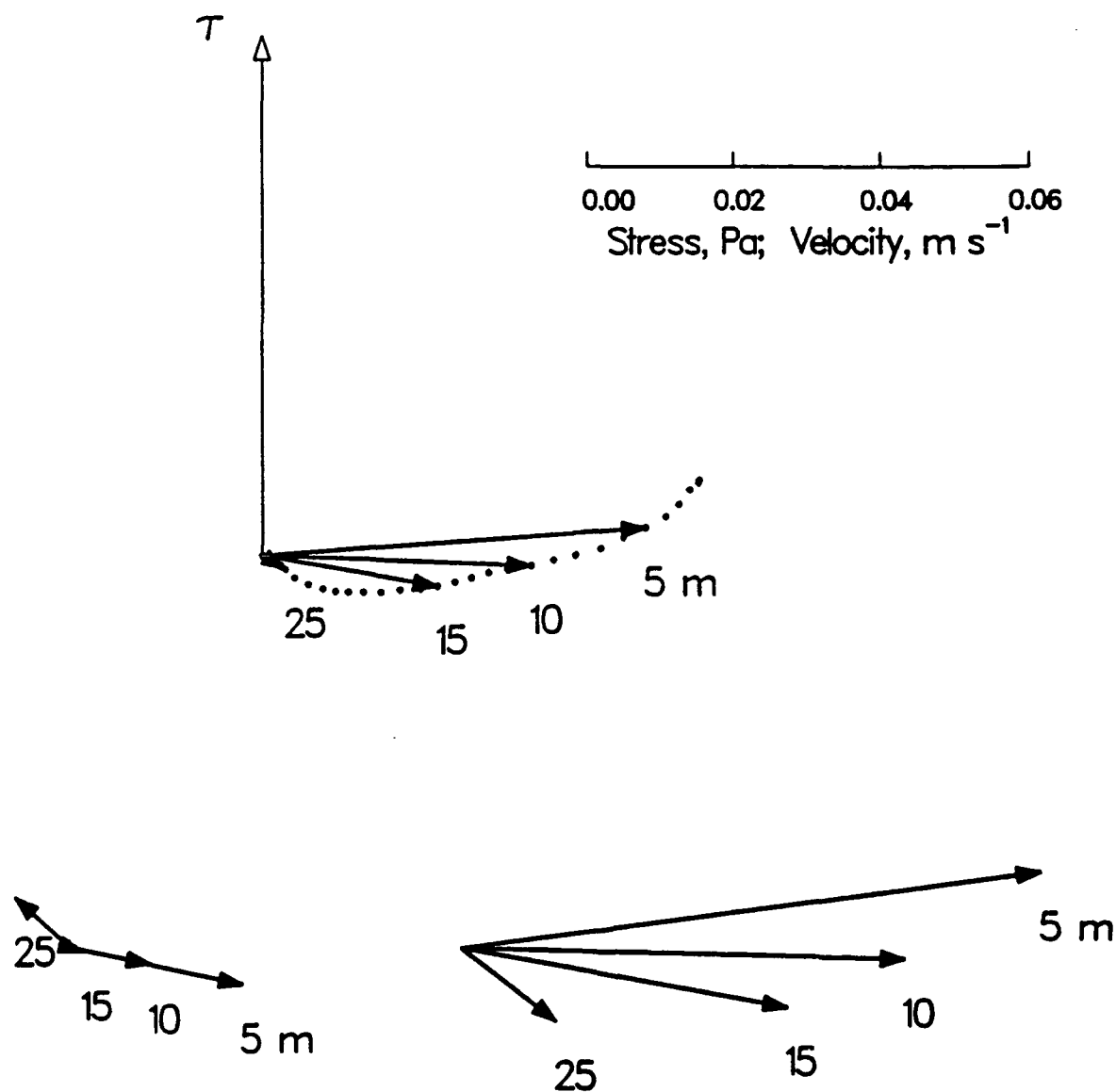


FIGURE 2.18. Numerical simulation of the LOTUS 3 mean current spiral and its diurnal variability. The mean is shown in the upper plot; the vectors correspond to the VMCM depths during LOTUS 3, and the dots are at 1-m intervals. The mean simulated transport (not shown) is exactly equal to the Ekman transport. At the lower left is the mean simulated current during the nighttime hours (20 to 8 LST), and at the lower right is the mean during the daytime hours (8 to 20 LST). The model reproduces the overall shape and depth of the mean current spiral (Figure 2.6) and its diurnal variability (Figure 2.11).

accurately simulates the effect of wind stress and solar heating on the depth of the surface mixed layer and on the vertical structure of the wind-driven current.

Price et al. (1987) used this model to predict how the mean current spiral would vary with wind stress, heating, and latitude when the diurnal cycle controls the upper ocean stratification. In the next chapter we will discuss the wintertime portion of the LOTUS observations (LOTUS 4), when the diurnal cycle is not a controlling factor.

2.7 SUMMARY AND CONCLUSIONS

Despite a small signal-to-noise ratio at the LOTUS site, the upper ocean shows a long-term mean Ekman balance. During the fair weather, summertime conditions of LOTUS 3, net heating and light winds lead to a shallow seasonal stratification and an Ekman layer that penetrates to about 50 m, e-folding in 12 m. Diurnal cycling produces a mean current with a spiral-shaped structure that is closely coupled to the mean stratification. The wind-driven transport is given by the classical Ekman relation.

Averaging in a wind-relative way isolates the wind-driven signal from the eddy-like currents that dominate the LOTUS observations. The success in this case is due to several factors: a high-quality, long-term data set with sufficient vertical resolution to capture the very surface-trapped wind-driven current, as well as a wind variation that was very different than the mesoscale current variation. Wijffels and Bryden (1991) and Weller et al. (1991) have looked at currents in a wind-relative reference frame and have also found improved agreement with Ekman theory, even over much shorter records and at lower latitudes, where the inertial period is greater than 2 days (Wijffels and Bryden, 1991).

Chapter 3

Observations of the Ekman Balance in Winter Conditions

In this chapter, the analysis of the LOTUS observations begun in Chapter 2 is continued into the first winter of the LOTUS experiment (the LOTUS 4 period), and we describe the observed long term balances seen during winter conditions. In Section 3.1 we discuss how the wind-relative averaging method introduced in Chapter 2 was applied to the winter LOTUS data. The resulting mean current spiral and transport are discussed in Section 3.2. In Section 3.3 we analyze a numerical simulation of the mean current, and in Section 3.4 we estimate the effect of surface waves on the measured current. A concluding summary is given in Section 3.5.

3.1. APPLYING THE WIND-RELATIVE METHOD TO LOTUS 4

3.1.1. Choice of reference level

As we discussed in Chapter 2, the LOTUS 4 period was dominated by winter conditions (strong winds and net surface heat loss), and the seasonal thermocline created during the previous summer (LOTUS 3) continually eroded throughout LOTUS 4 (see Figure 2.3). To choose an appropriate reference level for our calculations we estimated the mixed layer depth during this period just as we did for the LOTUS 3 period. The mixed layer depth is quite variable but is never deeper than 100 m during the period from November 1 to February 19 (see Figure 3.1). In this sense, a reference level of 100 m would have been desirable, and consistent with our choice of 50 m during the LOTUS 3 period. However the VMCM positioned at 100 m failed after only a few days (as we discuss in the next section), so to capture the full wind-driven signal we used a reference level at the next

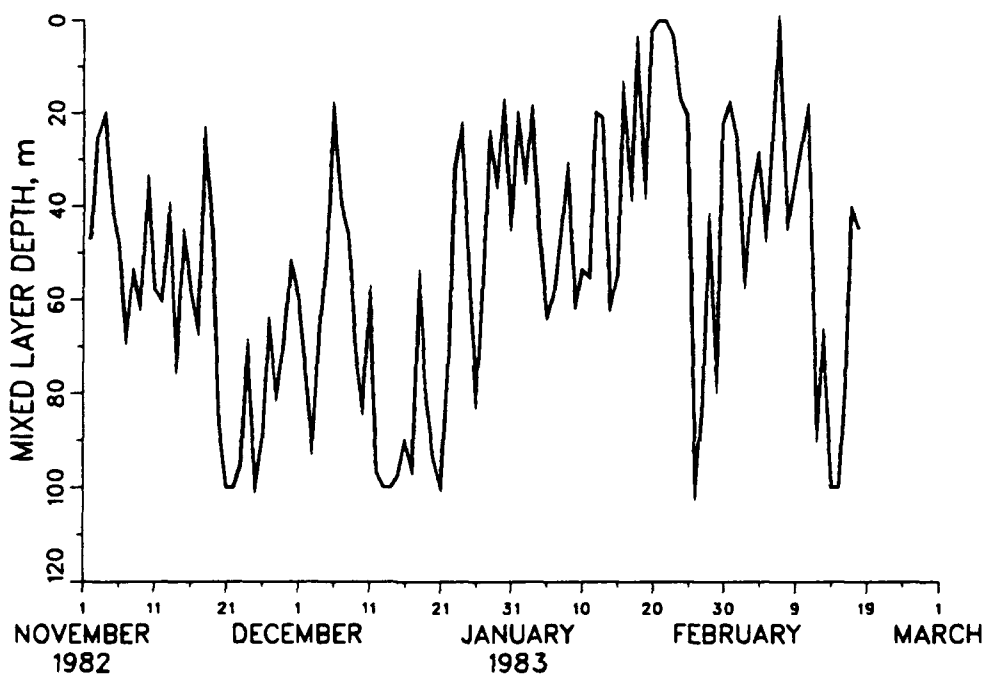


FIGURE 3.1. Mixed layer depth during the LOTUS 4 period estimated at 15-minute intervals using a temperature difference of 0.05°C from the surface, then averaged over one day. The mixed layer depth is quite variable but is never deeper than 100 m during the period from November 1 to February 19.

deepest VMCM, which was at a depth of 129 m on the adjacent sub-surface mooring 766, 7.9 km NNW of mooring 770 (Figure 3.2). (The next deepest current meter on surface mooring 770 was an Aanderaa current meter at 150 m, see Figure 2.2. We chose not to use this current meter because Aanderaa current meters do not give reliable measurements of current from surface moorings (Weller and Davis, 1980).) The sensitivity of our results to this choice of a reference level is examined in Section 3.2.2.

3.1.2 Data quality

The LOTUS 4 period extended from October 31, 1982 to February 19, 1983, spanning 109 days. Currents and temperature were measured from surface mooring 770 during this period at depths of 5, 10, 15, 25, 50, 75, and 100 m by VMCMs, with the exception of the current at 15 m, which was measured by a vector-averaging current meter (VACM), see Figure 2.2. Unfortunately, the VMCM at 100 m depth on mooring 770 failed after only 8 days, so we have temperature but practically no current measurements at 100 m for LOTUS 4. This is part of the reason we chose to reference the currents to the 129 m current measurements from mooring 766. Because the shortness of the 100 m record results in a statistically insignificant mean current, we exclude the 100 m current from our calculations.

The 75 m VMCM failed after 50 days on December 21, and the 25 m VMCM failed after 99 days on February 8. We treated these records in the same way as the failed 5 m VMCM in LOTUS 3 (i.e. the average current at 75 m is a 50-day mean and at 25 m it is a 99-day mean, and at all other depths the mean currents are 109-day averages).

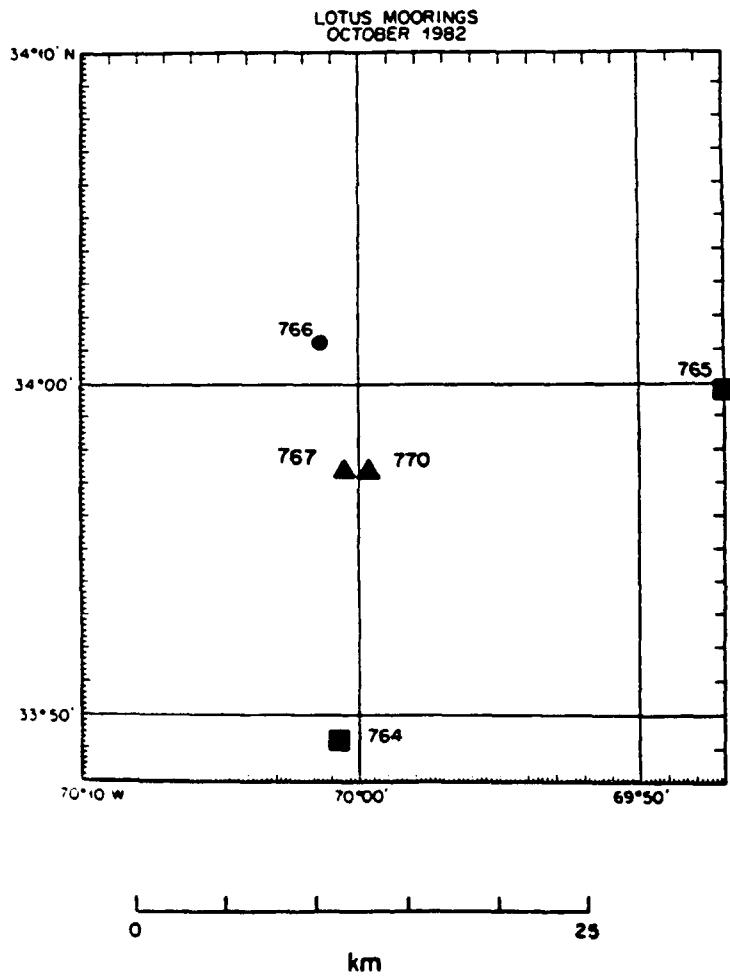


FIGURE 3.2. Positions of the LOTUS moorings shown in Figure 2.2. We use currents measured by VMCMs on moorings 767 and 770 for our analysis of the LOTUS 4 observations.

3.2. WINTERTIME MEAN CURRENT SPIRAL AND TRANSPORT

3.2.1. Mean spiral and transport

The mean current profile for the LOTUS 4 period is found by referencing currents to 129 m and averaging relative to the wind direction as described in Chapter 2. The mean wind stress during the LOTUS 4 period was a fairly strong 0.147 Pa, about twice the LOTUS 3 mean value. The mean current at the seven depths above 129 m and the resulting transport are shown in Figure 3.3 (notice that this figure is plotted on a different scale than the mean spiral for LOTUS 3 shown in Figure 2.8). Numerical values for the mean velocity at each depth and their uncertainties (as standard errors) are listed in Table 3.1. The mean currents at 50 m and above are thus fairly well defined, but the 75 m and 100 m values are not distinguishable from zero.

The mean wind-driven current profile is qualitatively very different from the LOTUS 3 spiral, spread over a greater vertical scale. In a sense, the LOTUS 4 mean spiral looks more like a classic Ekman spiral than the LOTUS 3 current spiral. The current at 5 m has an amplitude of about 7 cm s^{-1} , and is about 43° to the right of the wind. The mean current decays rapidly with depth, e-folding over about a 25 m scale. The current rotates about 36° over the e-folding depth. The resulting eddy viscosities are thus $250 \times 10^{-4} \text{ m}^2\text{s}^{-1}$ for shear and $650 \times 10^{-4} \text{ m}^2\text{s}^{-1}$ for rotation, substantially larger than those inferred from the LOTUS 3 mean spiral.

The shear in the mean current profile has a very different character than the LOTUS 3 spiral. The shear is almost entirely in the direction of the wind (downwind) in the upper 15 m, and almost entirely perpendicular to the wind below this depth. Below 15 m, the shear looks qualitatively like the LOTUS 3 spiral (see Figure 2.8). The downwind shear in

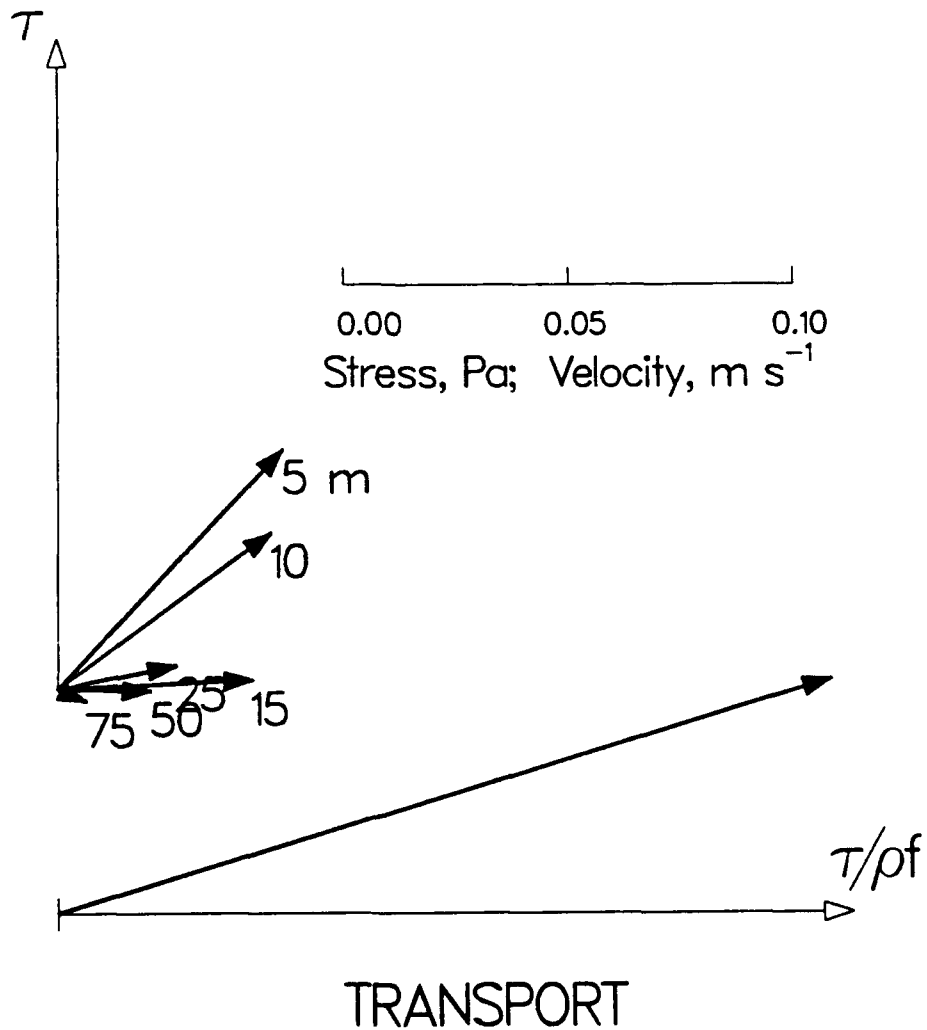


FIGURE 3.3. Mean current spiral and transport during the LOTUS 4 period. Uncertainties are given in Tables 3.1 and 3.2. The current spiral has a large downwind shear in the upper 15 m, and the shear abruptly changes to the crosswind direction below 15 m. The observed transport agrees with the predicted Ekman transport except for the large downwind component. As described in the text, the 75-m current is a 50-day average, the 25 m current is a 99-day average, and all other currents are 109-day averages.

TABLE 3.1.

Mean current and uncertainties during the LOTUS 4 period. Uncertainties on the data are statistical standard errors; 90% confidence limits are larger by a factor of 1.7, and 95% confidence limits are larger by a factor of 2.0.

DEPTH (m)	CROSSWIND CURRENT (cm s ⁻¹)	DOWNWIND CURRENT (cm s ⁻¹)
5	5.0 ± 1.8	5.4 ± 1.5
10	4.7 ± 1.7	3.5 ± 1.5
15	4.3 ± 1.8	0.2 ± 1.5
25	2.6 ± 1.5	0.5 ± 1.3
50	2.1 ± 1.5	-0.1 ± 1.4
75	0.7 ± 1.2	-0.3 ± 1.0
100	-1.4 ± 1.3	-0.5 ± 0.8
129*		

* The 129-m depth was chosen as the reference level, where the simple time-mean current was 1.8 cm s⁻¹ westward and 4.4 cm s⁻¹ northward.

TABLE 3.2.

Mean transport and errors during LOTUS 4. The Ekman transport was computed using the mean wind stress magnitude of 0.147 Pa, which is presumed to be uncertain to 20% because of uncertainty inherent in the bulk aerodynamic method (Large and Pond, 1981); the standard error for the Ekman transport estimate (based on 109 daily estimates over the LOTUS 4 record) is ± 0.21 m²s⁻¹.

	CROSSWIND TRANSPORT (m ² s ⁻¹)	DOWNWIND TRANSPORT (m ² s ⁻¹)
OBSERVED	1.71 ± 1.21	0.65 ± 1.03
EKMAN	1.76 ± 20%	0

the upper 15 m is a puzzling feature of the wintertime observations, since no such downwind shear was observed during the summertime portion of the observations. Richman et al. (1987) have also observed a strong downwind shear in the upper 9 m of the water column in the Pacific ocean under conditions of moderately strong wind stress (0.145 Pa). We will examine the near-surface downwind shear during LOTUS 4 in more detail in Section 3.4.

While the winter current spiral may appear more Ekman-like than the summer, the observed transport does not agree as well with the Ekman balance. The downwind shear in the upper 15 m of the mean current profile causes a downwind component of transport, see Figure 3.3 and Table 3.2. Without the downwind component there would be good agreement with the theoretical Ekman transport as was found for the summertime portion of the LOTUS observations.

3.2.2. Sensitivity to reference level

The chosen reference level of 129 m was the only reasonable choice deeper than 50 m for the LOTUS 4 data set, since the VMCMs at 75 and 100 m failed after 50 and 8 days, respectively, of the 109-day long record. There were no other VMCMs on any of the LOTUS 4 moorings other than the one at 2500 m (see Figure 2.2), and the next deeper current meter was a VACM at a depth of 178 m on mooring 766, which certainly would have been too deep in the water column based on our estimates of mixed layer depth during the LOTUS 4 period (Figure 3.1).

As we discussed in Chapter 2 for the LOTUS 3 case, the observed volume transport varies quite a bit with the choice of a reference level. If we had referenced the currents to any of

the current meters shallower than 100 m, the observed transport becomes a successively smaller fraction of the predicted Ekman transport (Table 3.3).

TABLE 3.3.
Observed transport and standard errors during the LOTUS 4 period for different reference levels. The Ekman transport is $1.76 \text{ m}^2\text{s}^{-1}$.

REFERENCE LEVEL (m)	CROSSWIND TRANSPORT (m^2s^{-1})	DOWNWIND TRANSPORT (m^2s^{-1})
15	0.07 ± 0.60	0.03 ± 0.06
25	0.41 ± 0.53	0.16 ± 0.15
50	0.62 ± 0.75	0.25 ± 0.19
75*	0.99 ± 0.48	0.76 ± 0.38
100**	2.96 ± 1.62	0.84 ± 1.09
129	1.71 ± 0.52	0.67 ± 1.03

* The VMCM at 75 m failed after 50 days so this estimate of observed transport is a 50-day average. The mean wind stress during this period was 0.140 Pa and the predicted Ekman transport was then $1.68 \text{ m}^2\text{s}^{-1}$.

** The VMCM at 100 m failed after only 8 days. The mean wind stress during this period was 0.137 Pa and the predicted Ekman transport was then $1.64 \text{ m}^2\text{s}^{-1}$.

3.2.3. Sensitivity to record length

The LOTUS 4 period was shorter than the LOTUS 3 period (109 vs. 160 days), and the variability in the wind-driven signal was more energetic. The mean currents and transport for the LOTUS 4 period are therefore less well-defined than they were for the LOTUS 3

data set. There is more scatter in the daily estimates of transport (Figure 3.4), and the average crosswind transport begins to approach the predicted Ekman transport only at the end of the 109-day record (Figure 3.5). The downwind component of observed transport remains positive (in the same direction as the wind) throughout the last 80 days of the record.

3.2.4. Diurnal variability of the current spiral

There is very little diurnal variability in the LOTUS 4 mean current spiral (Figure 3.6), in marked contrast to the large diurnal variation that was seen in the summertime (see Figure 2.11). This is consistent with the reduced diurnal cycle of stratification that is expected for increased wind and decreased surface heating that occur in the wintertime. The structure of the LOTUS 4 mean current spiral is characterized by a persistent downwind shear in the upper 15 m that has almost no diurnal variation, and which we explore in more detail in Section 3.4.

3.3. NUMERICAL SIMULATION OF THE LOTUS 4 MEAN CURRENT

To see if the mean current spiral is governed by the locally forced thermal stratification we simulate the mean current with the mixed layer model of Price et al. (1986). This model was quite successful in simulating the observed LOTUS 3 mean current structure and its large diurnal variability (Price et al., 1987). The LOTUS 4 period was simulated by integrating the model over 109 days with observed wind stress and surface heat fluxes. The simulated current was then averaged in a wind-relative way just as the observed currents were (though it is not necessary to subtract a reference current).

LOTUS 4 and EKMAN TRANSPORT

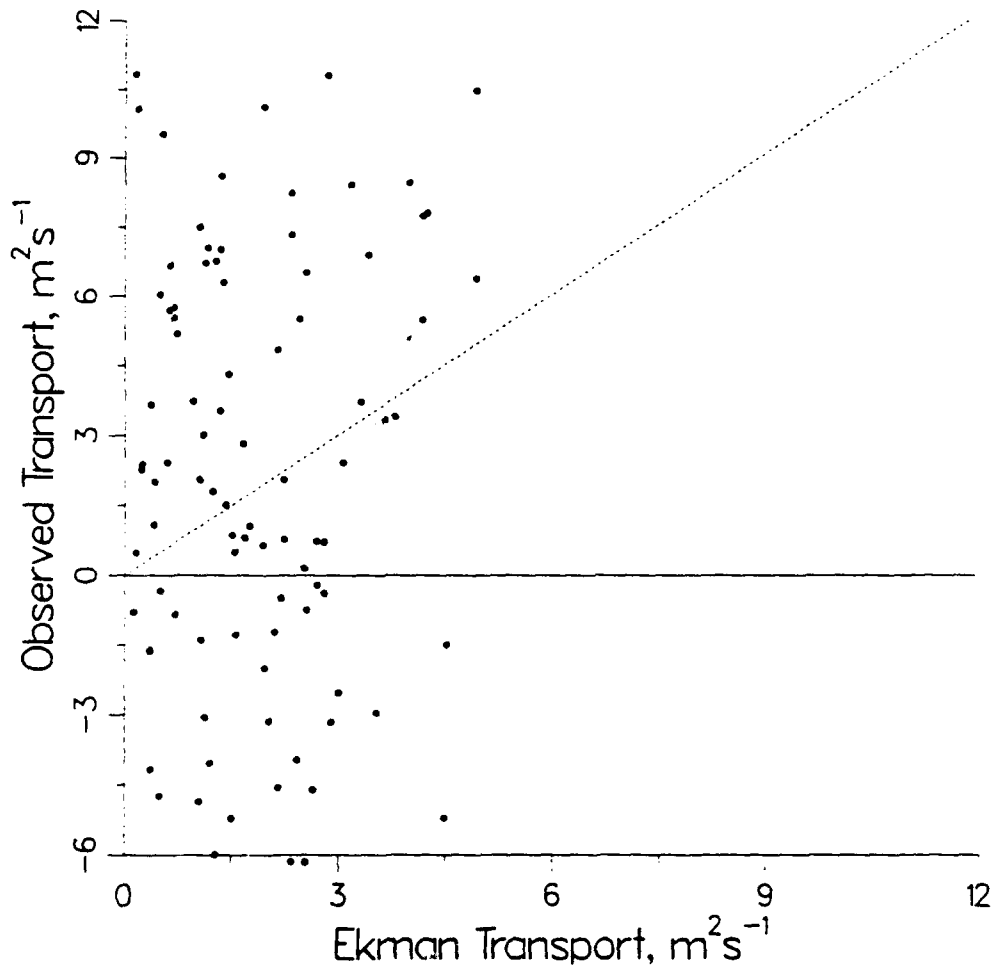


FIGURE 3.4. Crosswind component of observed transport relative to 129 m vs. the predicted Ekman transport for each of the 109 days in the LOTUS 4 period. The dashed line has a slope of one; if all days agreed exactly with the Ekman transport, all the points would lie along this line.

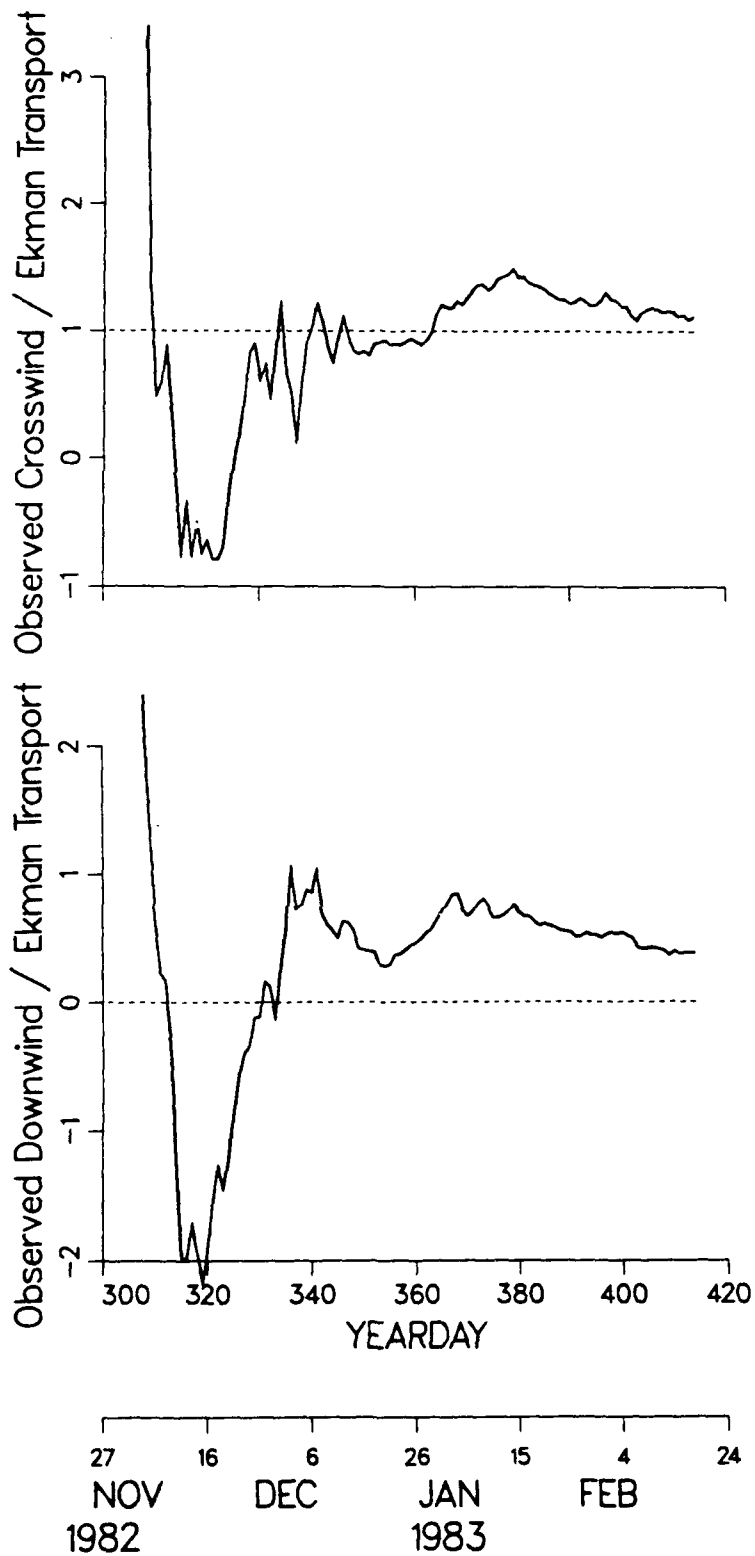


FIGURE 3.5. (a) Running average of the ratio of observed crosswind transport to Ekman transport during the LOTUS 4 period. A ratio near 1 is attained only near the end of the 109-day record. (b) Running average of the ratio of observed downwind transport to Ekman transport. A value of zero is never obtained, and the ratio remains greater than zero.

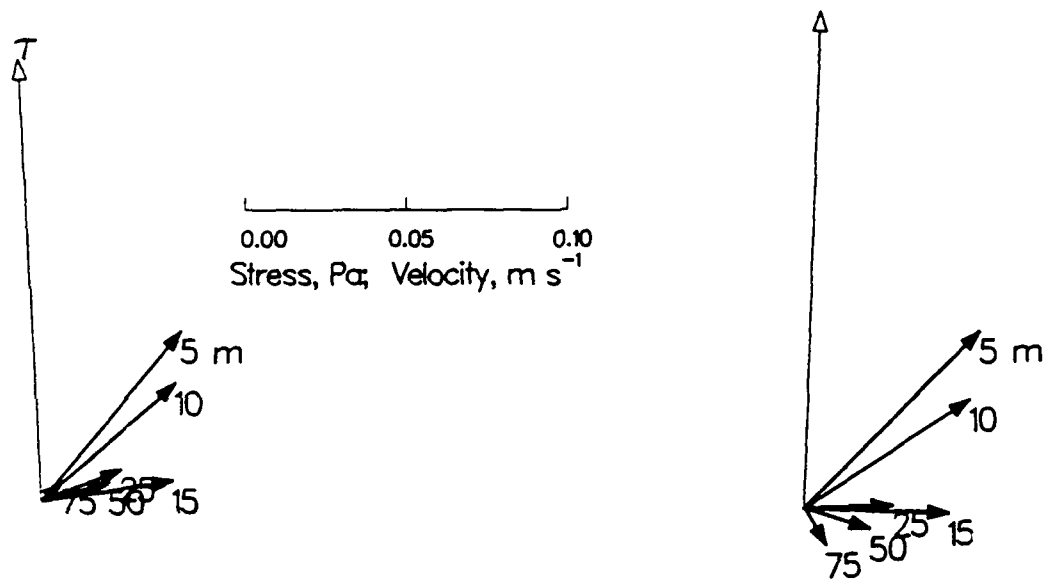


FIGURE 3.6. Diurnal variation of the wind stress and mean current spiral during the LOTUS 4 period. On the left is the mean current during the nighttime hours (20 to 8 LST) and on the right is the mean current during the daytime hours (8 to 20 LST). Note the lack of a diurnal variation and the persistent downwind shear in the upper 15 m.

The simulated mean current is somewhat similar to the observed mean current although it does not predict as much downwind shear in the upper 15 m as was observed (see Figure 3.7 and Table 3.4). The downwind shear in the observed mean current remains a mysterious aspect of the LOTUS 4 observations that will be explored in the following section. The most significant results of the simulation are that a) below 15 m the simulated mean currents are quite close to the observed means (compare Tables 3.1 and 3.4), and b) the model also predicts a similar depth scale of the mean current, with very small currents below 50 m and essentially vanishing currents at about 100 m.

The change in heat content in the model, which is due to surface heat fluxes alone, is quite close to the observed change in heat content in the upper 100 m and 129 m during LOTUS 4 (Figure 3.8). This implies that horizontal advection may have played no mean role in the upper ocean heat budget during this period. It also independently confirms that a reference depth of order 100 m is appropriate for the LOTUS 4 period.

TABLE 3.4.
Simulated mean current for the LOTUS 4 period.

DEPTH (m)	CROSSWIND CURRENT (cm s ⁻¹)	DOWNWIND CURRENT (cm s ⁻¹)
5	4.3	1.3
10	4.0	0.7
15	3.5	0.4
25	3.0	0.1
50	2.2	-0.3
75	-0.3	-0.3
100	0.0	-0.2
130	0.0	-0.1

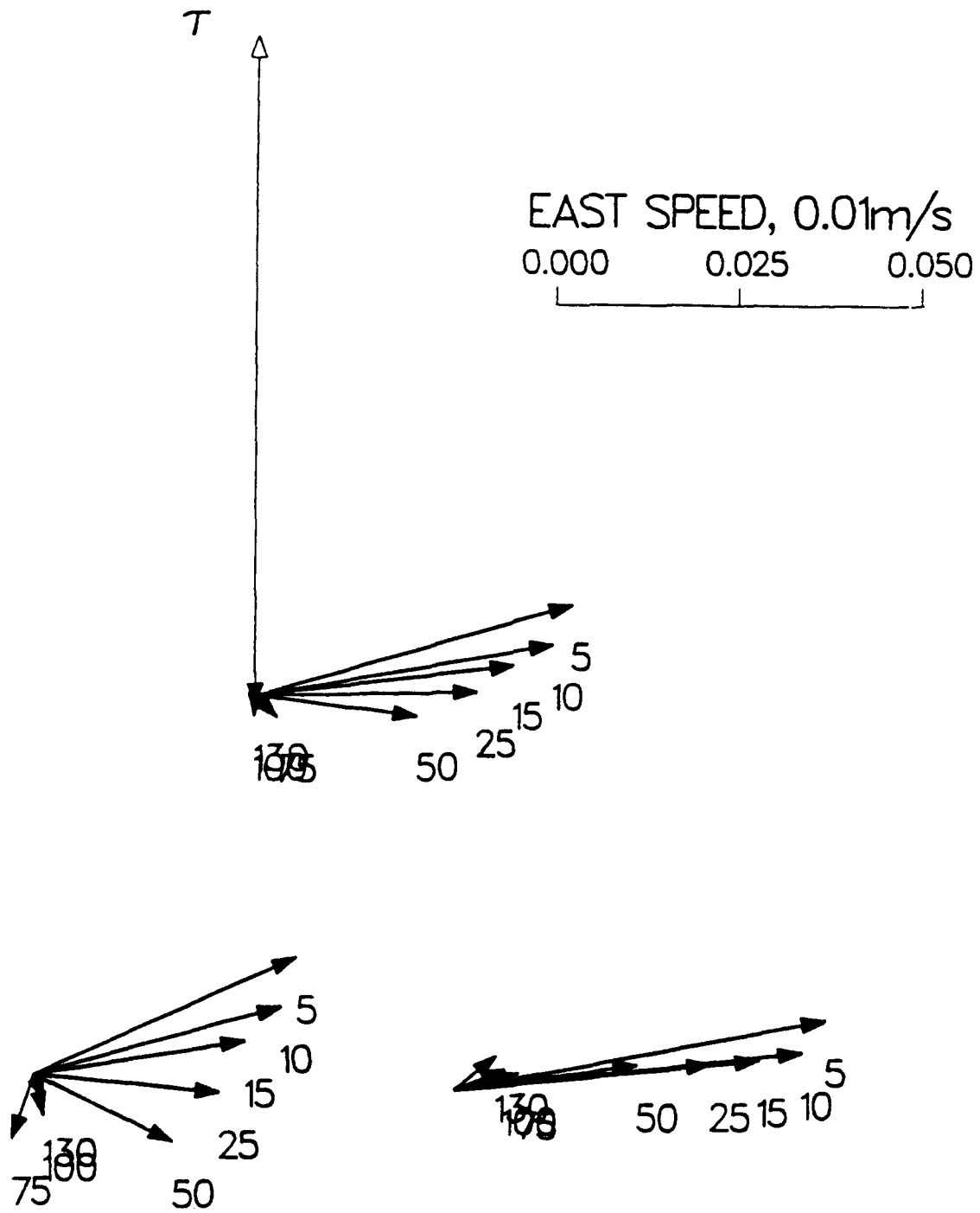


FIGURE 3.7. Simulation of the LOTUS 4 mean current spiral. Numerical values are listed in Table 3.4. The mean simulated transport (not shown) is exactly equal to the Ekman transport. The model a) shows no significant downwind shear in upper 15 m, and b) predicts that wind-driven velocities do not reach below 130 m.

At the lower left is the mean simulated current during the nighttime hours (20 to 8 LST), and at the lower right is the mean during the daytime hours (8 to 20 LST). There is some correspondence with the small amount diurnal variation observed below 15 m, see Figure 3.6.

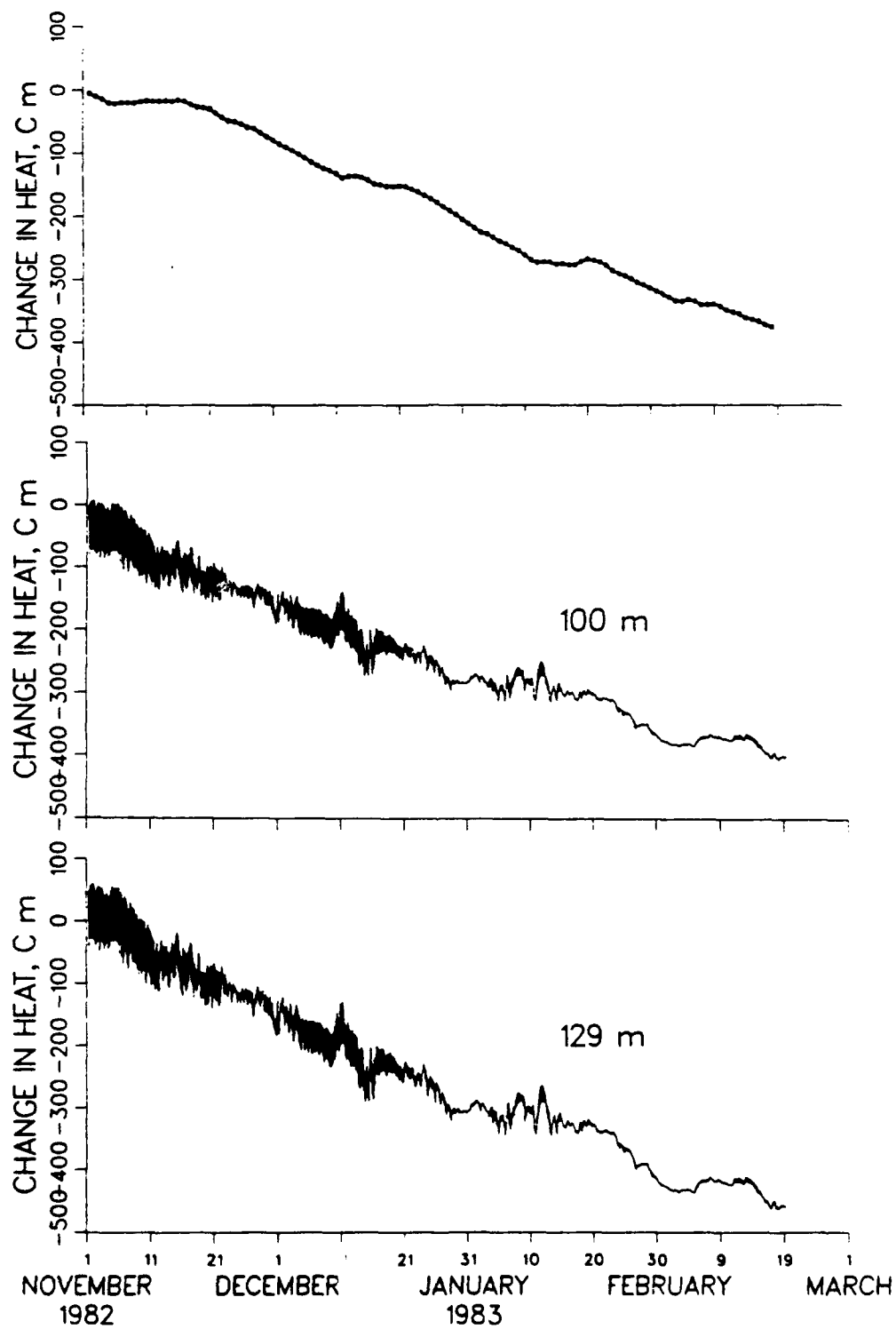


FIGURE 3.8. Simulated change in heat content based on observed heat fluxes, and observed change in heat content calculated as $\int_0^t \int_d^0 (T(z) - T(d)) dz dt$ over $t = 109$ days for $d = 100$ m and $d = 129$ m.

3.4. THE NEAR-SURFACE DOWNWIND SHEAR

Aside from the lack of diurnal variability and the deeper penetration of the mean current in the wintertime, which are both to be expected for the stronger wind and weaker heating typical of mid-latitude winters, the major difference between the summer and winter mean current spirals is the large downwind shear in the upper 15 m during the wintertime. This downwind shear is present not only in the mean current (Figure 3.3), but also throughout the entire LOTUS 4 time series. The shear above 15 m is generally in the same direction as the wind (Figure 3.9), despite the fact that the raw currents were dominated by large scale eddy-like motions and no wind-driven signal is apparent (Figure 3.10). The downwind shear is also consistently larger between 10 and 15 m than between 5 and 10 m; below 15 m the shear is much reduced and does not appear to be correlated to the wind (Figure 3.9).

We tried to look for evidence in the LOTUS 4 time series that would enable us to speculate on the nature of the downwind shear. Though we found the near-surface shear to be strongly correlated with the wind, there were no events that gave any clear indication of the phase relation between changes in the wind and the response of the downwind shear. This information might have allowed us to distinguish between wind-driven shear, which presumably would respond instantaneously to the wind, and surface wave processes, which would tend to lag the wind somewhat as the wave field responded to the local wind. Frustrated by this, we have turned instead to possible explanations for the *mean* downwind shear.

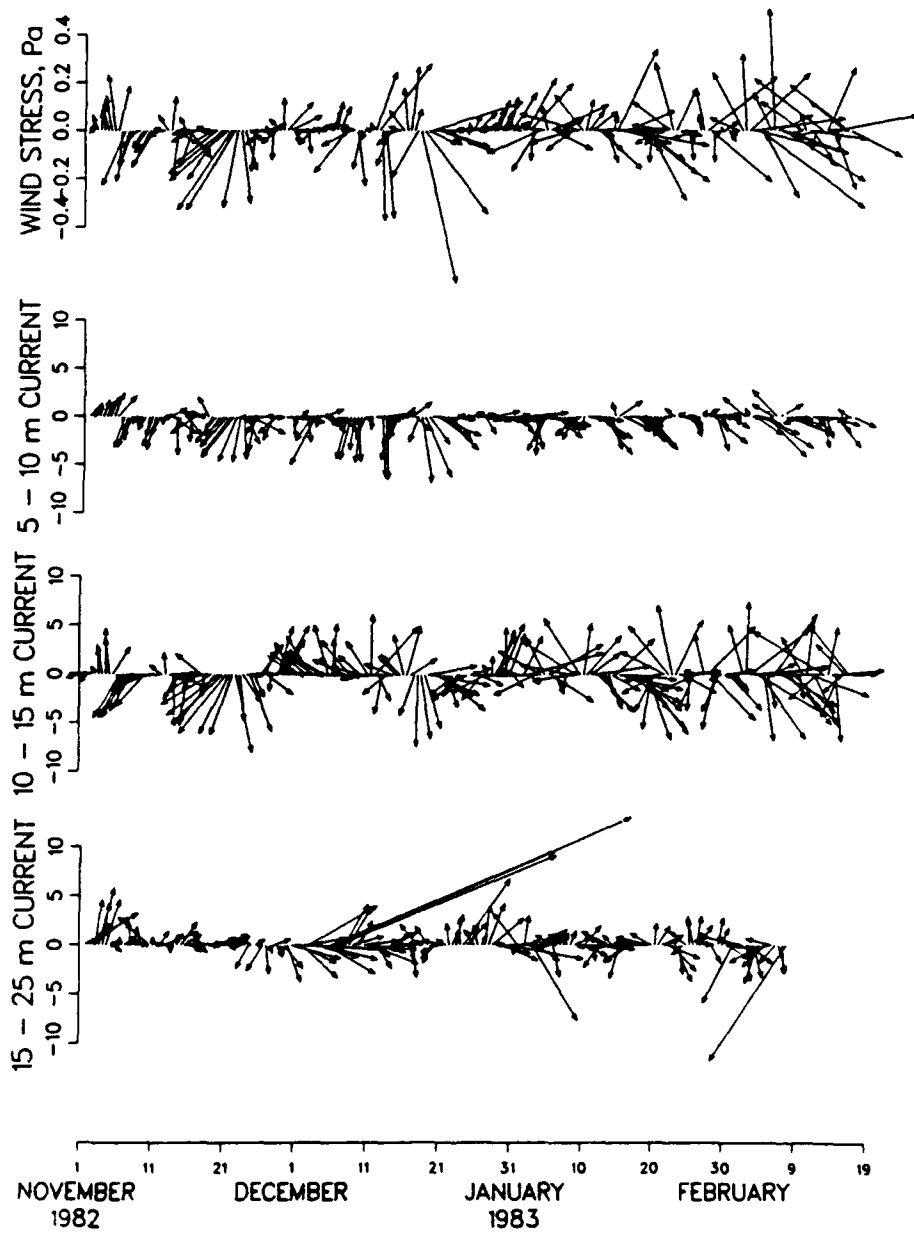


FIGURE 3.9. Wind stress and near-surface shear during LOTUS 4. North is up and east is to the right. Each vector is a 12-hour average. Note the wind-driven signal in the upper 15 m and the larger shear between 10-15 m than between 5-10 m (the current meter at 15 m depth is a VACM whereas at all other depths currents were measured by VMCMs). The shear in the upper 15 m is strongly correlated with the wind. The two large values in the 15-25 m shear during December are probably due to data dropout on the VMCM at 25 m. The VMCM at 25 m later failed on February 9.

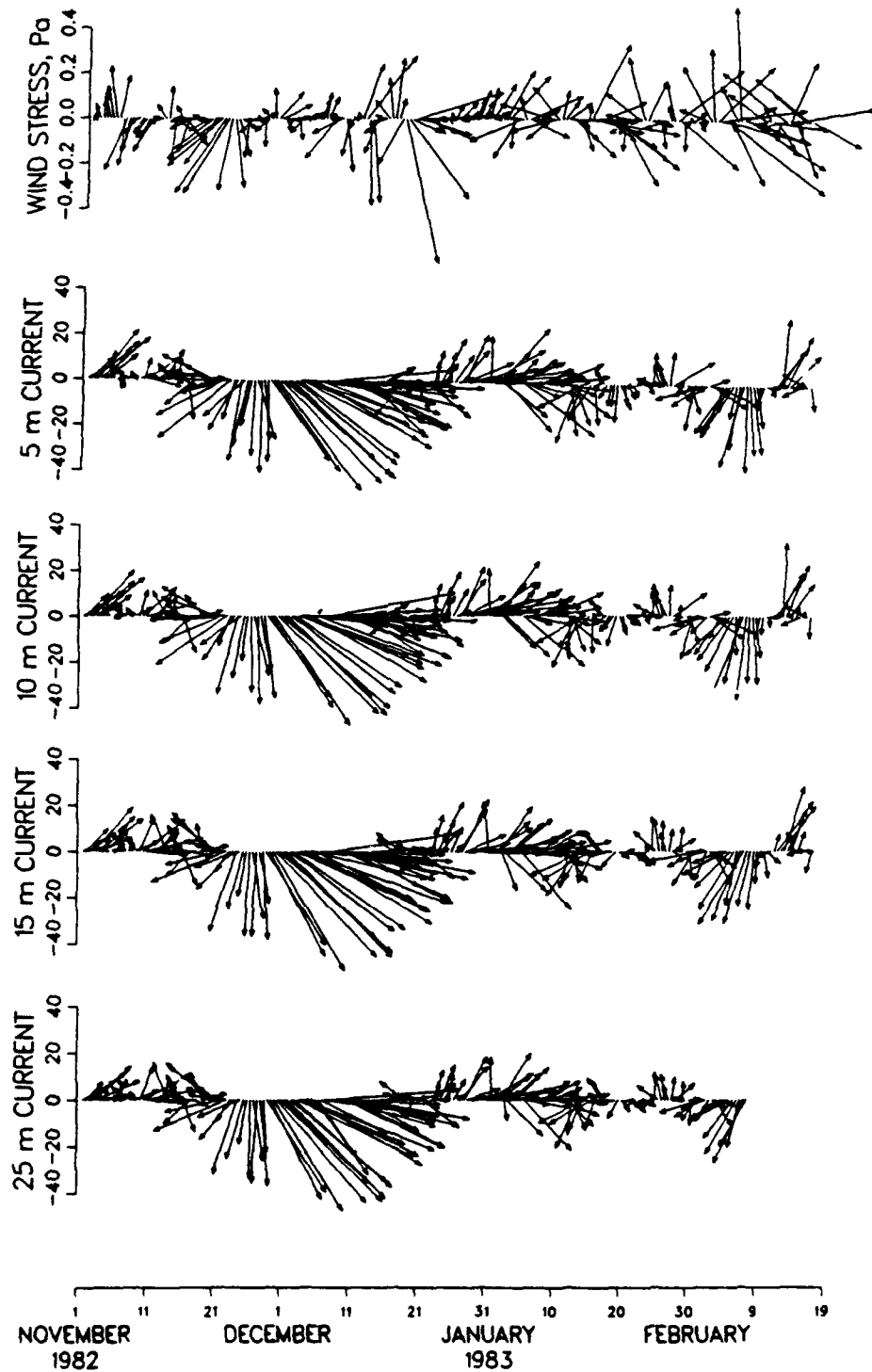


FIGURE 3.10. Wind stress and near-surface currents during LOTUS 4. North is up and east is to the right. Each vector is a 12-hour average. Note the lack of a wind-driven signal and the eddy-like character of the currents. The VMCM at 25 m failed on February 9, ten days before the end of the LOTUS 4 period.

3.4.1 Wall layer shear

The simplest model of the velocity profile near a boundary is the classic "law of the wall" logarithmic profile (see Turner, 1973). If stratification is unimportant and if there is a constant stress layer, then over distances from a solid surface that are small compared to the planetary boundary scale u_* / f , the current has a logarithmic profile $u(z) = u_* / \kappa \ln(z) + c$, where $\kappa = 0.4$ is von Karman's constant, $u_* = (\tau / \rho)^{1/2}$, and c is a constant of integration. The shear between two levels is then

$$\Delta u = u(z_1) - u(z_2) = u_* / \kappa \ln(z_2 / z_1) \quad (3.1)$$

and is in the direction of the wind stress. This model is quite appropriate for the atmospheric surface boundary layer, and logarithmic wind profiles near the earth's surface are a well-documented phenomenon (Stull, 1988). However this model vastly oversimplifies the ocean boundary layer, because the ocean surface is not a solid surface and often has large surface waves. Yet there have been observations of near-surface shear in the ocean that are consistent with wall-layer shear (Richman et al., 1987; Lentz, 1991), and the question of whether a logarithmic boundary layer exists in the ocean remains open.

3.4.2 Estimates of wave bias

Another possible explanation of near-surface downwind shear is that the motion of the LOTUS surface mooring during high seas may be biased into measurements of the current. Pollard (1973) showed that current meters whose motion is coupled to the surface suffer from a bias due to surface waves. A bias in the direction of the wave phase propagation arises because as the surface platform moves with the surface waves, the current meters suspended beneath it measure currents in different parts of the water column

relative to the mean sea level. The wave bias is dominated by short period wind waves rather than long period swell, and therefore tends to be in the direction of the local wind. The wave bias decays with depth and thus affects estimates of both the shear and the total current near the surface.

We have estimated the wave bias at each of the LOTUS current meter depths using a model developed by Santala and Terray (1990) that incorporates the mechanism described by Pollard (1973) into a directional wave spectrum. Ideally, then, both the directional wave spectrum and the current meter motion are needed to accurately estimate the wave bias. However neither of these are available for the LOTUS observations, so we estimated the wave spectrum from the wind speed after Donelan et al. (1985), assuming a duration of 12 hours. We assume the buoy is a perfect surface follower, as suggested by Boy (1986) for the discus buoys used in the LOTUS experiment. We also assume the instruments are rigidly attached to the buoy since the mooring line was very taut (5395 m of mooring line in 5366 m of water; scope = 1.0054). An upper bound on the size of the wave bias is calculated assuming both vertical and horizontal motion are biased into the measurements and a lower bound is found assuming only vertical motion is biased into the measurements.

For wind stresses typical of the LOTUS 4 period, estimates of the wave bias are the same size as the measured downwind *current* in the upper 15 m (relative to 129 m) during the winter (Figure 3.11). Furthermore, for winds typical of the summertime portion of LOTUS, the predicted wave bias is very small, and indeed no large component of downwind *current* was observed in the summer (Figure 2.8).

The downwind *shear* due to the wave bias is also similar to the observed near-surface downwind shear between 5 and 10 m, and grows with wind stress roughly as the observed

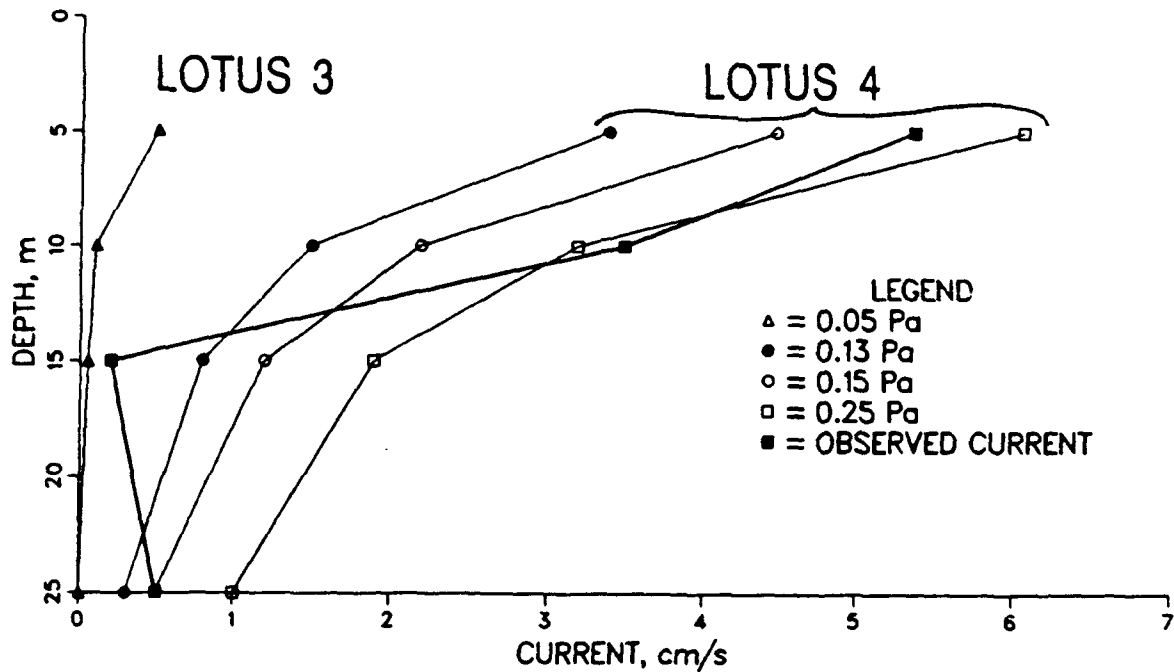


FIGURE 3.11. Profiles of observed mean LOTUS 4 downwind current and the predicted wave bias for four different values of wind stress. For LOTUS 4 (winter) conditions, the wave bias is the same size as the observed downwind near-surface current. For the lighter winds typical of the LOTUS 3 (summer) conditions, the wave bias is very small. This is consistent with the large downwind current observed in the winter (see Figure 3.2) and the lack of a downwind current in the summer (see Figure 2.8).

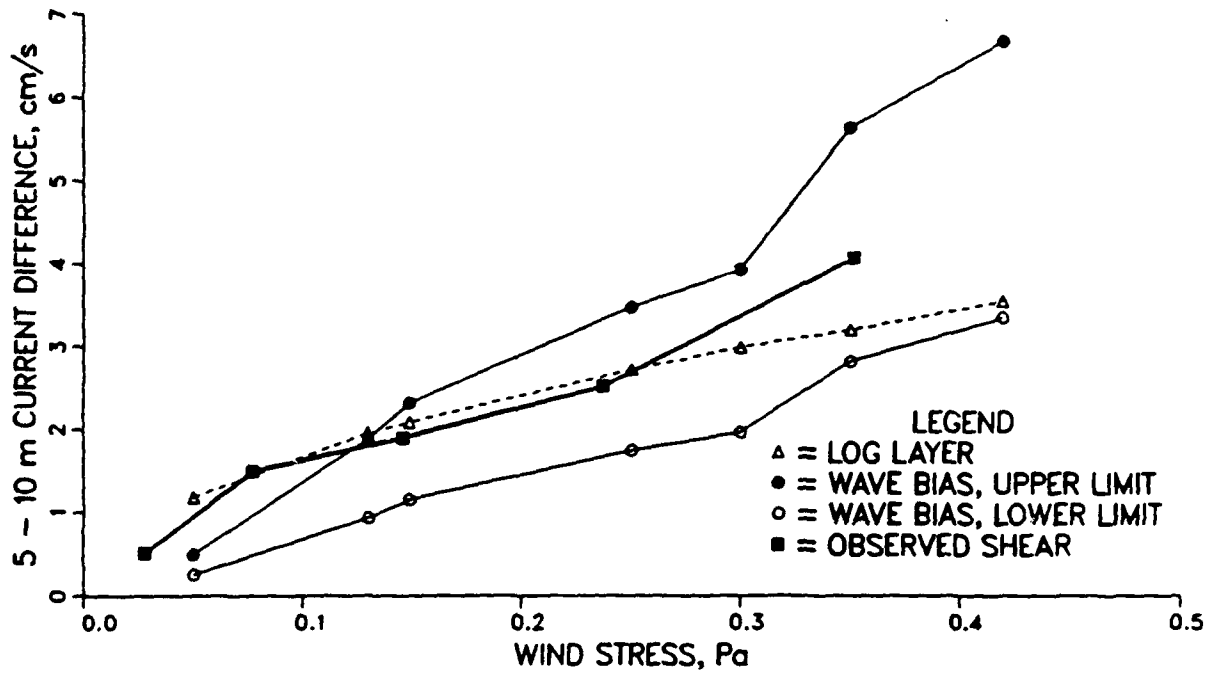


FIGURE 3.12. Near surface observed shear between 5 and 10 m, and the shear predicted by wave bias and log-layer theory vs. wind stress. The shear due to the wave bias is approximately the same as that in a log-layer, and both are similar to the observed shear, except at low and high wind stress, where the wave bias is closer to the observed shear.

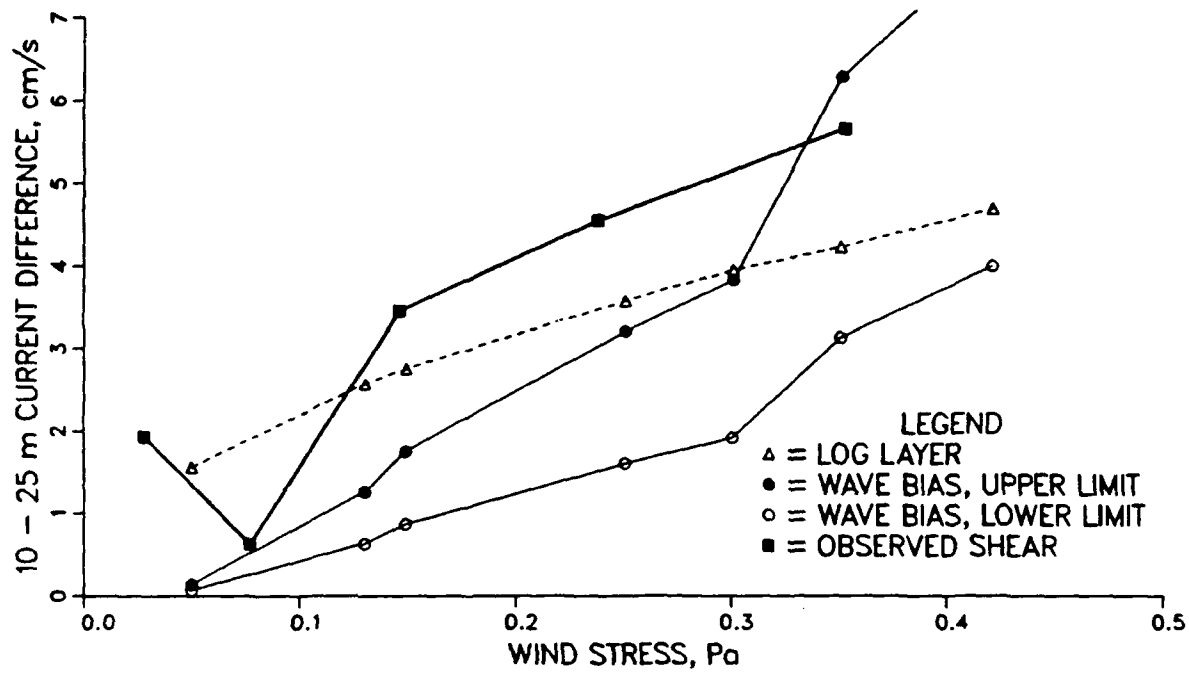


FIGURE 3.13. Near surface observed shear between 10 and 25 m, and the shear predicted by wave bias and log-layer theory vs. wind stress. The observed shear is larger than both the shear predicted in a log-layer and that due to the wave bias, except at high wind stress, where the wave bias is closer to the observed shear.

shear does (Figure 3.12). The shear predicted for a logarithmic boundary layer is also the same size as the observed shear, so the possibility that the observed shear is partially due to this mechanism cannot be eliminated. However at low and high values of wind stress the shear due to the wave bias is closer to the observed shear, and there is thus some evidence that the wave bias model is more like the observations than log layer theory for extreme values of wind stress. Deeper in the water column, the observed shear between 10 and 25 m is greater than both the shear due to the wave bias and the logarithmic boundary layer shear (Figure 3.13), and this information does not help us resolve the source of the downwind shear. If the downwind component of the current is partially an error due to a wave bias, then the true LOTUS 4 mean current spiral would be "flatter", like the LOTUS 3 mean spiral, and the agreement with Ekman transport would improve.

3.5. CONCLUSIONS AND COMPARISON OF SUMMER AND WINTER

By separating the wind-driven current from the total measured current and averaging relative to the wind direction over long records we find good agreement with the Ekman transport relation, with the exception of a downwind component in the LOTUS 4 period. A long term Ekman balance is seen in a wind-relative frame throughout summer and winter despite a small signal-to-noise ratio, with the exception of a downwind component in the winter.

For both LOTUS 3 and LOTUS 4 the mean current has a spiral structure qualitatively similar to an Ekman spiral, rotating to the right with depth. The depth scale of the spiral depends on stratification, which is very different in the summertime LOTUS 3 and the wintertime LOTUS 4 data. In the summer, net heating and light winds (average wind stress of 0.068 Pa) led to a shallow seasonal stratification and an Ekman layer that penetrates to about 50 m, e-folding in 12 m. In the winter, net cooling and strong winds

(average wind stress of 0.147 Pa) deepen the main thermocline through convection and the Ekman layer penetrates to about 100 m, e-folding in 25 m.

During the summer, the primary variability in the current structure was a diurnal variation. During the winter the current profile had very little diurnal variation, and its most striking feature is the persistent downwind shear in the upper 15 m. The downwind shear is consistent both with a logarithmic boundary layer and with the estimated error induced by a wave bias. In order to distinguish between these two possible explanations for the downwind shear it is necessary to estimate the wave bias more precisely, which requires simultaneous measurements of current, current meter motion, and the directional wave spectrum. The wave bias model, if nothing else, is another possible explanation (in addition to log layer theory) for the downwind near-surface shear during high wind, high sea conditions that causes the transport to differ from Ekman transport in the winter LOTUS observations.

Chapter 4

A Model of the Equatorial Upper Ocean

4.1 INTRODUCTION

To investigate how the equatorial undercurrent (EUC) may affect the diurnal cycle at the equator, we have developed a model of the equatorial upper ocean based on a simple upper ocean model that has successfully simulated mid-latitude cases (Price et al., 1986). In this chapter this model is presented and analyzed. First, the equatorial upper ocean model is described (Section 4.2). To give an indication of the typical conditions at the equator, we examine a case forced by climatological average meteorological conditions in Section 4.3. Using the climatological mean as a basic case, we examine the parameter dependence of the model on external variables such as wind stress, insolation, and the strength and depth of the EUC over ranges that span typical values for the equator, and report these results in Section 4.4. A concluding summary is given in Section 4.5. In Chapter 5 we will present a detailed analysis of a simulation of the 1984 TROPIC HEAT observations, as well as simulations of the 1987 TROPIC HEAT case.

4.2 A SIMPLE MODEL OF THE EQUATORIAL UPPER OCEAN

We use the one-dimensional upper ocean model of Price et al. (1986), modified for the equator, to simulate the zonal velocity and density of the equatorial upper ocean. The mid-latitude version of this model is described in Chapter 1. This model is different from previous models of the equatorial upper ocean in that vertical mixing occurs to satisfy stability requirements (Price et al., 1986), and turbulence in the model is entirely due to this mixing. A shear flow stability criterion acts to smooth out the sharp jump in velocity and density that would otherwise occur at the base of the mixed layer by extending mixing

below the well-mixed layer in a "transition layer". In this respect, the model more accurately simulates the vertical profiles observed in the upper ocean.

The model is adapted to the equator by including a zonal pressure gradient, upwelling, and the stratification and shear of the equatorial undercurrent. These are imposed externally, and are not generated or maintained by the model itself. Our goal is to see how diurnal cycling in the equatorial upper ocean is affected by these features of the large-scale equatorial circulation, and since they do not change over short time scales of a few days, they can be included in this simple way for short simulations (less than 10 days).

4.2.1. Momentum and Heat Budgets

The model simulates the equatorial upper ocean with one-dimensional budgets for momentum and heat,

$$u_t + \hat{w} u_z = - \frac{1}{\rho_o} \hat{P}_x - \frac{1}{\rho_o} \tau_z \quad (4.1a)$$

$$T_t + \hat{w} T_z = \frac{1}{\rho_o c_p} I_z - \frac{1}{\rho_o c_p} F_z \quad (4.1b)$$

$$\rho = \rho_o (1 + \alpha(T - T_o)) \quad (4.1c)$$

where the flux profiles of momentum and heat, τ_z and F_z , are determined by mixing criteria. I_z is the vertical penetration of solar insolation. The $\hat{\ }^{\prime}$ s indicate prescribed quantities; c_p is the specific heat of seawater. Density is calculated using a linearized equation of state, (4.1c), where α is a linear coefficient of thermal expansion. The model is forced at the surface by momentum and buoyancy fluxes due to wind stress, solar

heating, and cooling. The model extends to 150 m with a vertical resolution of 1 m and is integrated with a 15 minute time step.

To place the model at the equator we include a prescribed upwelling, $\hat{w}(z)$, a prescribed zonal pressure gradient (ZPG), $-1/\rho_0 \hat{P}_x(z)$, that partially balances the zonal wind stress, and include the shear and stratification of the equatorial undercurrent (EUC). The maximum amplitude of the upwelling and the zonal pressure gradient are prescribed and *held constant* in the model; the current and temperature profiles of the EUC are specified as an *initial conditions* for u and T , and evolve as they are modified by surface forcing and mixing in the water column.

4.2.2. Upwelling, Zonal Pressure Gradient, and Equatorial Undercurrent

Strong upwelling occurs at the equator due to divergent Ekman flow in the surface layer driven by prevailing easterly winds. The surface divergence is compensated from below by a geostrophic meridional inflow within the shallow thermocline due to the eastward pressure gradient and by a zonal convergence in the decelerating eastward Equatorial Undercurrent (Wyrтки, 1981; Bryden and Brady, 1985). This circulation results in an upwelling profile that is maximum in the shallowest part of the main thermocline where both Ekman divergence and geostrophic convergence contribute.

The upwelling profile we use is based on estimates made from field data (Wyrтки, 1981; Bryden and Brady, 1985; Halpern et al., 1989). Maximum upwelling is about 3×10^{-5} m s⁻¹ at the equator and occurs at depths of 50-80 m, however only roughly a third of the vertical velocity above the undercurrent core is true cross-isopycnal flow (Bryden and Brady, 1985; Brady and Bryden, 1987). Since a one-dimensional model can only represent w as cross-isopycnal flow, we use an upwelling profile with an amplitude of

$1 \times 10^{-5} \text{ m s}^{-1}$ (about 1 m day^{-1}) to get an accurate estimate of vertical advection. We make the maximum upwelling occur at the base of the model's mixed layer to simulate the Ekman divergence that drives equatorial upwelling (though later experiments have shown this to be unimportant for the purposes here; this is discussed further in Section 4.4). Since the mixed layer depth varies in time, the shape of the upwelling profile also varies (see Fig. 4.1a); the upwelling profile tapers linearly to zero at the surface and at the model base at 150 m.

We specify a zonal pressure gradient profile (ZPG) based on the results of Mangum and Hayes (1984), Figure 4.1b. The ZPG appears to provide the primary balance for the zonal wind stress at the equator (McCreary, 1981; Bryden and Brady, 1985). Turbulence generated directly by westward wind stress balances the ZPG above the EUC core; twenty one-day waves redistribute the wind momentum vertically to balance the ZPG below the EUC core (Brady, 1990), however this process is not included in our model. The total pressure gradient force of the ZPG we use (integrated from the surface to 150 m) is 0.08 Pa., and a westward wind stress of 0.05 Pa is balanced when the pressure gradient is integrated to a depth 66 m (an eastward wind stress contributes momentum in the same, rather than an opposing, direction, and thus is never balanced by the ZPG in this model). A westward wind stress stronger than 0.08 Pa can never be balanced by our pressure gradient. Fortunately, the model results are not sensitive to this momentum imbalance, nor are they sensitive to the vertical distribution of the zonal pressure gradient, as we discuss in Section 4.5.

The mean zonal current and temperature profiles of the EUC from the 1984 TROPIC HEAT experiment are specified as initial conditions, $u_o(z)$ and $T_o(z)$, Figure 4.1c and 4.1d. The undercurrent core is at 110 m with an amplitude of 1.2 m s^{-1} (Peters et al., 1988), typical of the yearly maximum value. Together, the mean current and temperature profiles

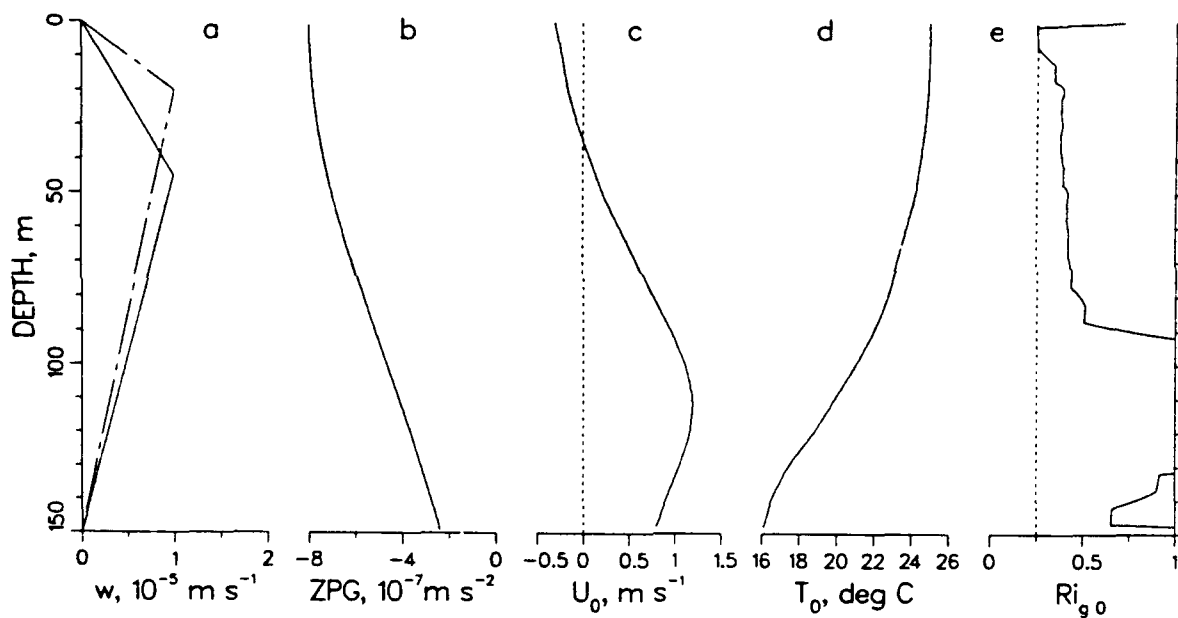


FIGURE 4.1. The prescribed dynamic profiles for (a) upwelling (as an example of how the upwelling profile varies with mixed layer depth, the solid line shows the profile for a mixed layer depth of 40 m and the chain-dashed line for a mixed layer depth of 25 m), (b) zonal pressure gradient, based on observations as described in the text; initial conditions for (c) current, and (d) temperature, from mean TROPIC HEAT 1984 observations (Peters et al., 1988), and (e) the resulting initial gradient Richardson number profile (the dashed line shows the critical value of 1/4).

give an initial gradient Richardson number profile (Fig. 4.1e) which is close to the shear flow stability limit ($Ri_g = 1/4$) down to the depth of the EUC core. During the 1984 TROPIC HEAT experiment the undercurrent core appeared to be "locked" to the density structure on time scales at least as long as twelve days (Chereskin et al., 1986). We therefore assume an initial zonal velocity profile with no dynamics of its own for our short (5-12 day) simulations. There may be times when the EUC does not have a mean structure that is near the shear stability limit above the undercurrent core. For instance, when the wind changes significantly it may take $O(20)$ days for Rossby-gravity waves to redistribute the momentum down to the EUC core (Brady, 1990), and during this time the Ri_g profile could be more stable. We consider cases like this in Section 4.4.

4.2.3. Vertical Mixing

The momentum and heat fluxes are imposed at each time step, and vertical mixing occurs until three stability conditions are satisfied, exactly as for the mid-latitude version of the model described in Chapter 1:

$$\rho_z \geq 0 \quad (4.2a)$$

$$Ri_{bulk} = - \frac{g}{\rho_o} \frac{\Delta \rho h}{(\Delta u)^2} \geq 0.65 \quad (4.2b)$$

$$Ri_{gradient} = - \frac{g}{\rho_o} \frac{\rho_z}{u_z^2} \geq \frac{1}{4} \quad (4.2c)$$

where h is the mixed layer depth and Δ is the difference in density or current across the base of the mixed layer (before 4.2c is applied). This mixing produces the vertical distributions of the momentum and heat fluxes, $\tau(z)$ and $F(z)$. The first two criteria (4.2a, 4.2b) simulate convection and entrainment, respectively, and produce a slab-like surface

mixed layer of depth h (see Fig. 1.1). The last criterion (4.2c) simulates shear flow instability and produces a sheared transition layer between the mixed layer and the fluid below, which in this case includes the equatorial undercurrent. Below the transition layer depth, d , the shear flow is stable. Because the EUC has strong vertical shear and is near instability in the upper 100 m, the transition layer is a particularly important feature of the equatorial upper ocean.

4.2.4. Surface Forcing

The model is forced at the sea surface by an air/sea heat flux and wind stress, τ_s , which we take to be purely zonal. The model is allowed to "spin up" for one day while the wind stress is ramped from zero to the initial value. The net surface heat flux, $F(0,t) = Q(t)$, positive downward, is equal to the solar insolation, I , minus the heat loss, L . The heat loss occurs directly at the sea surface (in the model's first depth bin), and then mixes downward, while solar insolation is absorbed in the water column with a double exponential depth dependence, $I(z,t) = I(0,t) (I_1 e^{-z/\lambda_1} + I_2 e^{-z/\lambda_2})$. Subscripts 1 and 2 refer to the shortwave and long-wave components of insolation, respectively, and z is positive downward with $z = 0$ at the sea surface. We use typical equatorial values for these constants: $I_1 = 0.6$ and $\lambda_1 = 0.5$ m, $I_2 = 1 - I_1 = 0.4$ and $\lambda_2 = 15$ m (Paulson and Simpson, 1977; Jerlov, 1968).

4.3 THE DIURNAL CYCLE IN THE EQUATORIAL UPPER OCEAN MODEL

To simulate conditions typical of the equator, we force the model with climatological mean meteorological forcing. Wind stress is a constant -0.05 Pa (westward), the climatological mean for the TROPIC HEAT area (Wyrki and Meyers, 1976). Solar heating has a half-sinusoidal variation with a daily maximum of 1000 W m^{-2} (which results in a net solar

heating of about 320 W m^{-2}), and the surface heat loss is a constant -200 W m^{-2} ; these values are consistent with observations of the surface heat flux during the 1984 TROPIC HEAT experiment (Peters et al., 1988; Moum et al., 1989). Cloudiness is not addressed, and neither is precipitation; these were not significant during the TROPIC HEAT experiments in the eastern-central Pacific (140°W), though they are important in the western Pacific. We show a four-day simulation of the typical diurnal cycle of current and temperature as profiles in Figure 4.2, and a time series of the surface forcing and the diurnal cycle of mixing is shown in Figure 4.3. One diurnal cycle of current and temperature at several depths in the upper 50 m is shown in Figure 4.4.

4.3.1. Daytime Phase of the Diurnal Cycle

The daytime phase of the diurnal cycle seen in these simulations follows a pattern that is very similar to that of the diurnal cycle at mid-latitudes. During the day, absorption of solar insolation tends to warm and stabilize a near-surface layer (5-10 m thick). In the absence of any wind-stirring the diurnal warm layer would have an e-folding thickness of only about 1 m given by the optical properties of sea water. However, wind-stirring acts continually to destabilize the near-surface layer, and mixes heat and momentum to a much greater depth, typically about 5 m for climatological conditions. The amplitude of the diurnal warming at the surface is thus much less than it would be in the absence of wind-stirring, about 0.3°C (see Figure 4.4). Observations (McPhaden and Peters, 1991) and the model simulations show that the diurnal cycle of sea surface temperature has a marked saw-toothed form in time, with comparatively rapid warming beginning at about 0800 local solar time and continuing only until about 1400 (Figure 4.4), again much like that noted for mid-latitude conditions by Price et al. (1986). The near-surface layer begins to cool in early afternoon even though the surface heat flux is strongly positive, because wind mixing transfers heat from the near-surface to depths of 10-20 m. Thus surface warming occurs

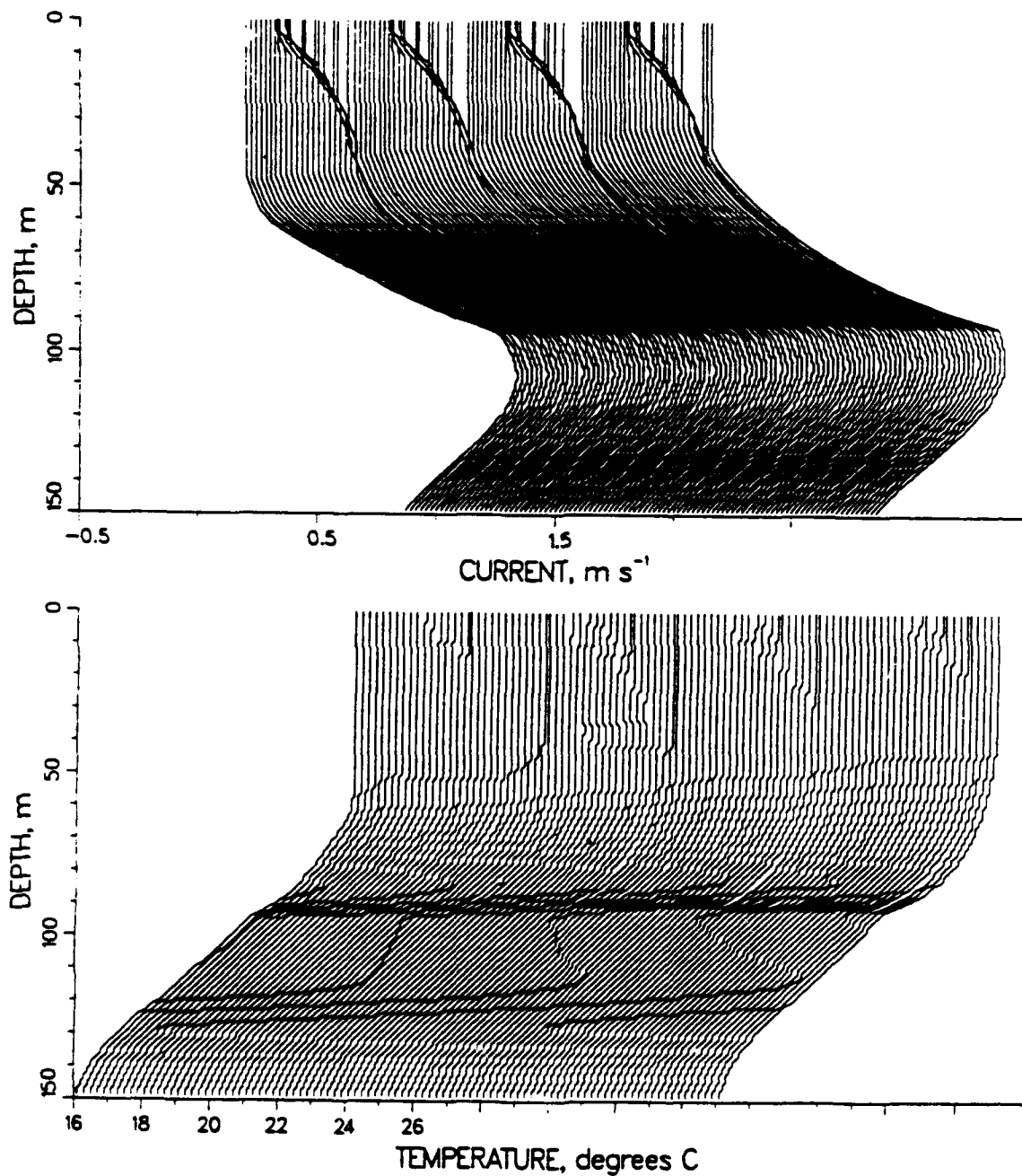


FIGURE 4.2. The diurnal cycle in current and temperature for four days of the climatological mean simulation. The horizontal axes apply to the first profile, which is at 6 a.m., and each successive profile is offset by a small amount. The time increment is 30 minutes. Notice that the diurnal range in current and temperature is much less than the vertical shear and stratification of the EUC.

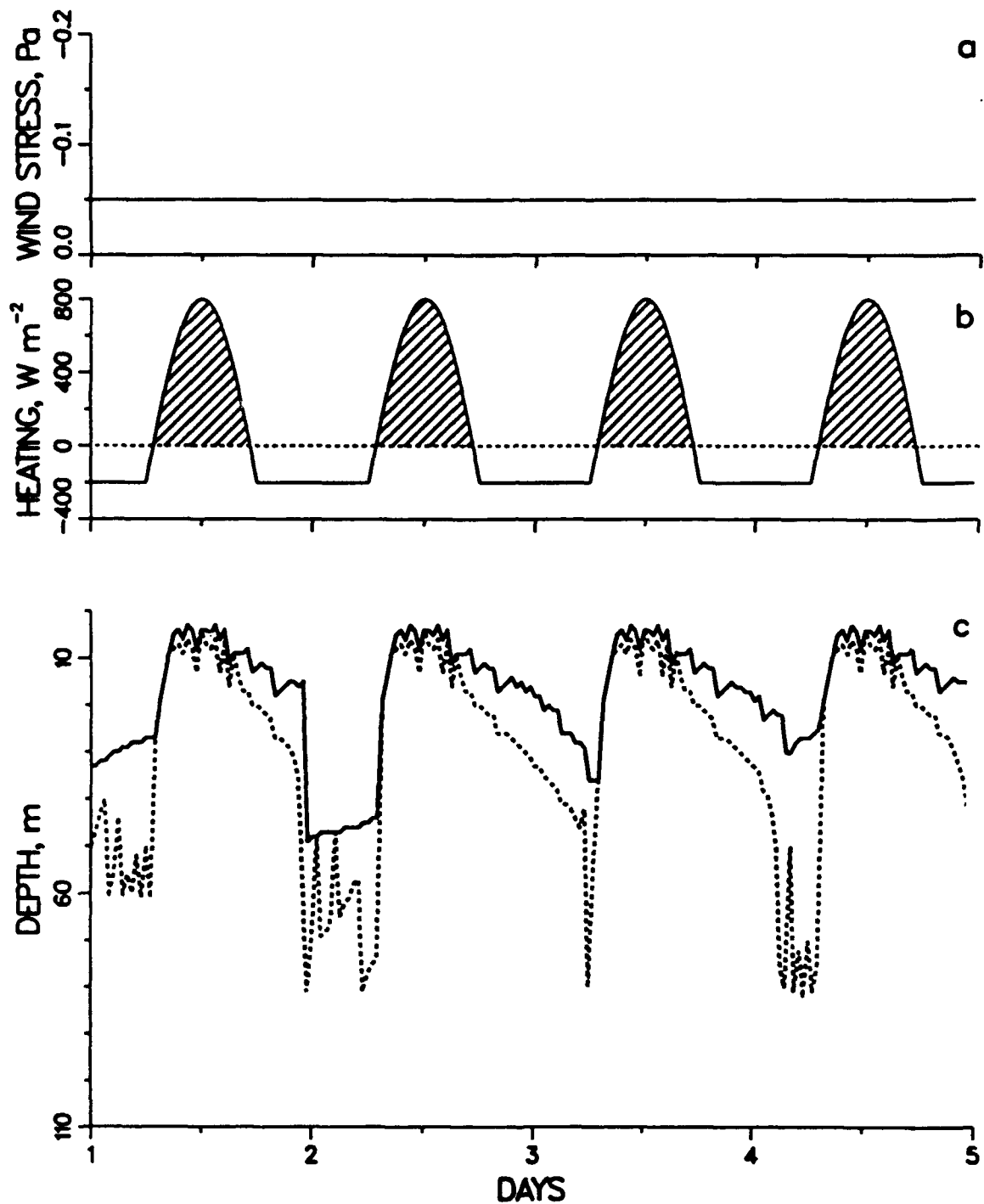


FIGURE 4.3. Meteorological forcing and simulated and observed mixing for four days of the climatological mean simulation: (a) wind stress, negative is westward, the direction of prevailing winds; (b) surface heat flux, positive is into ocean; (c) simulated mixed layer depth, h (solid line), transition layer depth, d (dashed line). Note the striking diurnal cycle and depth range of turbulent mixing in the transition layer.

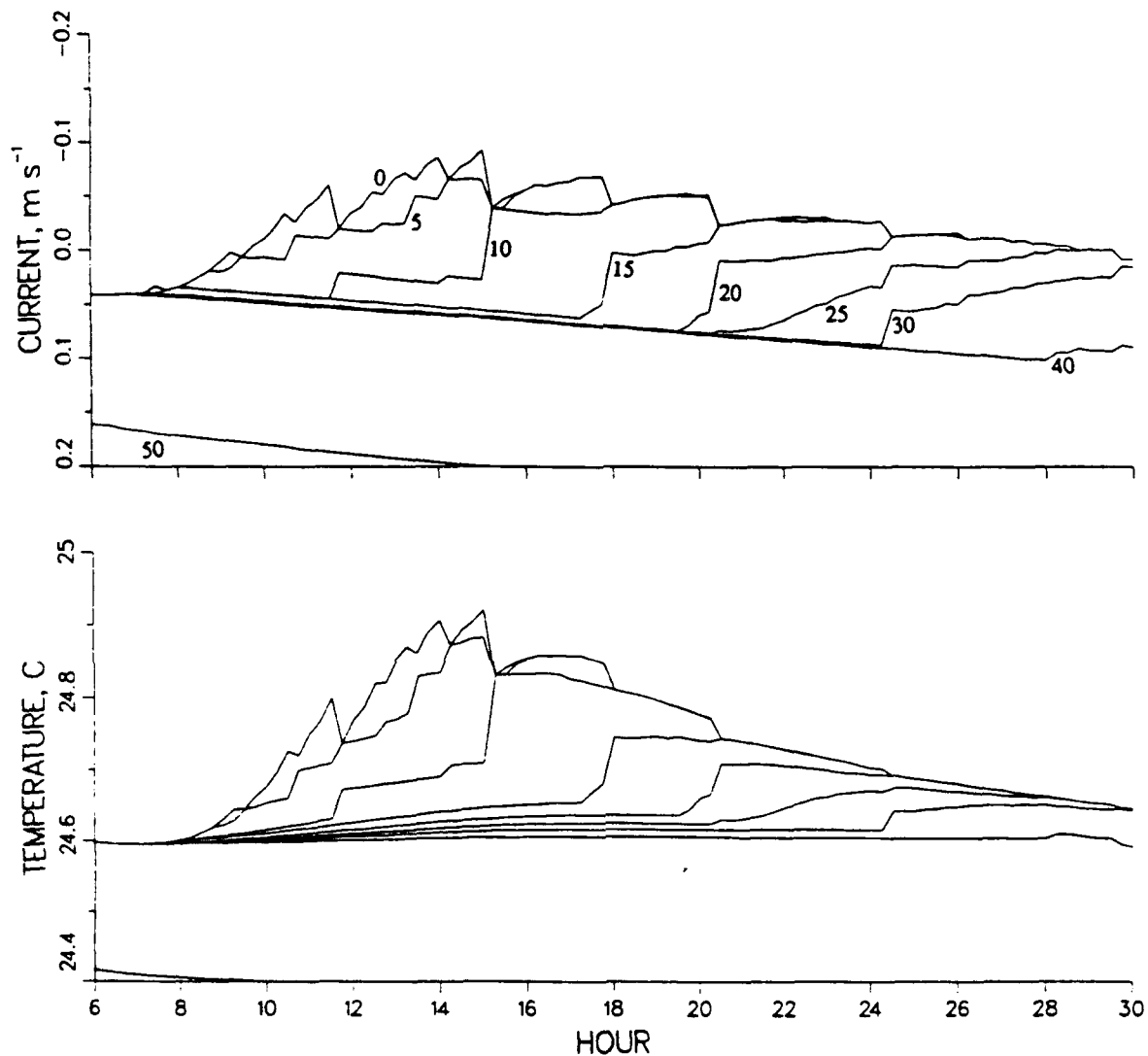


FIGURE 4.4. Simulated time series of current and temperature at depths of 0, 5, 10, 15, 20, 25, 30, and 40 m for a typical day with a wind stress of -0.05 Pa , the climatological mean. The amplitude of the diurnal cycle is 0.14 m s^{-1} and 0.32°C . Compare to the diurnal cycle amplitude for twice this wind stress but identical heating, 0.16 m s^{-1} and 0.19°C (Table 4.1). Notice that the current response is fairly constant as wind stress varies but the temperature response varies significantly with wind stress. This is consistent with the wind stress dependence of a mid-latitude diurnal response (Price et al., 1986; see Table 4.1 also), showing that the daytime phase of the diurnal cycle in the equatorial upper ocean has similar dynamics as a mid-latitude upper ocean.

over only about $1/4$ of the day, while a comparatively gradual cooling of surface temperature occurs during almost $3/4$ of the day.

The wind stress that is absorbed within the warmed diurnal layer accelerates the layer down-wind (recall in this model the wind is purely zonal, and westward in this case), and the resulting current, or diurnal jet, has an amplitude maximum occurring a few hours after noon of typically 0.13 m s^{-1} (Figure 4.4). Montgomery and Stroup (1962) inferred the existence of such a jet from surface drifter observations made near the equator. They suggested that the shear of this current was stabilized against turbulent mixing by the stratification of the diurnal thermal cycle, which is certainly what happens in this model. The equatorial diurnal jet is quite different from its mid-latitude counterpart in that an inertial rotation of the jet does not occur. Instead, the equatorial jet accelerates in the down-wind direction throughout the day. Its amplitude is reduced during the afternoon and evening only by vertical mixing.

4.3.2. Nighttime Phase of the Diurnal Cycle

During the late afternoon and early evening, continued wind-mixing and cooling act to destabilize the near-surface layer and form a nighttime mixed layer that has a thickness of about 35-40 m by the end of the night (Figures 4.2 and 4.3). Heat stored in the upper 20 m during the day is mixed downwards, and at the same time is lost through the surface so that on most days there is a more or less closed diurnal cycle of surface temperature.

Since the wind always blows from the east in this simulation, there is no similar diurnal cycle of the momentum supply to the upper ocean. Instead, the momentum stored in a shallow jet during midday is retained as the diurnal layer is mixed downwards. A long term balance is possible only by balancing the wind stress against some non-local

processes, particularly the zonal pressure gradient, which in this model has been prescribed.

As the momentum of the diurnal jet mixes down into the water column at night, it encounters the region where the mean profile of the EUC is nearly unstable, resulting in very deep mixing in a transition layer that typically extends about twice as deep as the mixed layer (see Figs. 4.3 and 4.5). This is remarkably different from a mid-latitude case, where this model predicts transition layers $O(5\text{ m})$ deeper than the mixed layer throughout the day (Price et al., 1986). The deep mixing at night is consistent with observations from the TROPIC HEAT experiment (see Section 4.4.2 and Chapter 5). In the model, the deep mixing is primarily due to the presence of the EUC and its low dynamic stability, as we discuss in the next section, and thus is truly unique to the equator.

4.4 PARAMETER DEPENDENCE OF THE DIURNAL CYCLE AT THE EQUATOR

We have run a series of numerical experiments to see how the equatorial upper ocean model depends on the external parameters: wind stress and surface heating, the depth and amplitude of the EUC, and the amplitude of the ZPG and upwelling. Our reference case, which we discussed at length in the previous section, has climatological mean forcing given by $\tau_s = -0.05\text{ Pa}$, $I_{max} = 1000\text{ W m}^{-2}$, $L = -200\text{ W m}^{-2}$, upwelling and ZPG as in Figure 4.1a and 4.1b, and an initial EUC as in Figure 4.1c-e. In our numerical experiments we vary only one parameter at a time while all other parameters retain the value of the reference case. This approach may be somewhat contrived, in that the dynamics of these processes are linked and therefore vary in conjunction with each other; for example, the EUC responds to changes in the ZPG, though perhaps with a lag of order 10-30 days as 21-day waves redistribute momentum above the EUC core (Brady, 1990). However, we retain this approach in order to isolate the effect of each process on the equatorial upper ocean. In

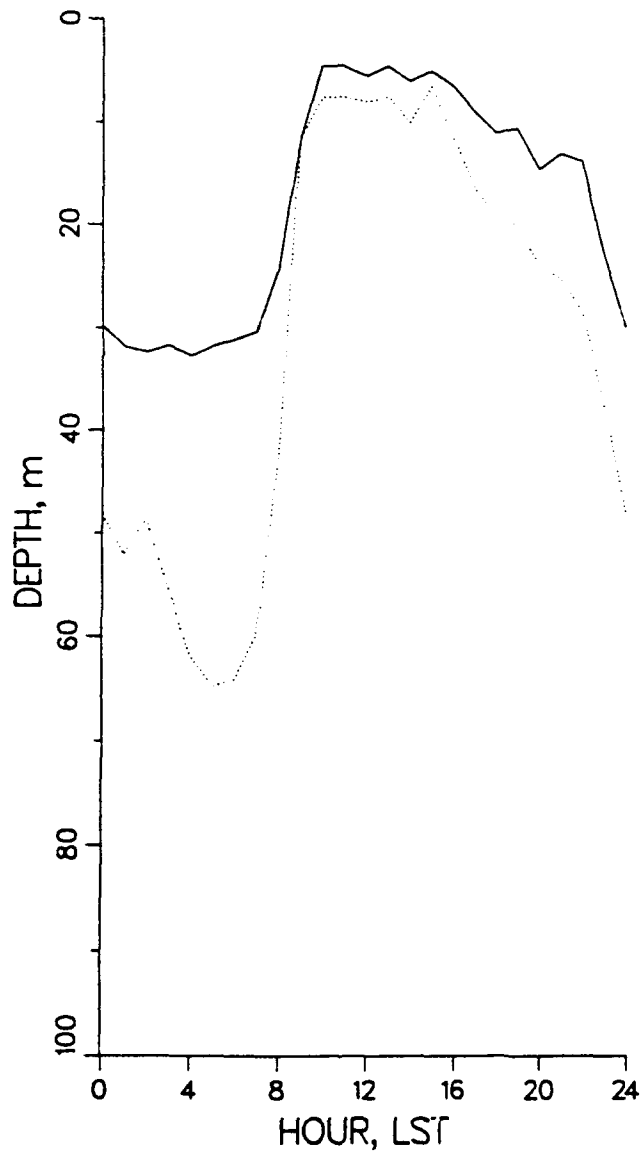


FIGURE 4.5. Ensemble average of 5 days of modeled mixed layer depth h (solid line) and transition layer depth d (dotted line). Note the large diurnal cycle, and the transition layer extending about twice as deep as the mixed layer at night.

the following sections we first discuss the sensitivity of the daytime phase of the diurnal cycle (Section 4.4.1) and then we discuss the nighttime phase (Section 4.4.2).

4.4.1. Daytime Phase: Amplitude of Diurnal Warming and the Diurnal Jet

4.4.1i. Surface forcing dependence

Variations in the daytime phase of the diurnal cycle due to wind stress and heat flux can be appreciable, and appear to be almost exactly as found at mid-latitudes; e.g., for a given heat flux, a stronger wind stress will cause a greater depth of the surface mixed layer, reduced warming of sea surface temperature (SST), but very little change in the amplitude of the diurnal jet (Price et al., 1986). Some numerical results are listed in Table 4.1, along with estimates of the simplified scale analysis "solution" of the Price et al. (1986) model, which is described in that paper. This comparison is also shown in Figure 4.6 for a wider range of heating and wind stress. Note that the simplified mid-latitude scale solution gives similar results to the full equatorial numerical model for forcing near the climatological mean (Table 4.1) and good agreement for ΔSST over all ranges of heating and stress (Figure 4.6).

The diurnal jet at the equator is somewhat different from its mid-latitude counterpart. For wind stresses weaker than -0.05 Pa, there is a tendency for the diurnal jet at the equator, Δu_{eq} , to be less than the predicted diurnal jet at mid-latitudes, $\Delta u_{mid\ lat}$; for winds stronger than -0.05 Pa, $\Delta u_{eq} > \Delta u_{mid\ lat}$ (Figure 4.6 and Table 4.1). Ironically, for $\tau_s = -0.05$ Pa, the climatological mean, Δu_{eq} and $\Delta u_{mid\ lat}$ are in close agreement. The reason for the lack of agreement for Δu and the good agreement for ΔSST may be that because there is no inertial rotation of the diurnal jet at the equator, τ_s and u are always parallel, and therefore more of the wind's kinetic energy gets into the upper ocean at the equator than at mid-

TABLE 4.1.

Amplitude of the mixed layer diurnal cycle compared to predictions from the scaling analysis of Price et al. (1986). Forcing is varied about the climatological mean: wind stress, τ_s , is -0.05 Pa (westward); amplitude of half-sinusoidal solar heating, I_{max} , is 1000 W m^{-2} ; constant heat loss, L , is -200 W m^{-2} ; and the EUC, ZPG and upwelling are as in Fig. 4.1.

Δ indicates the difference over a diurnal cycle. D_T is the daily minimum of the trapping depth, $D_T = 1/T'_s \int_{z_r}^{z_s} T' dz$, or the centroid of the temperature anomaly (T') profile. The trapping depth is a measure of the minimum depth scale of the mixed layer, which occurs during the heating phase of the diurnal cycle. T_{SC} , U_{SC} , and D_{SC} are predicted scales for the temperature, velocity, and depth amplitude of the diurnal response at mid-latitudes (Price et al., 1986). According to this scaling, $T_{SC} \sim Q^{3/2}\tau$, $U_{SC} \sim Q^{1/2}$, and $D_{SC} \sim \tau/Q^{1/2}$, where $Q = I - L$, the net solar heating.

	$\Delta SST, ^\circ C$	$T_{SC}, ^\circ C$	$\Delta V, \text{ m s}^{-1}$	$U_{SC}, \text{ m s}^{-1}$	$D_T, \text{ m}$	$D_{SC}, \text{ m}$
$\tau, \text{ Pa}$						
0	1.71	1.72	0.07	0	1	2
-0.025	0.46	0.51	0.10	0.12	3	5
-0.05	0.30	0.29	0.13	0.12	5	8
-0.10	0.19	0.18	0.16	0.13	10	13
$I_{max}, \text{ W m}^{-2}$						
600	0.10	0.10	0.07	0.08	9	11
800	0.19	0.19	0.11	0.11	6	9
1200	0.44	0.41	0.15	0.14	4	7

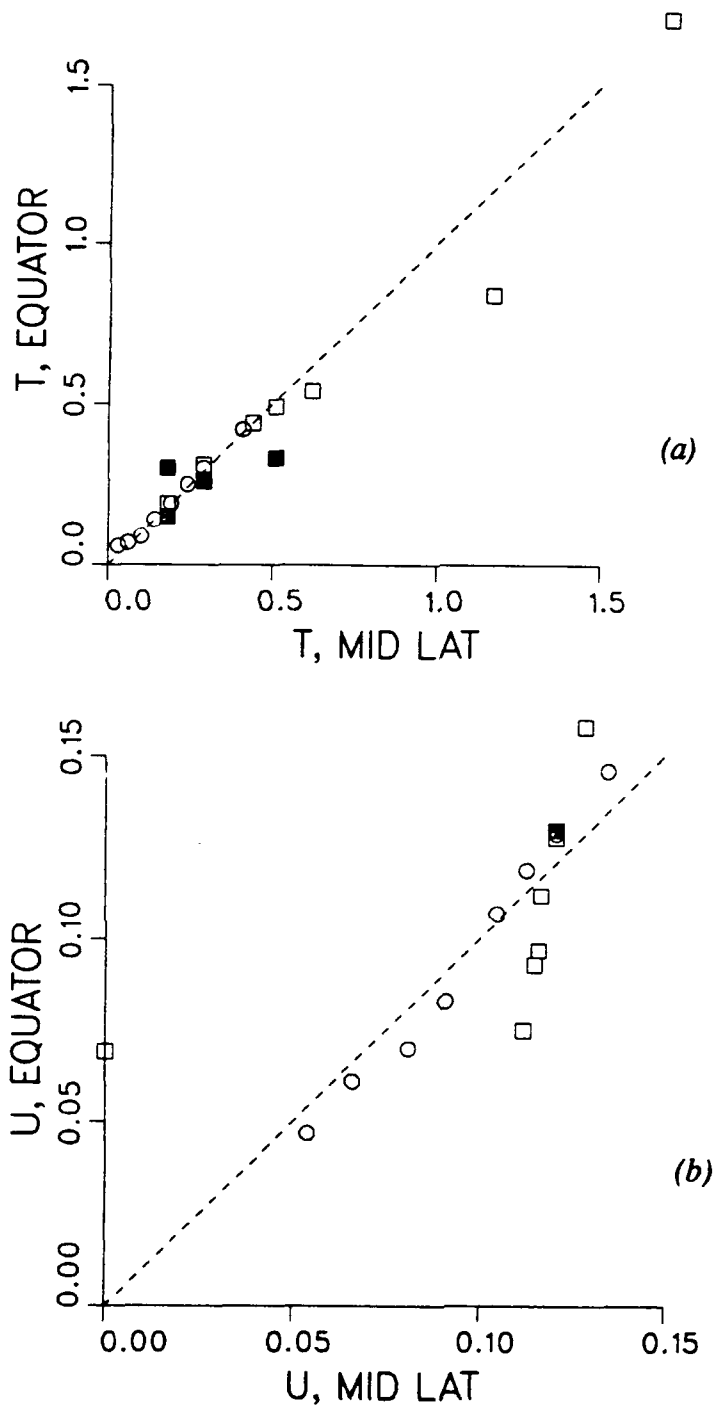


FIGURE 4.6. Amplitude of (a) diurnal SST warming and (b) diurnal jet amplitude at the equator vs. amplitudes predicted by a mid-latitude scaling argument (Price et al., 1986) for different values of surface heating and wind stress. Numerical values corresponding to some of these points are listed in Table 4.1. The open symbols are from the equatorial upper ocean model; solid symbols are observed values. Different values of surface heating are plotted as circles and different values of wind stress are plotted as squares. A line of slope one, indicating perfect agreement between equatorial and mid-latitude diurnal amplitudes, is shown as the dashed line. Note the very close agreement for ΔSST and the slightly less good agreement for Δu .

latitudes. Also, a background large-scale temperature stratification is assumed in the mid-latitude scale analysis, while a similar background large-scale current shear is not. This causes slight departures from the mid-latitude scaling results. The most dramatic example of this is the special case $\tau_s = 0$ (Figure 4.6); in this case the simulated equatorial diurnal jet is much larger than the scale solution (which predicts $\Delta u = 0$ for $\tau_s = 0$) because the shear of the EUC produces a variation in surface current in a freely convecting mixed layer even in the absence of wind stress.

Existing equatorial upper ocean observations represent only a limited range of forcing conditions, but can be used to make a semi-quantitative check of simulations of the diurnal cycle amplitude. These values are indicated as solid dots in Figure 4.6. For winds of about 0.06 Pa west (slightly larger than the climatological mean), surface drifter observations near the equator showed a diurnal cycle of 0.26°C and 0.13 m s^{-1} (Montgomery and Stroup, 1962), similar to the simulated diurnal cycle of 0.3°C and 0.14 m s^{-1} for climatological mean wind stress (Figure 4.6, Table 4.2). Kraus's (1987) model produced a diurnal variation of 0.3°C and 0.35 m s^{-1} for climatological mean forcing; the SST warming agrees well with both observations and our model, though the diurnal cycle in surface current is substantially larger than either our model or observations for reasons we can not explain. During the 1984 TROPIC HEAT experiment (mean wind stress 0.10 Pa west), SST warmed by $0.15\text{-}0.30^\circ\text{C}$ over a day (Moum et al., 1989); the model's diurnal variation of 0.19°C for a constant wind stress of -0.10 Pa (Table 4.2) is representative of that range. Unfortunately no observations of surface current were made during that experiment.

TABLE 4.2.

Amplitude of the diurnal cycle as it varies with wind stress, solar heating, depth of the undercurrent core, and undercurrent core speed. Δ is the difference during a diurnal cycle. Depths for h (mixed layer depth) and d (transition layer depth) are the maximum during the diurnal cycle. Forcing is varied about the climatological mean: $\tau = -0.05$ Pa, $I_{max} = 1000$ W m⁻², $L = -200$ W m⁻²; initial EUC core speed = 1.2 m s⁻¹ and EUC core depth = 110 m, as in Fig. 4.1; ZPG, and upwelling are as in Fig. 4.1. This standard case is in boldface.

	Δ SST, °C	Δ V, m s ⁻¹	h , m	d , m
$\tau = -0.05$ Pa (climatological mean)	0.3	0.13	33	65
$\tau = -0.20$ Pa	0.1	0.24	49	100
$\tau = -0.10$ Pa (1984 Tropic Heat mean)	0.2	0.16	46	86
$\tau = -0.025$ Pa (1987 Tropic Heat mean)	0.5	0.10	26	45
$\tau = 0$	1.7	0.07	12	12
$I_{max} = 1200$ W m ⁻²	0.4	0.15	32	56
$I_{max} = 800$ W m ⁻²	0.2	0.11	35	68
$I_{max} = 600$ W m ⁻²	0.1	0.07	43	72
$I_{max} = 0$	--	--	28	82
EUC core 0.90 m s ⁻¹	0.3	0.13	33	54
EUC core 0.60 m s ⁻¹	0.3	0.13	31	48
EUC = 0	0.3	0.12	26	39
EUC core at 90 m	0.3	0.13	34	62
Upwelling = 0	0.3	0.13	33	68
ZPG = half	0.3	0.15	37	65
ZPG = 0	0.3	0.17	38	69

4.4.1iii. EUC and ZPG dependence

The daytime phase of the diurnal cycle is found to be quite insensitive to any plausible variations in the EUC or ZPG, including the elimination of either one separately (Table 4.2). This is because the mixing dynamics in the model are unaffected by any depth-independent current or acceleration, and although the EUC and ZPG have large amplitudes, they have a depth scale much greater than the scale of the daytime mixed layer ($O(10\text{ m})$), and so appear depth-independent to the daytime phase of the diurnal cycle. On this basis, we conclude that aside from the fact that there is no inertial rotation of the diurnal jet at the equator, the special features of the equatorial upper ocean (the EUC, upwelling and the ZPG) do not significantly alter the dynamics of the daytime phase of the diurnal cycle; the nighttime phase, however, is affected by some of these features.

4.4.2. Nighttime Phase; Depth of Mixing

Numerical experiments indicate that the depth to which mixing extends at night in the model is very sensitive to the surface heat flux, wind stress, and the EUC (these are discussed further below). In comparison, the details of upwelling and the ZPG are unimportant for the *short term* integrations (10 days) of interest here, and, for example, a case with vanishing ZPG differs only slightly from the cases with a realistic ZPG (see Table 4.2). However, with ZPG vanishing, the upper ocean undergoes a westward acceleration due to wind stress that will eventually eradicate (and then reverse) the EUC, which would make a substantial difference over longer integrations (more than about 20 days). Similarly, upwelling is essential for balancing the downward flux of heat due to mixing, and without upwelling the thermal structure would eventually be altered substantially from the realistic profile used as the initial condition. This too would eventually change the nighttime phase of mixing by altering the mean flow and stratification.

4.4.2i. Surface Heating Dependence

A diurnal cycle of solar heating is, of course, essential for causing the diurnal cycle of mixing. If the insolation is shut off and cooling left at -200 W m^{-2} , for climatological wind stress (0.05 Pa westward) mixing in the transition layer and a substantial momentum flux from the wind stress reach to nearly the core of the EUC after about 3 days, until the EUC is eventually erased.

As solar heating is increased, the depth of the nighttime mixed layer and transition layer decrease (Table 4.2). For the climatological wind stress of 0.05 Pa westward (and a constant heat loss of -200 W m^{-2}), these simulations suggest that an appreciable diurnal cycle begins to occur when the maximum insolation reaches 600 W m^{-2} or higher (see Table 4.2), i.e. when there is a daytime maximum in net heating of at least 400 W m^{-2} .

4.4.2ii. Wind Stress Dependence

The depth of nighttime mixing depends most strongly on wind stress (Table 4.2). As τ_s increases, nighttime mixing deepens, allowing the wind to work against more of the shear of the EUC. Some observations are available to show how mixing varies with wind stress and, at least for these cases, the model agrees fairly well with the data, showing deeper mixing as wind stress increases (Figure 4.7). The observations of depths where turbulent dissipation is greater than $10^{-7} \text{ W kg}^{-1}$ indicate high levels of turbulent mixing associated with surface-forced mixing, and thus can be appropriately compared to the model's transition layer depth, d . The agreement is surprisingly good (Fig. 4.7a and c). Actual estimates of turbulent dissipation from the model will be described and compared to the TROPIC HEAT observations in Chapter 5.

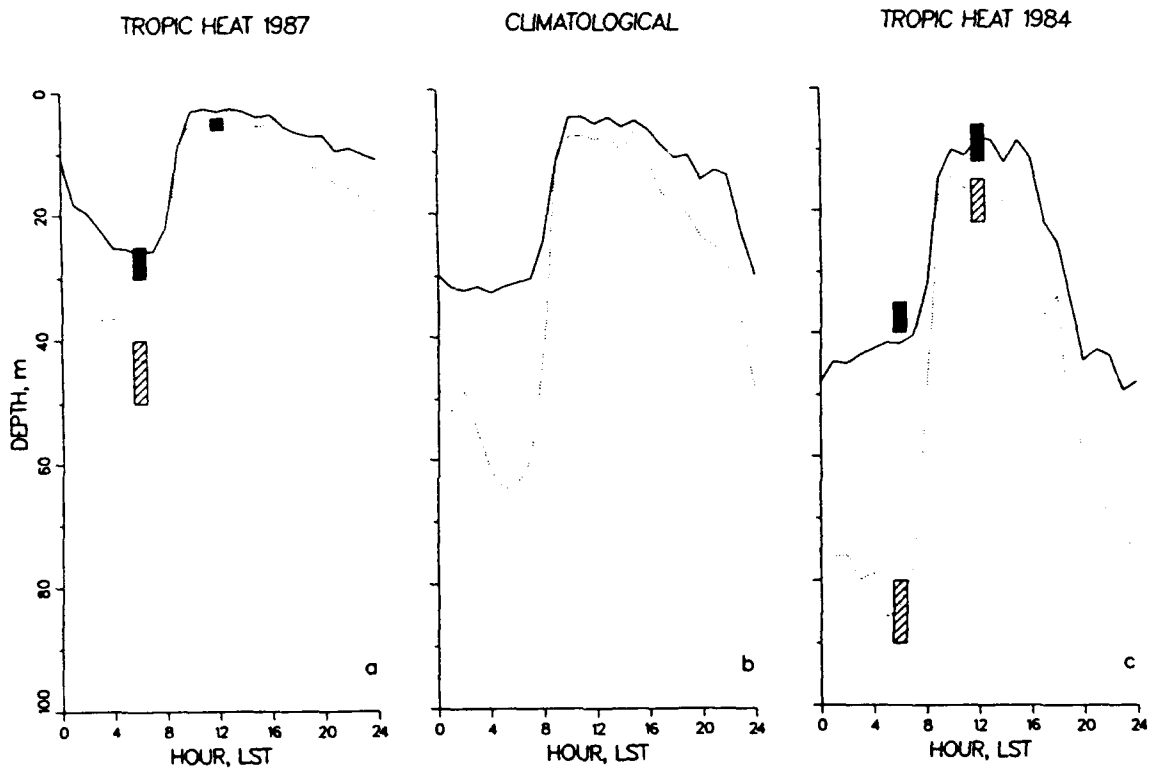


FIGURE 4.7. Ensemble averages of 5 days of modeled mixed layer depth (solid line) and transition layer depth (dotted line) for different values of wind stress. Observed mixed layer depth and extent of high dissipation are indicated by the solid and dashed bars, respectively. Wind stress is (a) 0.025 Pa westward (TROPIC HEAT 1987 mean wind stress; observations from Peters, personal communication), (b) 0.05 Pa westward (climatological mean wind stress), and (c) 0.10 Pa westward (TROPIC HEAT 1984 mean wind stress; observations from Peters et al., 1988 and Moum et al., 1989). All cases use the initial undercurrent and stratification and the profiles for the pressure gradient and upwelling indicated in Figure 4.1.

Our results also show some agreement with a model similar to ours in that it includes the EUC and mixed layer dynamics (Kraus, 1987). For climatological wind stress ($\tau_s = -0.05$ Pa), Kraus's model predicts a mixed layer that reaches 35 m at night and shallows to 2 m during the day, similar to our results (Fig. 4.7b). The turbulent domain in his model reaches 80-90 m at night, somewhat deeper than our model predicts, and remains at 60-70 m during the day, in marked contrast to our results and to the field data which show almost no mixing below about 10-20 m during the day.

4.4.2iii. Zonal Pressure Gradient Dependence

The zonal pressure gradient provides the primary balance for zonal wind stress at the equator (Bryden and Brady, 1985; McCreary, 1981) in a long term, integral sense. However it is unlikely that the ZPG and the zonal wind stress are in balance over short time scales, since the basin response time at the equator is of order 300 days in the Pacific Ocean and 100 days in the Atlantic (Philander and Pacanowski, 1980). Estimates of the distribution of stress in the water column show that it also seems unlikely that such a balance existed at any depth range in the upper 90 m during TROPIC HEAT 1984 (Dillon et al., 1989). In this simple one-dimensional model we can not expect to fully capture the zonal momentum balance at the equator, and fortunately the model results are not sensitive to this momentum imbalance, nor are they sensitive to the vertical distribution of the zonal pressure gradient.

We experimented with several different zonal pressure gradients, some which exactly balanced the mean wind stress when vertically integrated, and some which were more like reported profiles of the ZPG (Mangum and Hayes, 1984; Bryden and Brady, 1985) and did not completely balance the wind stress. The model was very insensitive to $\int \text{ZPG} dz$. Even a case with no pressure gradient was not very different than a case with a balancing

ZPG (see Table 4.2). Despite the fact that the wind stress is unbalanced in some of our experiments, the net effect is that the zonal velocity is slowly accelerated downwind while the diurnal cycle is little altered. This acceleration would eventually lead to an unrealistic zonal velocity profile, but for the short simulations considered here is relatively unimportant.

We also experimented with different vertical distributions of the zonal pressure gradient. We were concerned that the mixing was reaching deep in the model water column only in order to satisfy the simplistic momentum balance between the zonal pressure gradient and the wind stress. While there was some dependence of maximum depth of mixing on ZPG(z), it is not the primary factor in determining the depth of mixing. A ZPG profile that balanced the wind stress and was entirely distributed in the top 50 m of the water column (and zero below 50 m) still yielded mixing and high dissipation at night at depths of 80-90 m. The main factor determining mixing depth is the low stability of the equatorial undercurrent.

4.4.2iv. Equatorial Undercurrent Dependence

Observations show that the EUC can change on a time scale of days (as waves pass through); for example, during the 12 days of the 1984 TROPIC HEAT experiment (at 140°W), the core migrated between 140 m and 90 m and its speed varied between 0.80 and 1.50 m s⁻¹ (Moum et al., 1989). To test the possible consequences on the equatorial mixed layer, we experimented with several different profiles of the EUC by varying both the speed and the depth of the core.

We varied the speed of the undercurrent in the model by multiplying the entire initial EUC profile by a fraction. This changes the initial R_{ig} profile, making the water column more

stable above the EUC core when the EUC amplitude is reduced. With no EUC at all, the model develops a down-wind current that reaches 25-30 m and a transition layer that remains fairly thin, extending about 15-20 m below the mixed layer (see Table 4.2 and Figure 4.8). This is slightly deeper than a typical mid-latitude case, where the transition layer is 5-10 m thick, and quite different from the case with an undercurrent, where the transition layer is 30-40 m thick (Figure 4.8). Notice that the daytime phase of mixing is unaffected by the EUC. As the EUC amplitude increases from zero (and Ri_g decreases), the mixing becomes deeper and the transition layer becomes thicker. Thus, the shear of the EUC is critically important for producing deep nighttime mixing in the model.

The effect of the depth of the EUC core on the maximum depth of mixing is fairly direct. When the core is at 110 m, and for climatological mean wind stress, mixing reaches down to approximately 70 m (see Table 4.2). When the core is at 90 m (we vary the stratification also, to preserve the initial Ri_g profile above the undercurrent core as in Fig. 4.1e), mixing only reaches to 60 m. Thus mixing does not penetrate into the region of high stability near the nose of the undercurrent even if the core is comparatively shallow.

4.4.2v. Upwelling Dependence

As mentioned earlier, upwelling has little effect on the diurnal cycle in surface temperature (see Table 4.2) but is important in maintaining the long-term thermal structure of the EUC. Surface warming can reach to $O(100\text{ m})$ via deep mixing at night, and without upwelling, in just a matter of a few days the temperature at these depths begin to significantly warm (Figure 4.9b). This warming approximately equals the cooling that vertical advection provides, so that surface heating and upwelling are in rough balance, and the thermal structure is in quasi-steady state (Figure 4.9a). The relative importance of surface heating may seem surprising because the diurnal warming is so much smaller than the temperature

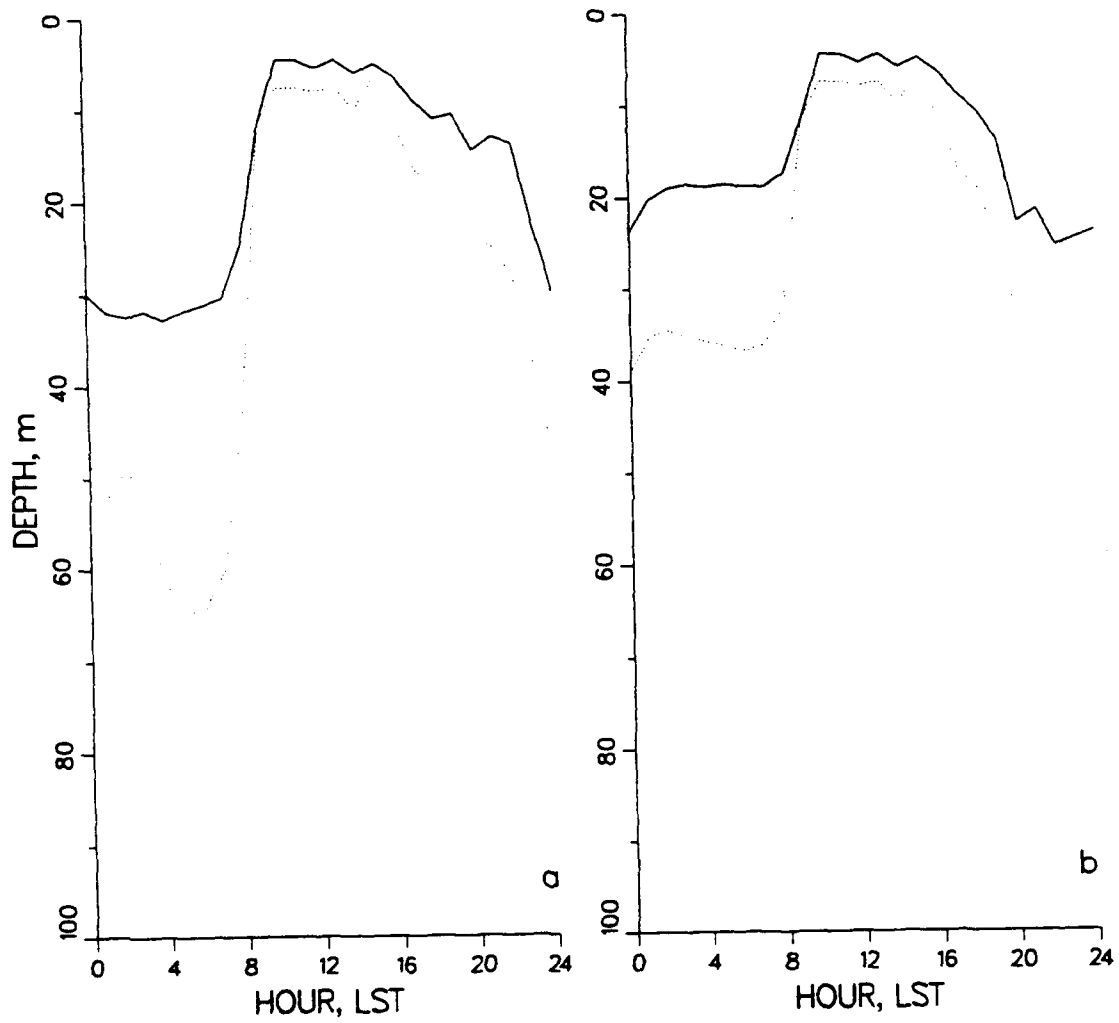


FIGURE 4.8. Ensemble averages of mixed layer depth, h (solid line), and transition layer depth, d (dotted line), for the climatological mean case (a) with the undercurrent and (b) without the undercurrent.

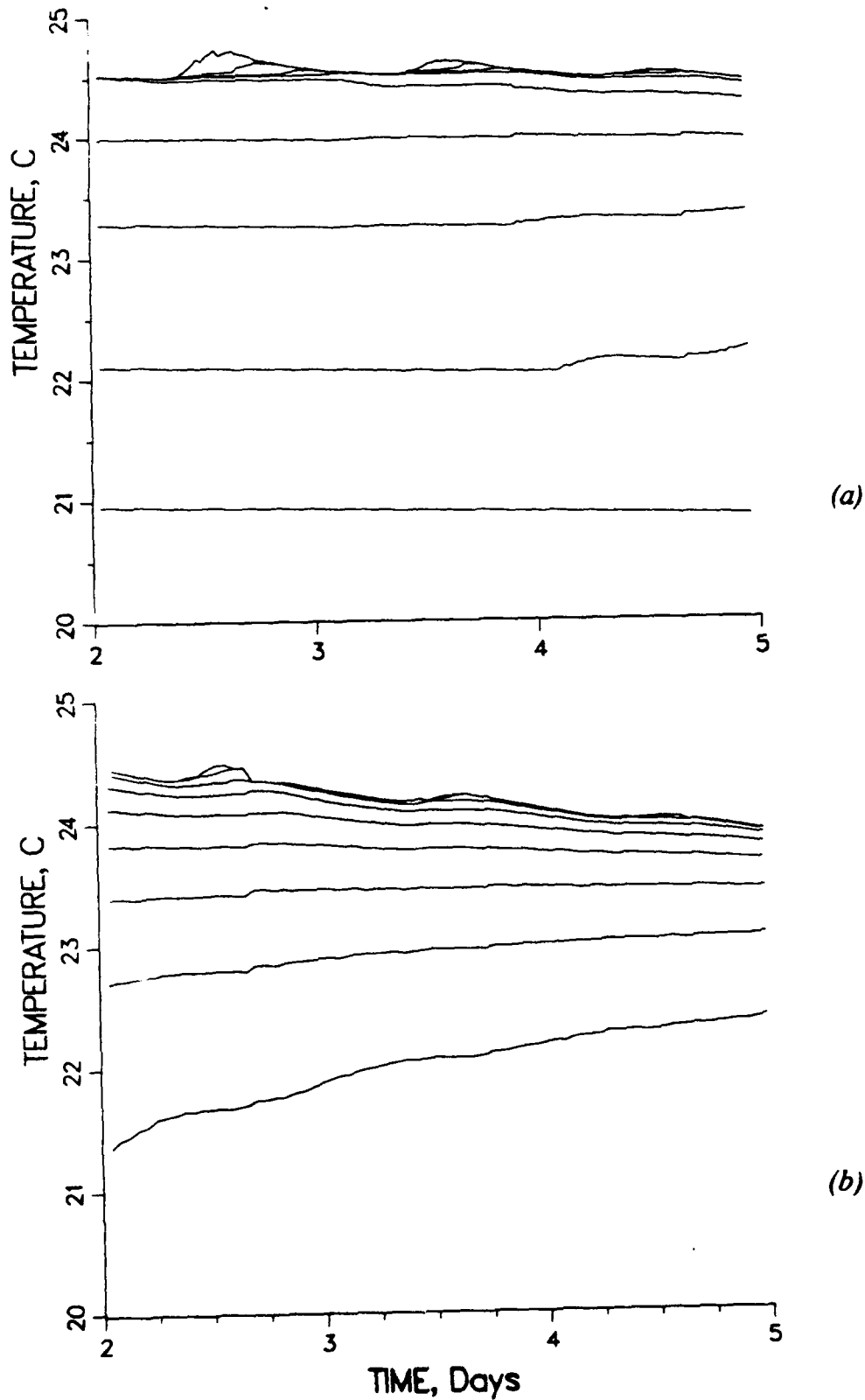


FIGURE 4.9. Time series of temperature at 2, 16, 28, 40, 52, 64, 76, 88, and 100 m for the last 3 days of a 5-day simulation of the climatological mean case, (a) with upwelling, and (b) without upwelling. The warming at depth in the absence of the undercurrent is approximately equal to the cooling produced by vertical advection.

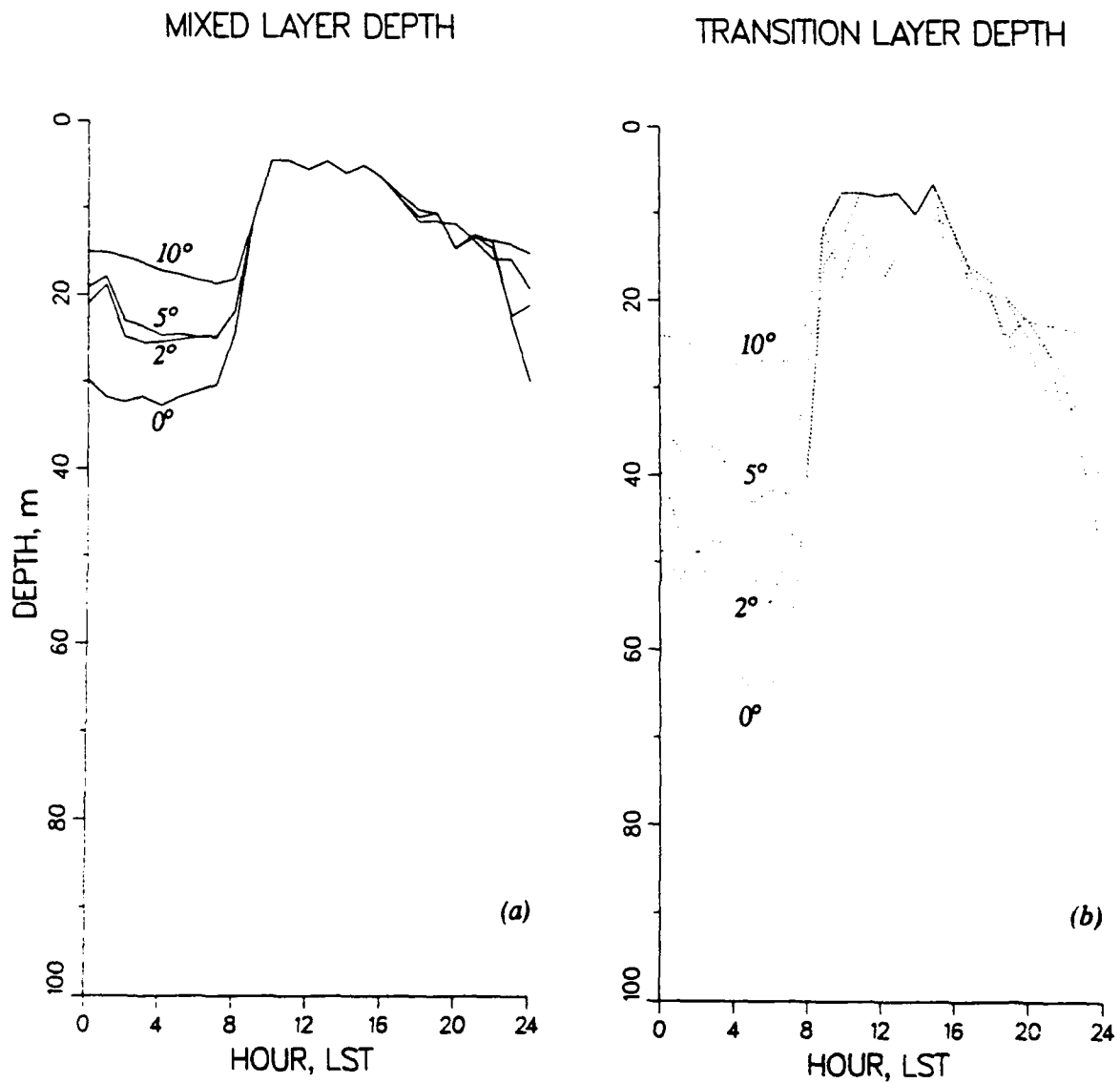


FIGURE 4.10. Variation of (a) mixed layer depth and (b) transition layer depth with latitude.

stratification above the EUC core. However, both surface heating and the vertical advection of heat have magnitudes of about $3\text{ }^{\circ}\text{C m day}^{-1}$, and are important terms in the local heat balance of the equatorial upper ocean.

4.4.2vi. Latitude Dependence

Finally, we would like to note that simply increasing f is sufficient to radically alter the depth to which mixing penetrates, even if we retain other equatorial features (ZPG, EUC, and upwelling). This introduces a meridional velocity and a meridional momentum balance of the form $v_t + wv_z + fu = 0$; the zonal momentum balance has the $-fv$ term added. Notice that the daytime phase of mixing is not affected by the presence of the Coriolis force (Fig. 4.10), while the nighttime phase is significantly altered. The depth of mixing at the equator is thus enhanced by the absence of the Coriolis force as well as by the low stability of the undercurrent. At latitudes as low as 5° from the equator, inertial rotation limits the growth of the diurnal jet enough to significantly affect the amount of momentum available to mix downwards at night. We should note, however, that we have isolated the effect of inertial rotation in this calculation. Observations indicate that the mixed layer generally becomes deeper (rather than shallower) off the equator (Levitus, 1982; Wyrki and Kilonsky, 1984; Peters et al., 1989). The mixed layer is shallowest at the equator due to the meridional circulation which concentrates strong upwelling at the equator (Wyrki, 1981; Muller and Ross, 1987).

4.5. SUMMARY AND CONCLUDING REMARKS

We have found that the nighttime phase of the diurnal cycle in the equatorial upper ocean is strongly affected by the equatorial undercurrent, which causes mixing to be about twice as deep at night as without an undercurrent. Other equatorial ocean features such as the zonal

pressure gradient and persistent upwelling are of little direct importance for the diurnal cycle, though they are of great importance for the long-term maintenance of the mean flow and stratification.

The daytime phase of the diurnal cycle appears to be unaffected by the EUC, and is very similar to the daytime phase observed at mid-latitudes. Solar heating warms and stabilizes a surface layer having a thickness of 5-10 m. The resulting diurnal warming of the surface is only about 0.2°C , but is nevertheless sufficient to insulate the eastward-flowing EUC from vertical mixing and the (generally) westward wind stress. The diurnal cycle of surface heating thus serves to modulate and limit the depth to which the westward wind stress can mix into the eastward-going EUC.

As the warm layer is erased by nighttime cooling, vertical mixing and the wind stress can penetrate well into the upper EUC given only moderate wind stress (0.05 Pa). This produces very deep mixing in a thick transition layer that extends to about 70 m, about twice the depth of the mixed layer. The westward wind stress penetrates to about the same depth. In the absence of solar heating, the model suggests that the nighttime structure would occur around the clock, or until the EUC was erased. This is consistent with the results of Pacanowski and Philander (1981) and Schopf and Cane (1983), who found that simulations of the equatorial ocean which did not include a mean surface heat flux could not maintain an EUC. Here we have found that the diurnal cycle in solar heating determines the local vertical structure above the core of the EUC. The diurnal cycle in vertical mixing is thus an important element in the overall heat and momentum balances in that layer, and by extension, for the equatorial region as a whole.

Chapter 5

Tropic Heat Case Studies

In this chapter, the equatorial upper ocean model described in Chapter 4 is compared to observations made during the TROPIC HEAT field experiments. In Section 5.1 we summarize the historical motivation for the dissipation measurements made during the TROPIC HEAT experiments and the major findings. A method for estimating dissipation from the model is described in Section 5.2. In Section 5.3, we present a detailed comparison to the observations of the first TROPIC HEAT experiment, which took place in 1984 and has been thoroughly described in published papers (Gregg et al., 1985; Moum and Caldwell, 1985; Chereskin et al., 1986; Toole et al., 1987; Niiler, 1987; Peters et al., 1988; Moum et al., 1989; Dillon et al., 1989). Fewer papers on the 1987 TROPIC HEAT experiment have appeared at this time, so that our comparison to these observations in Section 5.4 is more qualitative in nature. In Section 5.5 we discuss how dissipation varies with wind stress, surface heating, and the Undercurrent in our simulations, and in Section 5.6 a concluding summary is presented.

5.1 MOTIVATION FOR THE TROPIC HEAT EXPERIMENT

Before the TROPIC HEAT observational program, relatively few turbulence measurements had been made at the equator. These measurements, from the central Pacific and Atlantic oceans, showed strong turbulence in the highly-sheared zones above and below the Undercurrent core (Gregg, 1976; Crawford and Osborn, 1979). The strong turbulence above the core appeared to be narrowly confined to the equator (Figure 5.1), but lack of extensive data made this conclusion uncertain. Small-scale turbulence plays an important role in the equatorial upper ocean because it reflects how wind stress is mixed into the

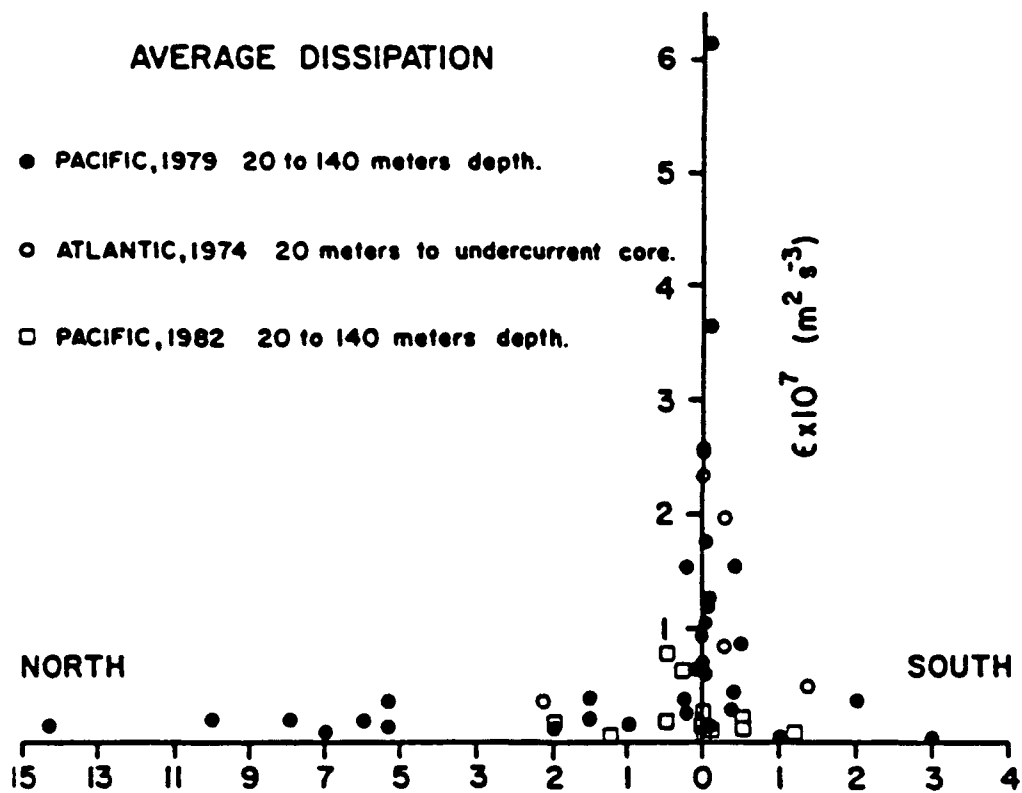


FIGURE 5.1. Average dissipation vs. latitude in the Atlantic and Pacific oceans. Originally from Crawford (1982). The 1982 data was added by Moum et al. (1986), from which this figure is taken.

upper water column to balance the zonal pressure gradient. While the wind stress profile cannot be measured, the turbulent fluctuations of velocity and temperature that reflect small-scale mixing can be. These fluctuations are measured by microstructure profilers and are usually expressed in terms of the turbulent dissipation of mechanical energy, ϵ . Within the water column, dissipation has the units W kg^{-1} , or $\text{m}^2 \text{s}^{-3}$. Values of $10^{-7} \text{ W kg}^{-1}$ are typical of the intense mixing in wind-driven surface mixed layers, while values several decades lower are typical "background" values away from boundaries in the interior of the ocean (Gargett, 1984; Gregg, 1987).

Dissipation is measured using a dropped sensor such as the Advanced Microstructure Profiler (AMP), the Multi-Scale Profiler (MSP), or the Rapid Sampling Vertical Profiler (RSVP). As the instrument falls, it measures a time series of the small fluctuations in the velocity field, u' , that are due to turbulence and are much smaller than the speed with which the instrument falls, W . Because $W \gg u'$, it can be assumed that the turbulence field does not change as it is being measured, or that the instrument is measuring a "frozen" turbulence field. Using this assumption, $\partial u'/\partial t = W \partial u'/\partial z$, and the signal is recorded directly as $\partial u'/\partial z$. These instruments are thus often referred to as "shear probes". Assuming isotropic turbulence, dissipation is then calculated from the measurements as $\epsilon = \frac{15}{2} \nu \langle (\frac{du'}{dz})^2 \rangle$, where ν is kinematic molecular viscosity, and the angled brackets indicate a Reynolds' average. Sources of error in this estimate of turbulence are errors in measuring u' and in estimating W , as well as the assumption of isotropic turbulence, which alone can introduce an error of 50%. Individual estimates of ϵ are from this measurement method are considered to be known within a factor of 2 (Oakey and Elliott, 1982; Peters et al, 1988).

The intense turbulence that had been measured at the equator was thought to be modulated principally by the annual cycle in twenty-one day instability waves. The goal of the

TROPIC HEAT experiments was to measure this variability, with one cruise in the late fall, when the waves are strongest, and a second cruise in the spring, when the waves are weakest. The fall cruise took place in 1984, and the spring cruise in 1987.

During the 1984 TROPIC HEAT experiment the Undercurrent and twenty-one day instability waves were at their annual maximum. Wind stress was fairly strong, averaging -0.10 Pa (twice the climatological mean) and the cold tongue was well developed, with average sea surface temperatures of 25°C . The principal result of the 1984 TROPIC HEAT experiment was the discovery of a diurnal cycle in turbulent dissipation extending to 70-80 m, much deeper than the 30-40 m maximum mixed layer depth. Large values of dissipation of order 10^{-7} W kg^{-1} occurred at night below the mixed layer, and tended to be intermittent, vertically coherent, and were often greater than values of dissipation that occur within the mixed layer at the same time (see Figure 5.2). The 1984 TROPIC HEAT measurements also confirmed the equatorial maximum in dissipation, and peaks in ϵ coincided with the high-shear zone above the core of the Undercurrent.

The 1987 TROPIC HEAT experiment, on the other hand, took place when the Undercurrent and instability waves were at their annual minimum. This was reinforced by a moderate El Nino which occurred during the spring of 1987. Wind stress was light, 0.25 Pa westward on average at 140°W , and the Undercurrent was in general weaker and shallower than in 1984. The diurnal cycle in surface heating was about the same as in 1984. The diurnal cycle of mixing was weaker than before, with dissipation bursts to 50-60 m, though again this was about twice as deep as the maximum mixed layer thickness of 25-30 m. It is unclear whether the weaker diurnal cycle was due to the weaker wind or the weaker Undercurrent. A major problem in interpreting the 1987 results and comparing them to the 1984 experiment has been separating out the relative contributions of the wind and the Undercurrent.

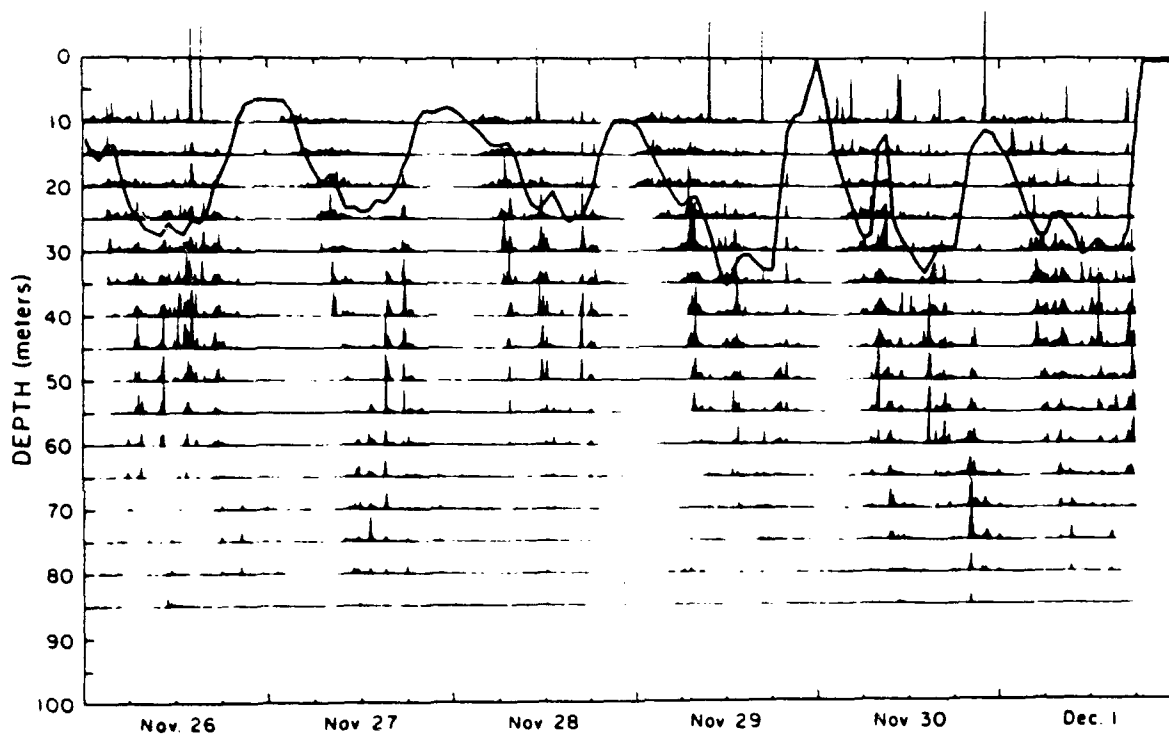


FIGURE 5.2. Dissipation averaged over 5-m depth intervals and plotted as a time series over the last 6 days of the 1984 TROPIC HEAT experiment, from Moum et al. (1986). The solid line is the base of the surface mixed layer, and shows a clear diurnal cycle that is in phase with the surface heating. The uppermost series of dissipation, at 10 m, has been averaged over 7.5 to 12.5 m and may occasionally be contaminated by ship wake or instrument instability as it begins its free fall near the surface (Moum et al., 1986); notice the occasional large spikes in that series.

5.2 ESTIMATING DISSIPATION FROM THE EQUATORIAL UPPER OCEAN MODEL

To directly compare the model formulated in Chapter 4 to the TROPIC HEAT dissipation measurements, we have calculated the turbulent dissipation implicit in the mixing scheme. If one assumes steady, homogeneous, vertically-sheared turbulence, the turbulent dissipation rate, ϵ , is equal to the sum of buoyancy and shear production (Phillips, 1980),

$$\epsilon = \langle w'b' \rangle - \langle w'u' \rangle u_z = \alpha g F - \tau u_z \quad (5.1)$$

where b is the buoyancy of a parcel, $-g\rho/\rho_o$, and the angle brackets indicate Reynolds' averages.

In our model, the turbulent fluxes of momentum and buoyancy, $\langle w'u' \rangle$ and $\langle w'b' \rangle$, arise solely from the mixing processes (4.2a)-(4.2c), and can be estimated from the changes, δ , in the momentum and temperature profiles produced by mixing within each time step, i.e., from (4.1a) and (4.1b),

$$\langle w'b' \rangle (z) = -\alpha g \int_{z_b}^z \left(\frac{1}{\rho c_p} I_z + \frac{\delta T}{\delta t} + \hat{w} T_z \right) dz \quad (5.2)$$

$$\langle w'u' \rangle (z) = - \int_{z_b}^z \left(\frac{1}{\rho} \hat{P}_x + \frac{\delta u}{\delta t} + \hat{w} u_z \right) dz \quad (5.3)$$

where $z_b = 150$ m (the depth of the model). The flux profiles are used together with the shear of the current profile to calculate ϵ as in (5.1). Shear production of dissipation is the

dominant term in (5.1), and in the model is non-zero only in the transition layer (u_z vanishes in the mixed layer and $\langle w'u' \rangle$ vanishes below the transition layer).

5.3 TROPIC HEAT 1984 SIMULATION

To simulate the 1984 TROPIC HEAT conditions, we forced the model with meteorological measurements from that experiment. Wind and solar heating were measured from the R/V *Wecoma* for 12 days (Moum and Caldwell, 1985) and the R/V *Thompson* for 4¹/₂ days (Peters et al., 1988), see Figure 5.3. The two ships were within 10 nautical miles of each other while they were both on the equator, though they reported slightly different results for turbulent dissipation measurements (see Dillon et al., 1989, for a direct comparison).

5.3.1 The Diurnal Cycle of Current and Temperature

The simulated diurnal cycle of current and temperature in the model had a typical range of 0.19°C and 0.16 m s⁻¹ at the surface for these conditions (Figure 5.4). This compares reasonably well to the surface warming of 0.15 to 0.30°C during TROPIC HEAT 1984 reported by Moum et al. (1989). As discussed in Chapter 4, it is also consistent with the amount of warming and acceleration over one day with the same surface forcing at mid-latitudes.

5.3.2 The Diurnal Cycle of Mixing and Dissipation

While the diurnal cycle in current and temperature are relatively small, the diurnal cycle in mixing and dissipation that accompany it are very large. The model reproduces the striking diurnal cycle and depth range of turbulent dissipation (Figure 5.5). Note the general agreement between the modeled and observed diurnal cycle of mixing and dissipation,

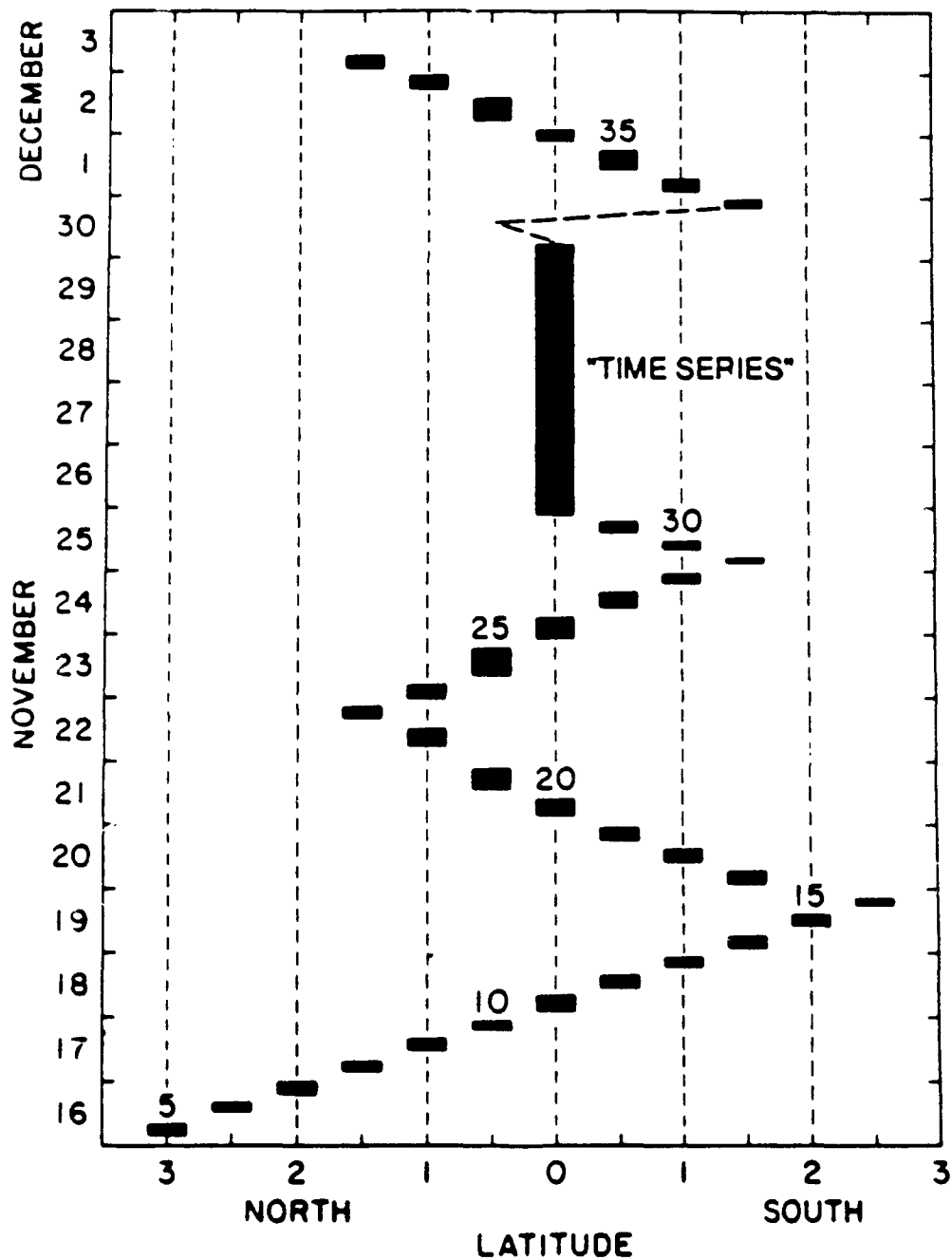


FIGURE 5.3. Position of the R/V *Thompson* during the 1984 TROPIC HEAT experiment, from Peters et al. (1988). The R/V *Wecoma* maintained a position on the equator from November 20 to December 1. Our four-day simulations correspond to the time that both ships were on the equator, and our 12-day simulations correspond to the time that the *Wecoma* was on the equator.

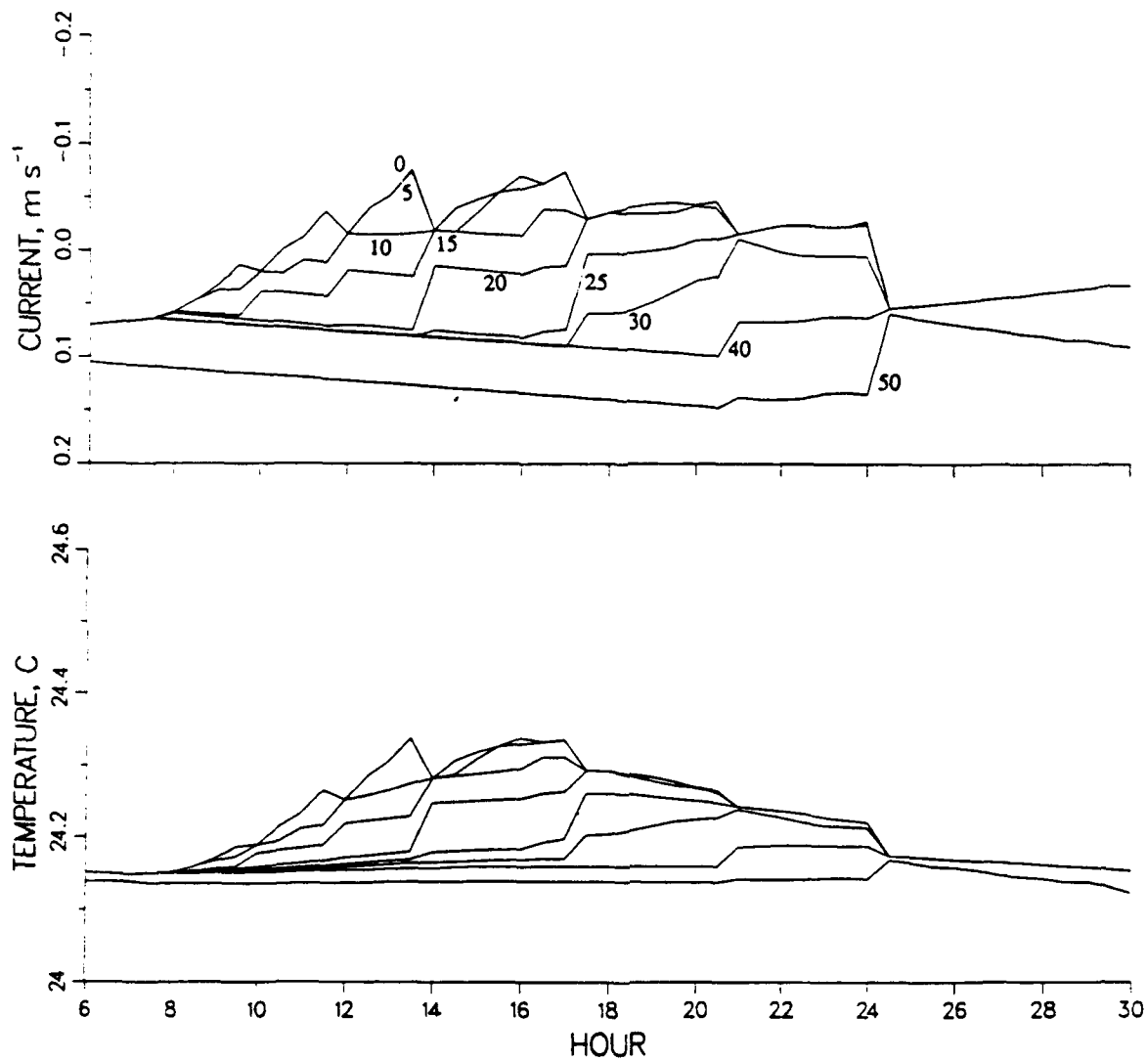


FIGURE 5.4. Simulated time series of current and temperature at depths of 0, 5, 10, 15, 20, 25, 30, and 40 m for a typical day with a wind stress of -0.10 Pa , the mean during the 1984 TROPIC HEAT field experiment. The amplitude of the diurnal cycle is 0.16 m s^{-1} and 0.19°C .

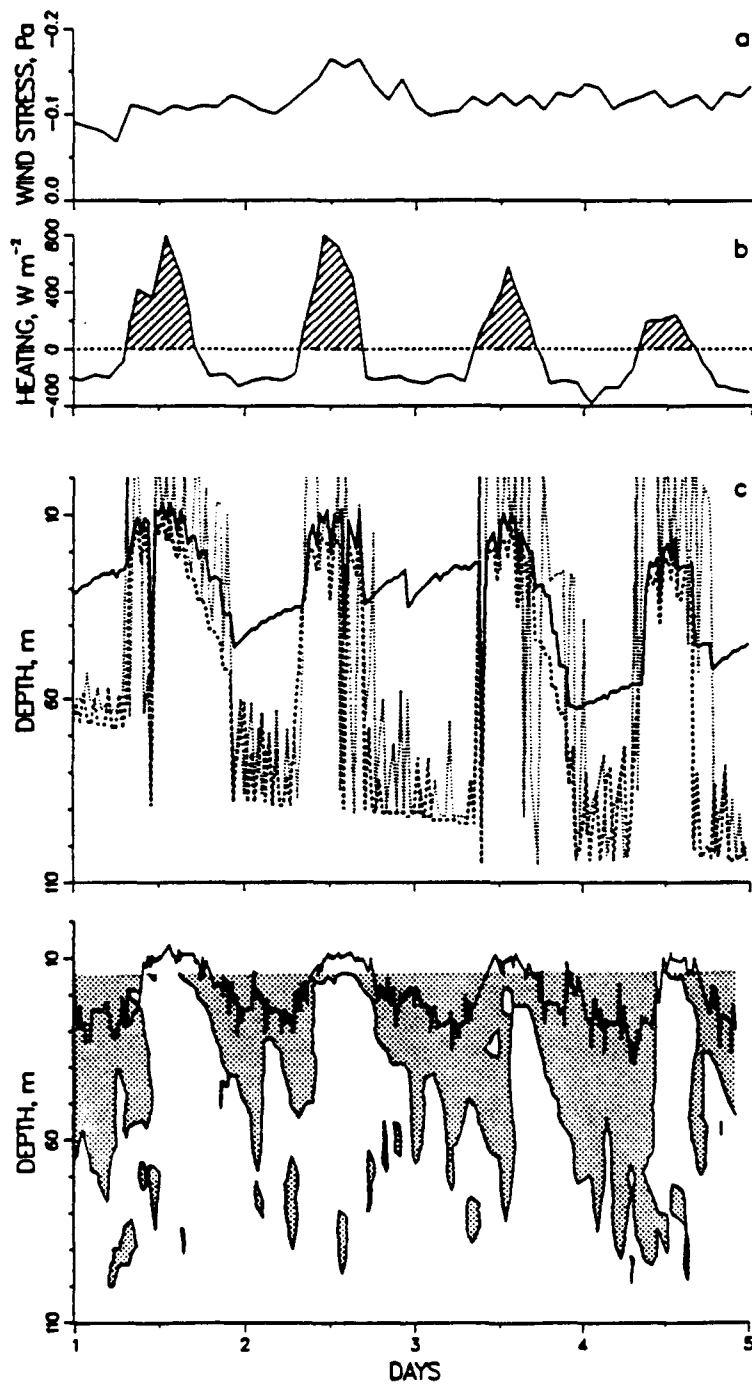


FIGURE 5.5. Meteorological forcing and simulated and observed mixing and dissipation for four days of the 1984 TROPIC HEAT experiment; model days 1-5 correspond to November 26-29, 1984: (a) wind stress observed from the R/V *Wecoma* (Moum et al., 1989), positive is westward, the direction of prevailing winds; (b) surface heat flux observed from the R/V *Thompson* (Peters et al., 1988), positive is into ocean; (c) simulated mixed layer depth, h (solid line), transition layer depth, d (heavy dashed line), and maximum depth where dissipation, ϵ , is greater than $10^{-7} \text{ W kg}^{-1}$ (light dotted line); (d) observed mixed layer depth (solid line) and region where hourly averaged dissipation is greater than $10^{-7} \text{ W kg}^{-1}$ (stippled area), from Peters and Gregg (1987).

though the modeled mixed layer is deeper than the observed mixed layer on the night and early morning of days 1-2 and 3-4. Notice also the close correspondence between the model's transition layer depth and the depth at which the model's dissipation drops below $10^{-7} \text{ W kg}^{-1}$.

5.3.2i. Daytime Dissipation

Overall dissipation values during the day are small, about $10^{-8} \text{ W kg}^{-1}$ in the observations and even smaller in the simulations (see Figures 5.5, 5.6 and 5.7). The primary source of turbulent energy is the work done by wind stress on the diurnal jet, $\tau_s \Delta u$, (rather than free convection, which is very small), and so during the day dissipation is unremarkable. Large values are confined to the upper 10-20 m, and are comparable to observations of dissipation at mid-latitudes under conditions of similar heating and wind stress (Lombardo and Gregg, 1989; Shay and Gregg, 1986).

The hourly values of modeled dissipation during the day are intermittent in a way that is not always realistic. Most of the time modeled dissipation is zero during the day, though observed values are typically $10^{-8} \text{ W kg}^{-1}$ (Fig. 5.7). Occasionally the model generates sudden mixing and extreme dissipation events, from which it then rapidly recovers. These occur near midday on days 1, 2 and 3 (Figure 5.5), when the wind stress is absorbed in a very thin layer, but not on day 4, when the daytime mixed layer is slightly deeper because of lower solar heating. We believe that both the occasional extreme values of daytime dissipation (and the associated mixing events) and the otherwise vanishing daytime dissipation are two aspects of the same shortcoming, namely, that the model does not include stochastic motions (such as internal waves) which in the ocean cause a background non-zero dissipation at all times and would presumably initiate mixing before extreme events occur.

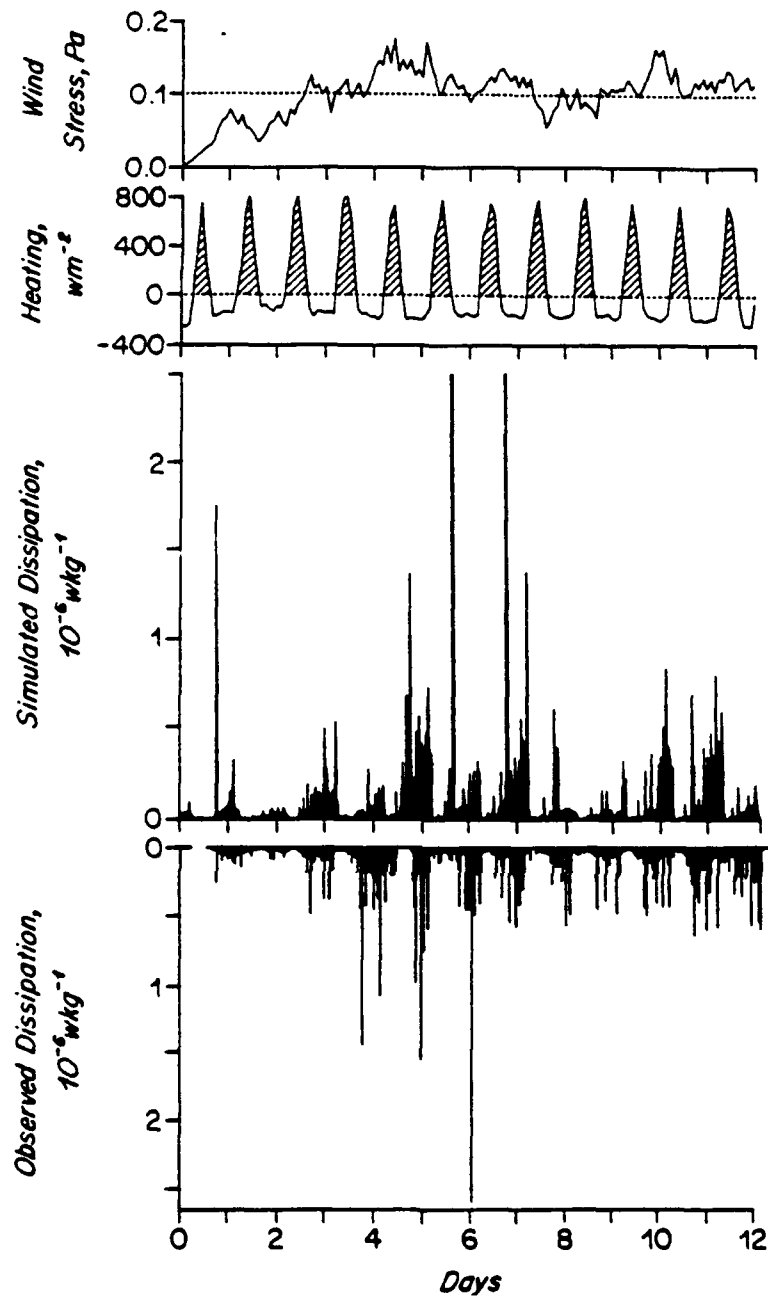


FIGURE 5.6. Meteorological forcing and simulated and observed dissipation for 12 days of the 1984 TROPIC HEAT experiment; model days 0-12 correspond to November 19-December 1, 1984: (a) wind stress, from Moum et al. (1989), ramped from zero to the observed value over the first day, positive is westward, the direction of prevailing winds; (b) net solar heating, from Moum et al. (1989), positive is into ocean; (c) simulated 10-110 m average turbulent dissipation; (d) observed 10-110 m average dissipation, from Moum et al. (1989).

Notice that the model reproduces the diurnal cycle and the intermittent character of the observed dissipation. The hourly intermittence is, however, uncorrelated with that seen in the data. On the afternoons of the fifth and sixth days, simulated dissipation is off the scale and has values of 8.6 and 4.2×10^{-6} , respectively. These large amounts of dissipation are produced by sudden deepenings of the mixed layer that sometimes occur as cooling begins in the afternoon which are discussed further in the text.

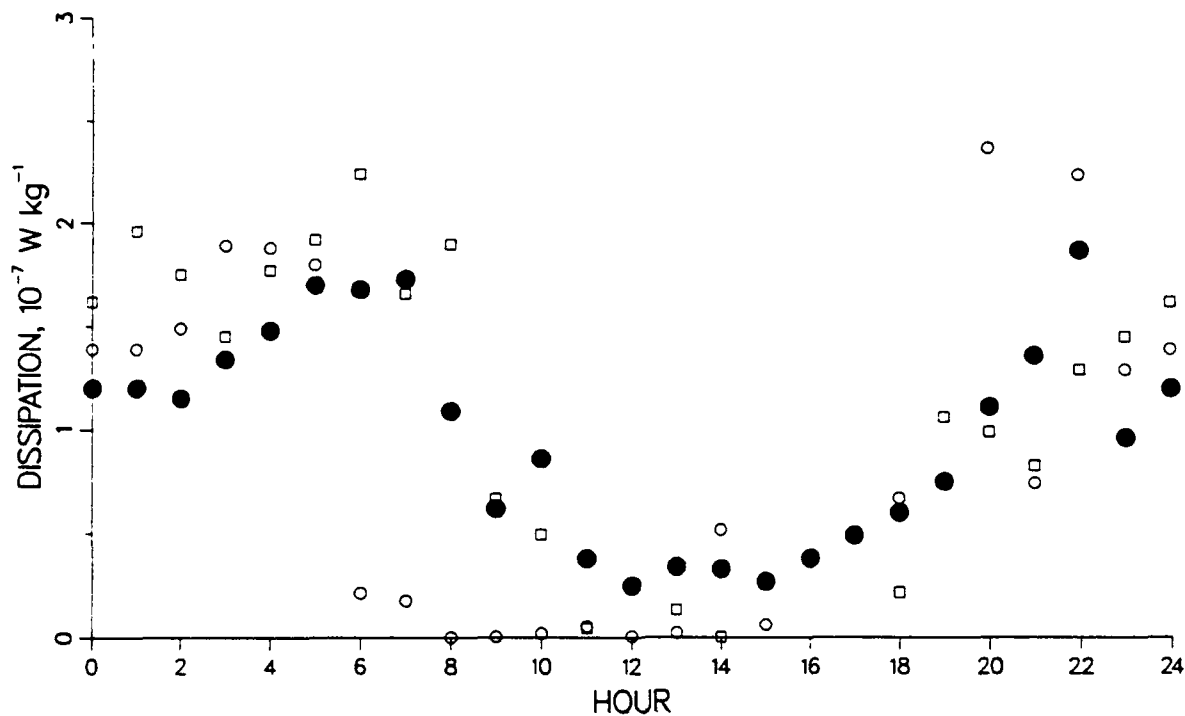


FIGURE 5.7. Ensemble averages of turbulent dissipation averaged between 10-100 m for each hour of the day over a period of several days. Solid dots are the average dissipation observed during the 12 days of the 1984 TROPIC HEAT experiment (November 19-December 1, 1984) from the R/V Wecoma (Moum et al., 1989). Two sets of simulated dissipation are shown: *open dots* are from a 12-day model integration forced by wind and heating observed from the Wecoma; *open squares* are from a 5-day model integration forced by wind and heating observed from the R/V Thompson (10 km away from the Wecoma) during November 27-December 1, 1984. It is unclear which is more appropriate to compare with observations. By the end of 12 days the model's EUC profile begins to differ from the initial realistic profile; this may affect the accuracy of the simulation (apparently most severely in the early hours of the warming phase between 0600 and 1000 LST). Differences between the two simulations give an indication of the sensitivity of simulated dissipation to small differences in surface heating and wind stress.

A few values of simulated dissipation are very large and lie off the graph. In the 12-day simulation, at hours 16, 17, and 19, dissipation has values of 4.1 , 9.3 , and $6.6 \times 10^{-7} \text{ W kg}^{-1}$, respectively. In the 5-day simulation, at hours 12, 16, and 17, dissipation has values of 5.1 , 5.2 , and $8.8 \times 10^{-7} \text{ W kg}^{-1}$ (at hour 15 the 5-day average simulated dissipation is $0.3 \times 10^{-7} \text{ W kg}^{-1}$, and overlays the observed value). The high values of dissipation are caused by sudden mixing events in the model as the mixed layer begins its diurnal deepening during the afternoon. This behavior in the model is discussed further in the text.

5.3.2ii. Nighttime Dissipation

During the late afternoon and early evening, continued wind-mixing and cooling act to destabilize the near-surface layer and form a nighttime mixed layer that has a thickness of about 50 m by the end of the night (Figure 5.5). The dissipation that occurs as the westward momentum of the diurnal jet mixes into the eastward-flowing EUC at night is remarkable; the model simulations give $O(2 \times 10^{-7} \text{ W kg}^{-1})$, consistent with observed values (Figure 5.7). The nighttime values of dissipation are almost an order of magnitude larger than the daytime values, and much larger than the dissipation found in mid-latitude sites with otherwise similar surface forcing. In the model, dissipation is confined to the transition layer, which is 40-50 m thick during the night (about the same thickness as the surface mixed layer). Thus, mixing and dissipation occur down to a depth of 80-90 m at night, also consistent with the observations (see Figure 5.5). As we will discuss in Section 5.5, the depth and amplitude of the dissipation are sensitive to the structure of the EUC and, for example, if the EUC is removed, the overall pattern of dissipation becomes more like that of a mid-latitude site.

We should note that the average dissipation shown in Figures 5.6 and 5.7 is a robust result of the model because it is an $O(1)$ term in the mean energy balance. Thus, any model that includes some form of an EUC and also gives a reasonably good simulation of the depth of mixing (which requires only a shear flow stability condition) would give a similar result for the overall dissipation, e.g., the models of Mellor and Durbin (1975) or Kondo et al. (1979) should do as well as this one if run under similar conditions.

The diurnal variation of dissipation is modeled well in some respects, and there is also a rough day-to-day correspondence of high and low levels of dissipation that correspond with high and low wind stresses (Figure 5.6). However the short term (hourly) variation

in dissipation is another matter entirely. Both the observations and the model show extreme hourly intermittence of dissipation. In the model, intermittence is somewhat sensitive to the size of the time step, but we suspect that the main difference between the intermittence of simulated and observed dissipation is due to the difference in the initiation of mixing events, as touched upon already. In the model, the *mean* profile has to be brought to the stability limit for mixing to occur. The only currents in the model are associated with the diurnal cycle and the EUC; in the ocean there are other currents and internal waves which may have appreciable vertical shear. It is likely that internal waves are the trigger for instability and mixing events in the ocean, and can cause mixing in a mean profile that is approaching but not quite at a stability limit. Thus the trigger for instabilities is probably different in the model than in the ocean. To the extent that internal waves play such a role in the ocean, the hourly intermittence of dissipation probably can not be modeled as a deterministic process the way that the diurnal variation evidently can be.

5.3.3 Mean Zonal Momentum Balance

This one-dimensional model does not fully simulate the zonal momentum balance at the equator since it cannot include either a dynamic ZPG or dynamic upwelling, and does not include the zonal convergence of zonal momentum, uu_x , which is also a significant term (Bryden and Brady, 1985). However, since the dominant balance in the equatorial upper ocean is between the turbulent stress divergence and the pressure gradient (McCreary, 1981), it may nonetheless be worthwhile to examine the momentum balance that the model does attain, mainly to note the depth to which the westward momentum flux of the wind stress penetrates. Dillon et al. (1989) emphasized that even if a balance existed between the depth-integrated ZPG and westward stress, there might not be even an approximate balance between the ZPG and stress divergence at most depths. The ZPG has a depth scale (e-

folding) of about 100 m that is well-defined from field data (Mangum and Hayes, 1984; Bryden and Brady, 1985), while Dillon et al. (1989) inferred that the penetration depth for wind stress is only about 40 m (e-folding).

The 12-day average momentum balance of the 1984 TROPIC HEAT simulation is shown in Figure 5.8 as profiles of the four terms that make up the model's zonal momentum balance (4.1a). Recall that the ZPG is imposed and held fixed, and that the upwelling amplitude and vertical profile are also imposed. In this simulation, the westward stress supplied by the wind is primarily balanced by the opposing ZPG and by local acceleration. Vertical advection plays a minor role in the momentum balance, though its relative importance would increase for lighter winds. Here the wind stress penetrates to about 100 m depth, which is deeper than inferred by Dillon et al. (1989) for these conditions, and considerably greater than the depth of the surface mixed layer. The depth of stress penetration is, in the model, the same as the depth of the vertical mixing and significant dissipation. The simulated stress divergence is greatest at about 75 m depth, though the stress itself is monotonic from the surface downward. While this simulation suggests that the stress may penetrate to surprisingly large depth, these results can at best only partially resolve the questions raised by Dillon et al. (1989) as there is still an acceleration in the model at most depths; the acceleration is eastward above 30 m, westward between 30 m and the core of the EUC, and eastward again below the core of the EUC. This acceleration would presumably be balanced by the non-local processes we have not included; for example, twenty-one day waves on the equator vertically redistribute horizontal momentum in a way that partially balances the residual acceleration in this simulation (Brady, 1990). However, recent studies have also suggested that the zonal momentum balance at the equator is not in a steady balance over short time scales (Dillon et al., 1989; Hebert et al., 1991), so some of the residual acceleration in this simulation may be a realistic feature of the equatorial ocean.

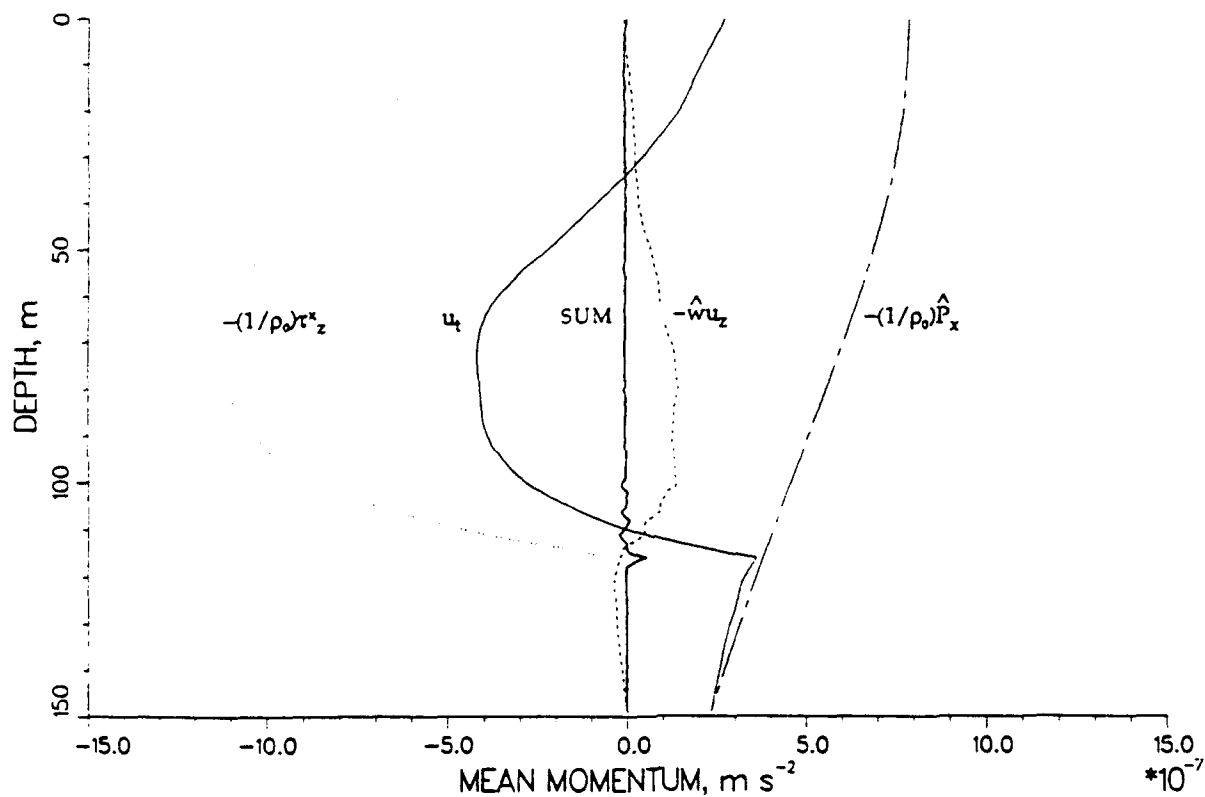


FIGURE 5.8. Mean zonal momentum balance profile (averaged over 12 days) for the 1984 TROPIC HEAT simulation. The solid line is the local acceleration, u_t ; the dotted line is the vertical divergence of zonal wind stress, $-(1/\rho_0)\tau_x^z$; the chain-dashed line is the zonal pressure gradient, $-(1/\rho_0)\hat{P}_x$; the dashed line is the upwelling of zonal momentum, $-\hat{w}u_z$; and the heavy line is the sum of all these. Notice that the stress divergence penetrates to nearly the depth of the Undercurrent core at 110 m.

5.4 TROPIC HEAT 1987 SIMULATIONS

The 1987 TROPIC HEAT experiment had a slightly different cruise plan than the 1984 experiment. While the R/V *Thompson* maintained a station on the equator near 140°W, the R/V *Wecoma* steamed eastward along the equator from 140° to 109°W during early April. The longitudinal equatorial section from the *Wecoma* was divided into three legs for analysis, each leg spanning about 9° of longitude and about 4 days of time. Some of the *Wecoma* data has been made available to us by Jim Moum and Dave Hebert of Oregon State University (prior to its publication) so we could run simulations of the 1987 observations. In this section we describe the results of these simulations and compare them to the observations that are available. The comparison here is less extensive than the 1984 case, as the 1987 observations have not been analyzed as thoroughly, but gives an indication of the seasonal and interannual variability in the upper equatorial ocean.

Simulations for each of the three legs of the 1987 TROPIC HEAT experiment were forced with an observed time series of surface heating and wind stress, and initialized with the mean Undercurrent over that leg (like the 1984 simulations). The zonal pressure gradient relative to 150 m was estimated for each leg by Dave Hebert. Upwelling is the same as in all previous simulations.

5.4.1. Diurnal Cycle of Current and Temperature near 140°W

The simulated diurnal cycle of current and temperature during Leg 1 near 140°W had a typical range of 0.10 m s⁻¹ and 0.45°C at the surface (Figure 5.9). This diurnal surface warming compares reasonably well to the surface warming observed at 140°W of up to 1.0°C but averaging 0.33°C in May-June 1987 (McPhaden and Peters, 1991). The observations also show a sharp rise in surface temperature between morning (7-10 am) and

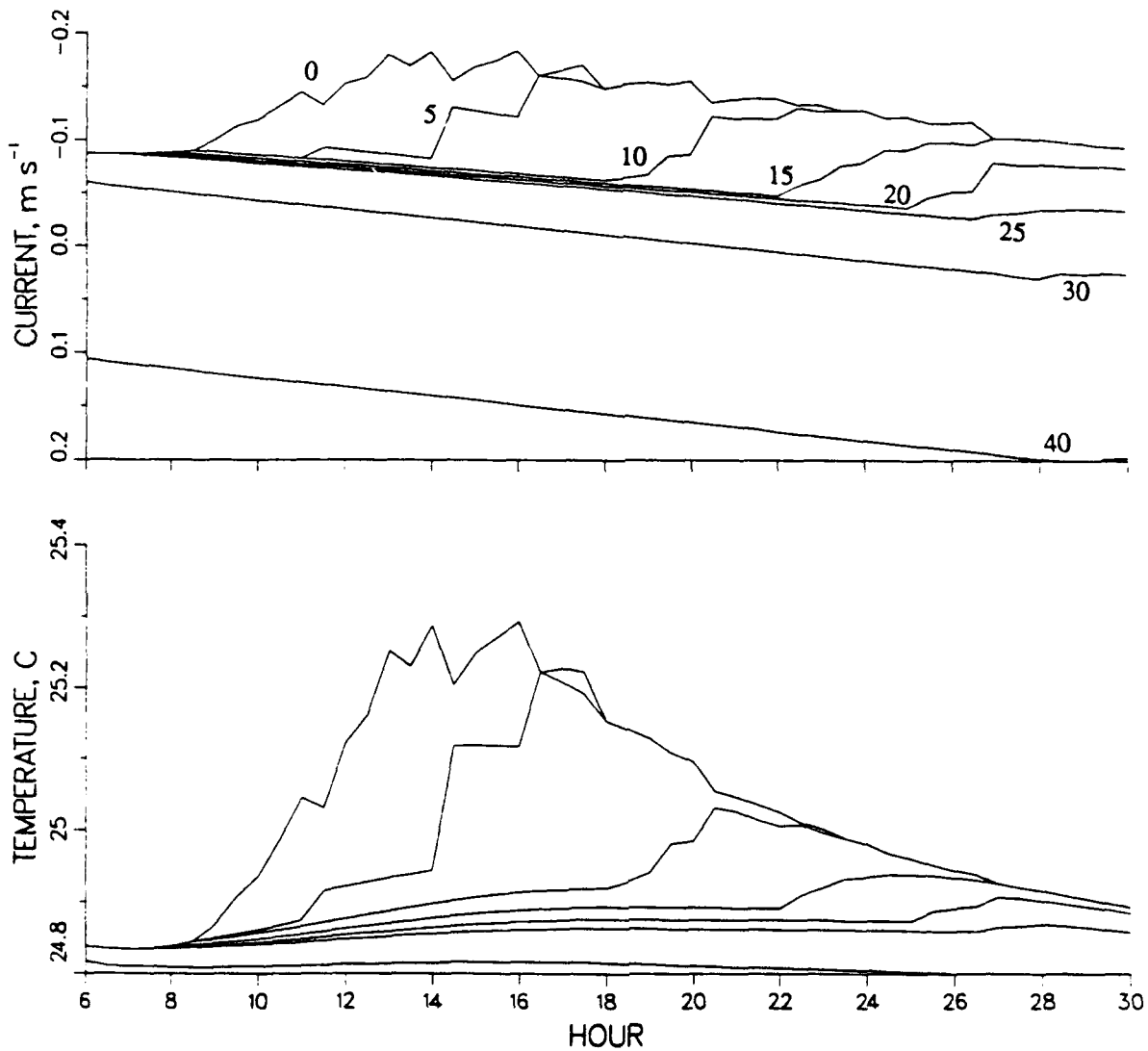


FIGURE 5.9. Simulated time series of current and temperature at depths of 0, 5, 10, 15, 20, 25, 30, and 40 m for a typical day with a wind stress of -0.025 Pa, the mean during early part of the 1987 TROPIC HEAT experiment. The amplitude of the diurnal cycle is 0.10 m s⁻¹ and 0.45°C .

early afternoon (1-4 pm) followed by a gradual cooling throughout the rest of the evening and early morning (McPhaden and Peters, 1991); temperatures at 10 m also tend to lag the surface temperature, and the maximum temperature at 10 m occurs in the early evening (7-10 pm). Both of these features are evident in the model (Figure 5.9), and also are typical of diurnal warming at mid-latitudes, particularly for light winds and strong heating such as these.

5.4.2. Diurnal Cycle of Mixing and Dissipation along the Equator, 140° to 110°W

The three legs of the equatorial longitudinal section were fairly different from each other. Leg 1 was most like the 1984 conditions in that both the wind and the zonal pressure gradient pointed in their climatological directions. The wind blew from the east with an average value of -0.025 Pa, about one quarter as large as the 1984 TROPIC HEAT mean, and the ZPG acted to accelerate the Undercurrent in an eastward direction. Further east, in Legs 2 and 3, the effect of the El Nino was more pronounced. Winds reversed direction and blew from the west, and both of these legs had a very light average wind stress of $+0.014$ Pa. The ZPG also changed sign in these legs, and the Undercurrent became shallower and weaker further east along the equator. The differences between the three legs were reflected in very different observations of mixing.

5.4.2i. Leg 1, 140° to 132°W

This leg was most like the 1984 observations in that an obvious diurnal cycle in mixing was observed (Hebert, personal communication). From the *Thompson*, near 140°W the mixed layer was estimated to be about 5 m deep during the day and about 25 m deep at night, while $O(10^{-7} \text{ W kg}^{-1})$ dissipation rates reached down to 40-50 m at night (Peters, personal communication). In observations from the PMEL mooring at 140°W slightly later

in the spring, May-June 1987, the isothermal layer was 30-34 m deep between 1-10 am (McPhaden and Peters, 1991). The model agrees reasonably well with these observations (Figure 5.10), both in the diurnal variation of the depth of mixing and in the hours of day when mixed layer depths are greatest.

5.4.2ii. Legs 2 and 3, 130° to 110°W

Legs 2 and 3 were very different from the 1984 observations in that almost no diurnal cycle of dissipation was observed. During Leg 2 there was almost no diurnal cycle in mixed layer depth, presumably due to weak solar heating during that leg, and during Leg 3 only a weak diurnal cycle in mixed layer depth was seen (Hebert, personal communication). No actual values of observed mixed layer depth are yet available from these legs. The model predicts a weak diurnal cycle of mixing for both of these legs (Figure 5.10), and it seems that this model is successful in predicting the diurnal penetration of mixing at the equator for a wide variety of conditions.

5.4.3 The Relative Role of Wind Stress and the Undercurrent in the 1987 TROPIC HEAT Observations

The 1987 TROPIC HEAT observations raised many questions. Why was the diurnal cycle of mixing so much weaker than in 1984? Since both the Undercurrent and the wind were very different than in 1984, it has been difficult to attribute the weaker diurnal cycle of mixing to any particular cause.

An interesting case to examine is one where the model is forced at the surface by the strong wind stress (average value -0.10 Pa) of the 1984 TROPIC HEAT experiment, but is initialized with the relatively weak mean Undercurrent of the 1987 TROPIC HEAT

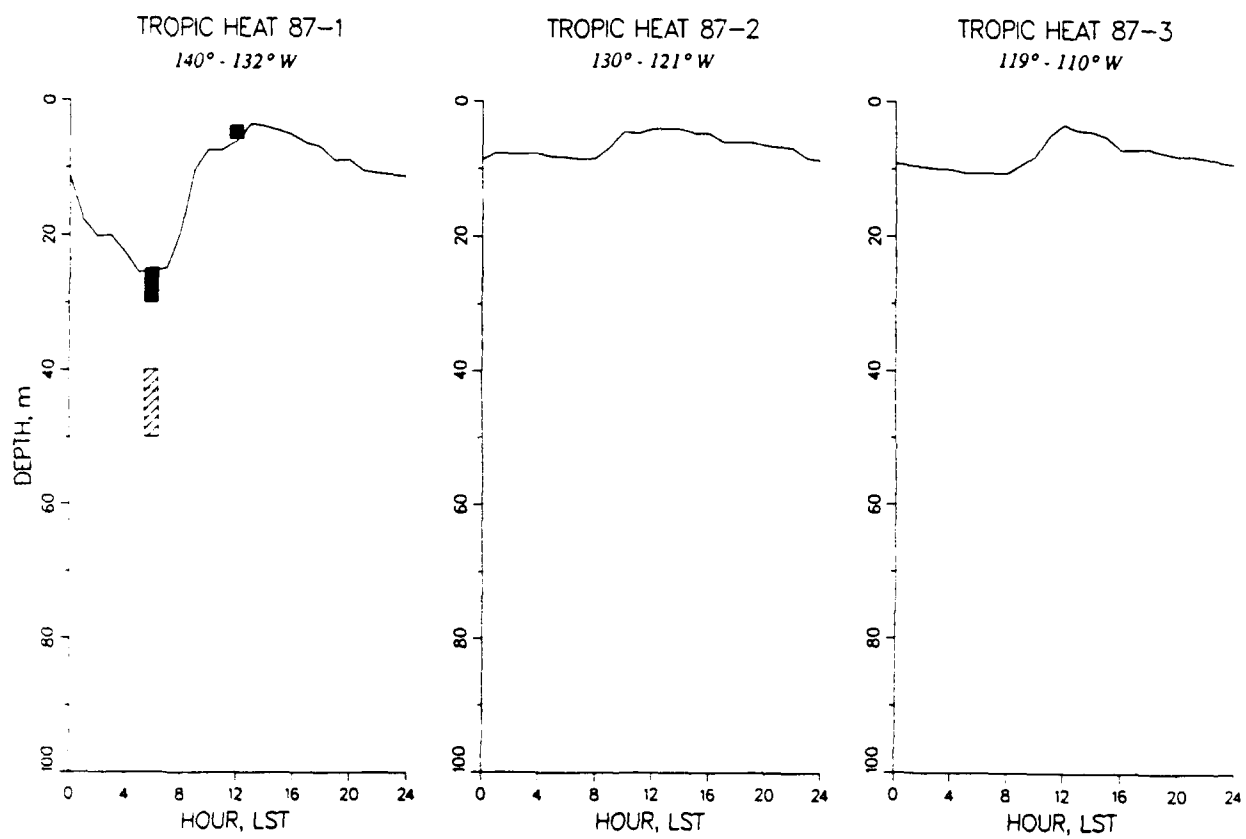


FIGURE 5.10. Ensemble averages of simulated mixed layer depth and transition layer depth for the 3 legs of the 1987 TROPIC HEAT experiment. Each figure represents an average over about 4 days and about 9° of longitude as the *Wecoma* steamed east along the equator from 140°W to 110°W.

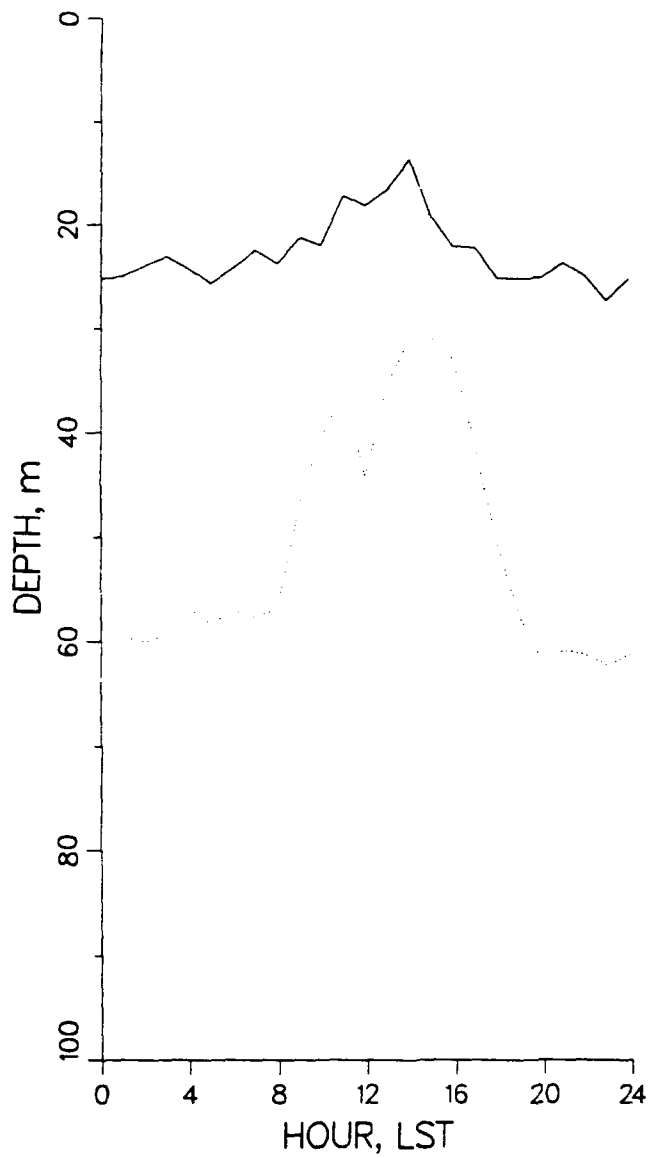


FIGURE 5.11. Ensemble average of simulated mixed layer depth, h (solid line), and transition layer depth, d (dotted line), over 4 days using the 1987 TROPIC HEAT (Leg 1) observed mean Undercurrent and the 1984 TROPIC HEAT observed wind stress.

experiment (Leg 1). Results from this case are summarized in Figure 5.11 and Table 5.1. Note that the mixing penetrates slightly deeper than when the much lighter wind stress (averaging -0.02 Pa) observed during Leg 1 of the 1987 TROPIC HEAT is used. The dissipation, however, is as large as during the 1984 TROPIC HEAT experiment. This implies that the wind stress, and not the shear of the EUC, was primarily responsible for the lower dissipation observed in 1987. On the other hand, the shallower mixing observed in 1987 seems to be due to the shallower and weaker structure of the Undercurrent.

TABLE 5.1.

Overall simulated dissipation in units of 10^{-7} W kg^{-1} for different combinations of wind stress and Undercurrent. These simulations suggest that the lower values of dissipation observed in 1987 were due to weaker wind stress rather than the weaker and shallower Undercurrent.

	1984 τ	1987 τ
1984 EUC	1.87	0.15
1987 EUC	1.84	0.16

5.5 DEPENDENCE OF TURBULENT DISSIPATION ON SURFACE HEATING, WIND STRESS, AND THE EQUATORIAL UNDERCURRENT

Numerical experiments indicate that the depth to which mixing and dissipation extend at night and the overall dissipation level in the model are very sensitive to the surface heat

flux, wind stress, and the EUC (these are discussed further below). As discussed in Chapter 4, a diurnal cycle of solar heating is essential for causing the diurnal cycle of mixing and dissipation. If the insolation is shut off and cooling left untouched at -200 W m^{-2} , for climatological wind stress (0.05 Pa westward) the transition layer and substantial dissipation reach to nearly the core of the EUC after about 3 days, and the overall dissipation is increased by about a factor of 4 from the reference case (which has the same wind stress and heat loss but a diurnally varying insolation, Table 5.2) until the EUC is eventually erased.

Wind stress is crucial in setting the overall level of dissipation. If $\tau_s = 0$, the only source of turbulent energy is free convection due to surface cooling, and the dissipation is several orders of magnitude smaller than observed during the 1984 TROPIC HEAT experiment (Table 5.2). As wind stress increases, the depth-averaged dissipation in the model rises approximately like $\tau_s^{3/2}$, or u_*^3 (Figure 5.12); this holds for both westward and eastward wind stress (though with different ϵ/u_*^3 ratios for each direction) and is consistent with the results of Oakey and Elliott (1982), who found that the turbulent dissipation within the mixed layer scales as u_*^3 . The u_*^3 dependence is reminiscent of the scaling of turbulent dissipation in a logarithmic boundary layer, where turbulence scales like the work done on the water by the wind, or like τu_z , where $u_*^2 = \tau_s/\rho$, and $u_z \sim u_*/\kappa z$ (see Turner, 1973, pp. 128-129). In this model wind stress acts on both the shear of the diurnal jet and on the shear of the upper EUC to produce turbulent dissipation, along with a smaller contribution from buoyant production. Dissipation is therefore lower when τ_s is eastward, because an eastward surface flow decreases the shear of the EUC (this is reflected in a different, lower ϵ/u_*^3 ratio for τ_s eastward). Thus the shear that enters the production term is not solely wind-driven, and the u_*^3 dependence is partly coincidental.

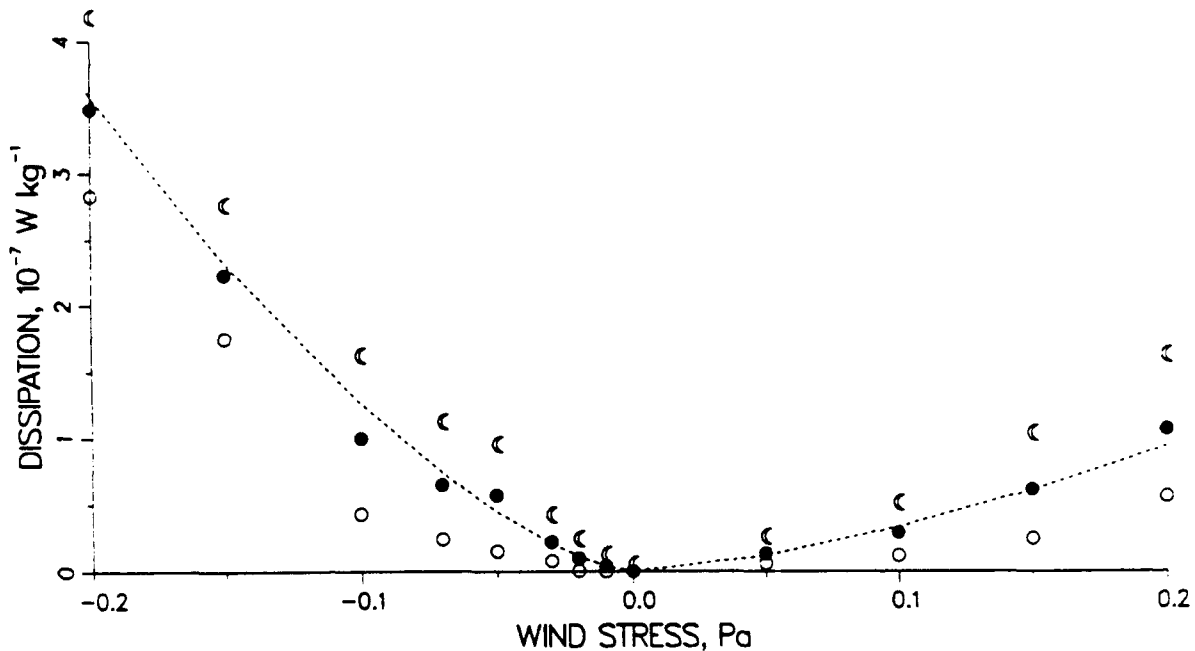


FIGURE 5.12. Variation of overall simulated turbulent dissipation, ϵ (averaged over the model domain, 0 to 150 m, and over 5 days), with wind stress. Positive wind stress is eastward and negative is westward. Prevailing winds on the equator are to the west. The dark circles represent overall average dissipation, the open circles are average dissipation during the daytime, and the crescents are average dissipation at nighttime. Note the consistently higher values at night and lower values during the day.

The dependence of ϵ on τ_s is roughly like $|\tau_s|^{3/2}$, shown as the dashed line, reminiscent of classic turbulence theories which scale ϵ as u_*^3 ($u_* = |\tau_s/\rho|^{1/2}$). The $|\tau_s|^{3/2}$ curve has different ϵ/u_*^3 ratios for $\tau_s < 0$ (west) and $\tau_s > 0$ (east) because dissipation is higher when τ_s is westward and the down-wind flow adds to the shear of the EUC (and lower when τ_s is eastward and the wind acts to decrease the shear of the EUC). For τ_s westward, the ratio is $4.0 \times 10^{-6} \text{ W kg}^{-1} \text{ Pa}^{-3/2}$; for τ_s eastward, the ratio is $1.1 \times 10^{-6} \text{ W kg}^{-1} \text{ Pa}^{-3/2}$. These are comparable to values of $O(10^{-5} \text{ to } 10^{-6} \text{ W kg}^{-1} \text{ Pa}^{-3/2})$ for the upper 8 to 20 m of the mid-latitude ocean (Oakey and Elliott, 1982). However, note that these ϵ/u_*^3 ratios are for depth-averaged dissipation; at the equator high levels of dissipation extend deeper into the water column, so the *total* amount of turbulent dissipation in the equatorial upper ocean is almost an order of magnitude higher than in the mid-latitude upper ocean.

TABLE 5.2.

Variation of overall simulated dissipation with wind stress, surface heating, and the Undercurrent. For ease of comparison to Table 4.2, depths for maximum h (mixed layer depth) and d (transition layer depth) are repeated, and forcing is varied about the climatological mean: $\tau_s = -0.05 \text{ Pa}$, $I_{max} = 1000 \text{ W m}^{-2}$, $L = -200 \text{ W m}^{-2}$; initial EUC core speed = 1.2 m s^{-1} and EUC core depth = 110 m , as in Fig. 4.1; ZPG and upwelling also are as in Fig. 4.1. This standard case is in boldface.

	$\epsilon, \text{ W kg}^{-1}$	$h, \text{ m}$	$d, \text{ m}$
$\tau_s = -0.05 \text{ Pa}$ (climatological mean)	0.57	33	65
$\tau_s = -0.20 \text{ Pa}$	3.48	49	100
$\tau_s = -0.10 \text{ Pa}$ (1984 Tropic Heat mean)	1.00	46	86
$\tau_s = -0.025 \text{ Pa}$ (1987 Tropic Heat mean)	0.15	26	45
$\tau_s = 0$	**	12	12
$I_{max} = 1200 \text{ W m}^{-2}$	0.38	32	56
$I_{max} = 800 \text{ W m}^{-2}$	0.79	35	68
$I_{max} = 600 \text{ W m}^{-2}$	0.97	43	72
$I_{max} = 0$	2.00	28	82
EUC core 0.90 m s^{-1}	0.34	33	54
EUC core 0.60 m s^{-1}	0.33	31	48
EUC = 0	0.18	26	39
EUC core at 90 m	0.43	34	62

** $\epsilon = 0.25 \times 10^{-9} \text{ W kg}^{-1}$ when $\tau_s = 0$.

We can develop some intuition for the τ_s dependence of dissipation by estimating the shear production term. At least in the model, both $\tau(z)$ and $u(z)$ are very roughly linear with depth, and thus $\int_0^H \tau(z) u_z dz = \tau_s \Delta u / 2$, where H is the depth of the transition layer and Δu is the change of u from the surface to $z = H$. By ignoring the buoyant production of turbulence (which is small compared to the approximation already made), we get $\rho \varepsilon \approx \tau_s \Delta u / 2$. This approximation overestimates ε by about a factor of 2 because, in actuality, u_z tends to be somewhat larger at depths where $\tau(z)$ is small. This estimate does, however, show why ε varies by roughly a factor of five from day to night in the 1984 TROPIC HEAT simulation as Δu goes from the diurnal jet amplitude ($\approx 0.15 \text{ m s}^{-1}$) to the EUC amplitude ($\approx 0.80 \text{ m s}^{-1}$). It also suggests that variations of ε will be more than linear in τ_s because H and Δu both increase with τ_s , and thus the approximate $\varepsilon \sim \tau_s^{3/2}$ dependence of the model noted above. Some observations are available to show how dissipation varies with wind stress and, at least for these cases, the model agrees fairly well with the data, showing larger dissipation as wind stress increases (Figure 5.12; see also Table 5.2).

As we discussed in Chapter 4, the shear of the EUC is critically important for producing deep nighttime mixing and thus large dissipation in the model. Without an Undercurrent (and with a climatological mean wind stress), the model suggests that dissipation would be only a third as large and would reach about two-thirds as deep in the water column (Table 5.2).

The effect of the depth of the EUC core on the maximum depth of mixing is fairly direct. When the core is at 110 m, and given a climatological mean wind stress, mixing reaches down to approximately 70 m (see Table 5.2). When the core is at 90 m (we vary the stratification also, to preserve the initial Ri_g profile above the Undercurrent core as in Fig.

4.1e), mixing reaches to only 60 m. The dissipation, however, is relatively unchanged. This indicates that apparently the same amount of shear in the EUC is worked on by the wind stress. For any plausible wind stress, mixing does not penetrate into the region of high stability near the nose of the Undercurrent even if the core is comparatively shallow. This is consistent with our results for TROPIC HEAT 1987.

5.6 CONCLUSIONS AND SUMMARY

We have found that a simple model of the upper ocean can simulate the dramatic diurnal cycle of dissipation observed during the 1984 TROPIC HEAT field experiment, provided that the model includes forcing by wind stress and heat fluxes, a reasonable treatment of vertical mixing, and an EUC. Large values of dissipation, $O(10^{-7} \text{ W kg}^{-1})$, occur at night in a thick transition layer below the mixed layer where the wind stress works directly against the large vertical shear of the Undercurrent. During the day, diurnal stratification is sufficient to confine the wind stress to a shallow surface layer in which dissipation is much smaller, $O(10^{-8} \text{ W kg}^{-1})$. The model also simulates the weak diurnal cycle of mixing and dissipation observed during the 1987 TROPIC HEAT experiment, when lighter winds and a weaker Undercurrent were prevalent, and suggests that the lower levels of dissipation observed in 1987 were due to the lower wind stress rather than the weaker Undercurrent.

Overall dissipation values are set by the strength of the wind stress rather than the structure of the Undercurrent, and rise like u_*^3 for a given Undercurrent. However, the shear of the EUC is crucial in producing large values of dissipation; if there were no Undercurrent, the model suggests that overall dissipation values would be only about 1/3 as large. Thus both wind stress and the EUC are instrumental in producing large mixing and dissipation at the equator. On the other hand, the vertical structure of mixing, while somewhat dependent on wind stress, is controlled by the structure of the Undercurrent. Richardson numbers close

to the critical value of $1/4$ above the Undercurrent core permit mixing to penetrate deeper, and the higher and more stable values of the Richardson number at the Undercurrent core limit the extent of mixing.

It has been suggested that internal waves radiating downward from the mixed layer might produce the observed deep mixing and a deep penetration of the wind stress in a critical layer above the EUC core (Toole et al., 1987; Peters et al., 1988; Moum et al., 1989; Dillon et al., 1989; Wijesekera and Dillon, 1991). Twenty-one day Rossby-gravity waves also play an important role in the energy balance of the EUC core, and in fact account for as much energy dissipation in the EUC as the TROPIC HEAT observations showed (Brady, 1990). Our model is simpler than this, depending entirely upon an instability of the mean current and density profile to produce vertical mixing. While this does yield a realistic simulation of the diurnal cycle of dissipation, it does not give a similarly realistic intermittence (hourly time scale) of the dissipation. We too suspect that internal waves and 21-day waves are important mixing processes in the equatorial upper ocean, at least by serving as triggers for instability in a mean flow already close to instability and also by maintaining a background mixing even in the absence of direct wind forcing.

Chapter 6

Summary and Conclusions

6.1 SUMMARY

This thesis examines the vertical structure of the upper ocean 1) at mid-latitudes, away from strong mean currents, and 2) at the equator, where strong and persistent mean circulation exists. To investigate these cases, we use observations of current from the mid-latitude LOTUS moored array, observations of the dissipation of turbulent kinetic energy from the equatorial TROPIC HEAT experiments, and models of the mid-latitude and equatorial upper ocean.

In Chapters 2 and 3, we found that the effect of mean currents on the wind-driven flow in the upper ocean could be neglected in the LOTUS observations. Averaging relative to the wind direction and over low frequencies acts to isolate the wind-driven signal and resulted in the first quantitative observational verification of the Ekman transport. We find good agreement with the Ekman transport relation throughout the first summer and winter of the LOTUS experiment, with the exception of a downwind component of transport in the wintertime (LOTUS 4) period which is discussed in more detail below. This then allows us to then examine the vertical structure of the currents that make up the mean Ekman transport.

During both the summer (LOTUS 3) and the winter (LOTUS 4) the mean upper ocean current has a spiral structure qualitatively similar to an Ekman spiral, rotating to the right with depth. The depth scale of the spiral depends on stratification, which is very different in the summertime LOTUS 3 and the wintertime LOTUS 4 data. In the summer, net

heating and light winds (average wind stress of 0.068 Pa) leads to a shallow seasonal stratification and an Ekman layer that penetrates to about 50 m, e-folding in 12 m. In the winter, net cooling and strong winds (average wind stress of 0.147 Pa) deepen the main thermocline through convection and the Ekman layer penetrates to about 100 m, e-folding in 25 m.

During the summer, the primary variability in the current structure is a diurnal variation. The diurnal shoaling and deepening of the well-mixed layer produces a mean current profile that is sheared, with a spiral-shaped structure that is flatter than the classic Ekman spiral. Several other investigators have reported similar flat mean current spirals which may also be a direct result of strong diurnal cycling (Weller, 1981; Price et al., 1986). This provides further evidence that when the diurnal cycle is strong, it is the controlling factor in the upper ocean's vertical structure.

During the winter the current profile has very little diurnal variation, and its most striking feature is the persistent downwind shear in the upper 15 m. The downwind shear is consistent with both a logarithmic boundary layer and with the estimated error induced by a wave bias. In order to distinguish between these two possible explanations for the downwind shear it is necessary to estimate the wave bias precisely. This in general would require simultaneous measurements of current, current meter motion, and the directional wave spectrum; the latter two of these had to be estimated for the LOTUS observations. However, the wave bias model does account for the downwind near-surface shear during high wind, high sea conditions found in the winter LOTUS observations.

The Price et al. (1986) model is fairly successful in simulating the current structure during the summer. Both the mean current and its strong diurnal variation are reproduced well by the model. The model appears less successful in the winter case, in that it does not give the

downwind shear noted before, though it does predict the vertical penetration of the mean wind-driven current to $O(100 \text{ m})$.

In Chapter 4, we extend the Price et al. (1986) model to the equatorial upper ocean to assess the effect of the mean equatorial circulation on the equatorial upper ocean. We find that the nighttime phase of the diurnal cycle in the equatorial upper ocean is strongly affected by the Equatorial Undercurrent (EUC), which causes mixing to be about twice as deep at night as without an Undercurrent. Other equatorial ocean features such as the zonal pressure gradient and persistent upwelling are of little direct importance for the diurnal cycle, though they are of great importance for the long-term maintenance of the mean flow and stratification.

The daytime phase of the diurnal cycle appears to be unaffected by the EUC, and is very similar to the daytime phase observed at mid-latitudes. Solar heating warms and stabilizes a surface layer having a thickness of 5-10 m. The resulting diurnal warming of the surface is only about 0.2°C , but is nevertheless sufficient to insulate the eastward-flowing EUC from vertical mixing and the (generally) westward wind stress. The diurnal cycle of surface heating thus serves to modulate and limit the depth to which the westward wind stress can mix into the eastward-going EUC.

As the warm daytime layer is erased by cooling at night, vertical mixing and the wind stress can penetrate well into the upper EUC even for relatively moderate wind stress (0.05 Pa). This produces very deep mixing in a thick transition layer that extends to about 70 m, about twice the depth of the mixed layer at night. The westward wind stress penetrates to about the same depth. In the absence of solar heating, the model suggests that the nighttime structure would occur around the clock, or until the EUC was erased. This is consistent with the results of Pacanowski and Philander (1981) and Schopf and Cane (1982), who

found that simulations of the equatorial ocean which did not include a mean surface heat flux could not maintain an EUC. Here we have found that the diurnal cycle in solar heating determines the local vertical structure of the equatorial upper ocean above the core of the EUC. The diurnal cycle in vertical mixing is thus an important element in the overall heat and momentum balances in that layer, and by extension, for the equatorial region as a whole.

In Chapter 5, we found that the simple model of the equatorial upper ocean developed in Chapter 4 can simulate the dramatic diurnal cycle of dissipation observed during the 1984 TROPIC HEAT field experiment. Large values of dissipation, $O(10^{-7} \text{ W kg}^{-1})$, occur at night in a thick transition layer below the mixed layer where the wind stress works directly against the large vertical shear of the Undercurrent. During the day, diurnal stratification is sufficient to confine the wind stress to a shallow surface layer in which dissipation is much smaller, $O(10^{-8} \text{ W kg}^{-1})$. The model also simulates the weak diurnal cycle of mixing and dissipation observed during the 1987 TROPIC HEAT experiment, when lighter winds and a weaker Undercurrent were prevalent, and suggests that the lower levels of dissipation observed in 1987 were due to the lower wind stress rather than the weaker Undercurrent.

Overall dissipation values in the model are set by the strength of the wind stress rather than the structure of the Undercurrent, and rise like u_*^3 for a given Undercurrent. However, the shear of the EUC is crucial in producing large values of dissipation; if there were no Undercurrent, the model suggests that overall dissipation values would be only about 1/3 as large. Thus both wind stress and the EUC are instrumental in producing large mixing and dissipation at the equator. On the other hand, the vertical penetration of mixing, while somewhat dependent on wind stress, is controlled mainly by the structure of the Undercurrent. Richardson numbers close to the critical value of 1/4 above the Undercurrent core permit mixing to penetrate to nearly the depth of the core at night, and

the higher and more stable values of the Richardson number at the Undercurrent core limit the extent of mixing.

6.2 DISCUSSION

This dissertation shows that the vertical structure of currents in the upper ocean is very dependent on the thermal stratification of the upper ocean and on the presence of strong large-scale currents. Our analysis of both the LOTUS and TROPIC HEAT experiments illustrates that when the diurnal cycle of insolation is strong, the resulting diurnal cycle of mixing plays an important role in determining the vertical structure of the upper ocean. When the diurnal cycle is weak, as in the winter portion of the LOTUS observations, the vertical structure is determined by the extent of convection produced by cooling at the surface. The LOTUS and TROPIC HEAT experiments also illustrate the fundamental effect of strong large-scale mean currents on the upper ocean. We found we could neglect the effect of large-scale currents and eddies in the LOTUS observations because they were fairly barotropic in the upper ocean, and indeed by doing so we were able to observe a mean Ekman balance. Large-scale currents could not be neglected in the TROPIC HEAT observations; the presence of the vertically-sheared equatorial Undercurrent greatly alters the diurnal cycle in the equatorial upper ocean and changes its mean structure.

In mid-latitude summers, and essentially year-round at the equator and in the tropics, upper ocean stratification is affected significantly by solar insolation. The strong diurnal cycle in insolation therefore plays a major role in determining the local vertical structure of the upper ocean. In these cases the upper ocean model of Price et al. (1986) and its extension to the equator simulate the structure of the upper ocean quite well. Both the observations and the modelling results suggest that when the diurnal cycle of insolation is strong, it will be

necessary to make measurements very near the surface, shallower than 10 m, in order to fully resolve the wind-driven flow.

In mid-latitude winters, conditions of weak surface heating and/or very strong wind stress prevail and diurnal cycling is essentially non-existent. The penetration of wind stress into the upper ocean is then determined by the amount of cooling and the background stratification. Furthermore, during high wind conditions, observations of current from surface-moored platforms are also subject to a bias induced by surface wave motion. This bias can be as large as several cm s^{-1} , comparable to the wind-driven Ekman currents. If measurements are made from a surface mooring, when surface waves are strong it will be necessary to measure the wave spectrum and the current meter motion as well as the current in order to accurately estimate the wave bias. Due to the combined effects of wave bias and instrument failure due to surface waves, Ekman dynamics may be harder to observe in the winter or during any prolonged windy period; this is rather ironic since the Ekman transport is largest when the wind is strongest.

At the equator, the diurnal cycle of mixing is greatly enhanced by the presence of the Undercurrent which is often near the dynamic stability limit in the upper equatorial ocean. Though the daytime phase of the diurnal cycle appears to be unaffected by the EUC, the nighttime phase is strongly amplified by the shear of the EUC. In this sense, the effects of large-scale currents cannot be ignored in the equatorial upper ocean as they often can be in mid-latitudes. Furthermore, the strong diurnal cycle at the equator suggests that forcing on all scales from hourly to interannually are important at the equator. This makes the simulation of the full equatorial response to wind stress forcing a very difficult problem.

REFERENCES

- Beardsley, R. C., 1987. A comparison of the vector-averaging current meter and New Edgerton, Germeshausen, and Grier, Inc. vector-measuring current meter on a surface mooring in Coastal Ocean Dynamics Experiment 1. *Journal of Geophysical Research* 92, 1845-1859.
- Bennett, S. L., 1986. The relationship between vertical, diapycnal, and isopycnal velocity and mixing in the ocean general circulation. *Journal of Physical Oceanography* 16, 167-174.
- Bevington, P. R., 1969. Data reduction and error analysis for the Physical Sciences. McGraw-Hill Book Company, 336 pp.
- Bowers, C. M., J. F. Price, R. A. Weller, and M. G. Briscoe, 1986. Data tabulations and analysis of diurnal sea surface temperature variability observed at LOTUS. Woods Hole Oceanogr. Inst. Tech. Rep. WHOI-86-5, 51 pp.
- Boy, R. L., 1986. Semi-empirical study of moored buoy hulls for air-sea interaction applications. M.S. Thesis, Massachusetts Institute of Technology.
- Brady, E. C., 1990. Observations of wave-mean flow interaction in the Pacific Equatorial Undercurrent. Ph. D. Thesis, MIT-WHOI Joint Program in Oceanography, WHOI-90-51, 219 pp.
- Brady, E. C., and H. L. Bryden, 1987. Estimating vertical velocity on the equator. *Oceanologica Acta No. SP, Proceedings International Symposium on Equatorial Vertical Motion*, Paris, 6-10 May 1985, 33-37.
- Briscoe, M. G. and R. A. Weller, 1984. Preliminary results from the Long-Term Upper-Ocean Study (LOTUS). *Dynamics of the Atmosphere and Oceans* 8, 243-265.
- Bryden, H. L. and E. C. Brady, 1985. Diagnostic model of the three-dimensional circulation in the upper equatorial Pacific Ocean. *Journal of Physical Oceanography* 15, 1255-1273.
- Chereskin, T. K., J. N. Moum, P. J. Stabeno, D. R. Caldwell, C. A. Paulson, L. A. Regier, and D. Halpern, 1986. Fine-scale variability at 140°W in the equatorial Pacific. *Journal of Geophysical Research* 91, 12,887-12,898.
- Chereskin, T. K. and D. Roemmich, 1991. A comparison of measured and wind-derived Ekman transport at 11°N in the Atlantic Ocean. *Journal of Physical Oceanography*, in press.
- Davis, R. E., R. deSzoek, and P.P. Niiler, 1981. Variability in the upper ocean during MILE. Part II: Modelling the mixed layer response. *Deep Sea Research* 28A, 1453-1475.
- Deser, C., R.A. Weller, and M.G. Briscoe, 1983. Long Term Upper Ocean Study (LOTUS) at 34°N, 70°W: Meteorological sensors, data, and heat fluxes for May-October 1982 (LOTUS-3 and LOTUS-4). Woods Hole Oceanographic Institution Technical Report WHOI-83-32, 68 pp.

- Dillon, T. M., J. N. Moum, T. K. Chereskin, and D. R. Caldwell, 1989. Zonal momentum balance at the equator. *Journal of Physical Oceanography* 19, 561-570.
- Donelan, M. A., J. Hamilton, and W. H. Hui, 1985. Directional spectra of wind-generated waves. *Philosophical Transactions of the Royal Society of London, A*, 315, 509-562.
- Ekman, V. W., 1905. On the influence of the Earth's rotation on ocean currents. *Arkiv for Matematik, Astronomi och Fysik*, Bd. 2, No. 11, 1-53.
- Gargett, A. E., 1984. Vertical eddy diffusivity in the ocean interior. *Journal of Marine Research* 42, 359-393.
- Garwood, R. W., P. C. Chu, P. Muller, and N. Schneider, 1989. Equatorial entrainment zone: the diurnal cycle. *Western Pacific International Meeting and Workshop on TOGA COARE Proceedings*, ed. Joel Picaut, Roger Lukas, and Thierry Delcroix. Centre ORSTOM de Noumea, New Caledonia publication, pp. 435-443.
- Gregg, M. C., 1987. Diapycnal mixing in the thermocline: A review. *Journal of Geophysical Research* 92, 5249-5286.
- Gregg, M. C., H. Peters, J. C. Wesson, N. S. Oakey, and T. J. Shay, 1985. Intensive measurements of turbulence and shear in the equatorial undercurrent. *Nature* 318, 140-144.
- Halpern, D., R. A. Weller, M. G. Briscoe, R. E. Davis, and J. R. McCullough, 1981. Intercomparison tests of moored current measurements in the upper ocean. *Journal of Geophysical Research* 86, 419-428.
- Halpern, D., R. A. Knox, D.S. Luther, and S. G. H. Philander, 1989. Estimates of equatorial upwelling between 140° and 110°W during 1984. *Journal of Geophysical Research* 94, 8018-8020.
- Hebert, D., J. N. Moum, C. A. Paulson, D. R. Caldwell, T. K. Chereskin, and M. J. McPhaden, 1991. The role of the turbulent stress divergence in the equatorial Pacific momentum balance. *Journal of Geophysical Research* 96, 7127-7136.
- Huang, N. E., 1979. On surface drift currents in the ocean. *Journal of Fluid Mechanics* 91, 191-208.
- Hughes, R. L., 1980. On the equatorial mixed layer. *Deep Sea Research* 27A, pp.1067-1078.
- Jerlov, N. G., 1968. *Optical Oceanography*, Elsevier Press, 194 pp.
- Kondo, J., Y. Sasano, and T. Ishii, 1979. On wind-driven current and temperature profiles with diurnal period in the oceanic planetary boundary layer. *Journal of Physical Oceanography* 9, 360-372.
- Kraus, E. B., 1987. The torque and flux balances in the upper equatorial ocean. *Journal of Geophysical Research* 92, 14,242-14,250.
- Lentz, S. L., 1991. The surface boundary layer in coastal upwelling regimes. *Journal of Physical Oceanography*, submitted.

- Levitus, S., 1982. Climatological atlas of the world ocean. *NOAA Prof. Pap. 13*, 173 pp.
- Lippert, A., and M. G. Briscoe, 1990. Observations and EOF analysis of low-frequency variability in the western part of the Gulf Stream recirculation. *Journal of Physical Oceanography* 20, 646-656.
- Lombardo, C. P., and M. C. Gregg, 1989. Similarity scaling of viscous and thermal dissipation in a convecting surface boundary layer. *Journal of Geophysical Research* 94, 10,441-10,449.
- Mangum, L. J. and S. P. Hayes, 1984. The vertical structure of the zonal pressure gradient in the eastern equatorial Pacific. *Journal of Geophysical Research* 89, 6273-6284.
- McCreary, J. P., 1981. A linear, stratified ocean model of the Equatorial Undercurrent. *Philosophical Transactions of the Royal Society of London, A* 298, 603-635.
- McPhaden, M. J. and H. Peters, 1991. On the diurnal cycle of near-surface temperature variability in the eastern equatorial Pacific. *Journal of Physical Oceanography*, submitted.
- Mellor, G. L. and P. A. Durbin, 1975. The structure and dynamics of the ocean surface mixed layer. *Journal of Physical Oceanography* 5, 718-728.
- Montgomery, R. B. and E. D. Stroup, 1962. Equatorial waters and currents at 150°W in July-August 1952. *Johns Hopkins Oceanogr. Stud.*, 1, 68 pp., 1962.
- Moum, J. N., and D. R. Caldwell, 1985. Local influences on shear-flow turbulence in the equatorial ocean. *Science* 230, 315-316.
- Moum, J. N., D. R. Caldwell, and C. A. Paulson, 1989. Mixing in the equatorial surface layer and thermocline. *Journal of Geophysical Research* 94, 2005-2021.
- Muller, P. and H. Ross, 1987. On the meridional structure of the equatorial mixed layer. *Oceanologica Acta No. SP, Proceedings International Symposium on Equatorial Vertical Motion*, Paris, 6-10 May 1985, 7-14.
- Niiler, P. P., 1987. TROPIC HEAT - A science progress report. *Further Progress in Equatorial Oceanography, U. S. TOGA Workshop Proceedings*, ed. Eli J. Katz and Janet M. Witte, Nova University Press.
- Oakey, N. S. and J. A. Elliott, 1982. Dissipation within the surface mixed layer. *Journal of Physical Oceanography* 12, 171-185.
- Pacanowski, R. H. and S. G. H. Philander, 1981. Parameterization of vertical mixing in numerical models of tropical oceans. *Journal of Physical Oceanography* 11, 1443-1451.
- Paulson, C. A. and J. J. Simpson, 1977. Irradiance measurements in the upper ocean. *Journal of Physical Oceanography* 7, 952-956.

- Peters, H., and M. C. Gregg, 1987. Equatorial turbulence: mixed layer and thermocline. *Dynamics of the Ocean Surface Mixed Layer, Proceedings of the 'Aha Huliko'a Hawaiian Winter Workshop*, ed. Peter Muller and Diane Henderson, Hawaii Institute of Geophysics Special Publication, pp. 25-45.
- Peters, H., M. C. Gregg, and J. M. Toole, 1988. On the parameterization of equatorial turbulence. *Journal of Geophysical Research* 93, 1199-1218.
- Peters, H., M. C. Gregg, and J. M. Toole, 1989. Meridional variability of turbulence through the Equatorial Undercurrent. *Journal of Geophysical Research* 94, 18003-18009.
- Philander, S. G. H. and H. H. Pacanowski, 1980. The generation of equatorial currents. *Journal of Geophysical Research* 85, 1123-1136.
- Phillips, O. M., 1980. *The Dynamics of the Upper Ocean*. Cambridge University Press.
- Poliard, R. T., 1973. Interpretation of near-surface current meter observations. *Deep Sea Research* 20, 261-268.
- Pollard, R. T., P. B. Rhines, and R. O. R. Y. Thompson, 1973. The deepening of the wind-mixed layer. *Geophysical Fluid Dynamics* 3, 381-404.
- Price, J. F., R. A. Weller, and R. Pinkel, 1986. Diurnal cycling: observations and models of the upper ocean response to diurnal heating, cooling, and wind mixing. *Journal of Geophysical Research* 91, 8411-8427.
- Price, J. F., R. A. Weller, and R. R. Schudlich, 1987. Wind-driven ocean currents and Ekman transport. *Science* 238, 1534-1538.
- Richman, J. G., R. A. de Szoeke, and R. E. Davis, 1987. Measurements of near-surface shear in the ocean. *Journal of Geophysical Research* 92, 2851-2858.
- Santala, M. J., 1991. Surface-referenced current meter measurements. Ph. D. Thesis, MIT-WHOI Joint Program in Oceanography, 276 pp.
- Santala, M. J. and E. A. Terray, 1990. A technique for making unbiased estimates of current from a wave-follower. *Deep Sea Research*, submitted.
- Schopf, P. S. and M. A. Cane, 1983. On equatorial dynamics, mixed layer physics, and sea surface temperature. *Journal of Physical Oceanography* 13, 917-935.
- Shay, T. J. , and M. C. Gregg, 1986. Convectively driven turbulent mixing in the upper ocean. *Journal of Physical Oceanography* 16, 1777-1798.
- Stramma, L., P. Cornillon, R. A. Weller, J. F. Price, and M.G. Briscoe, 1986. Large diurnal sea surface temperature variability: satellite and in situ measurements. *Journal of Physical Oceanography* 16, 827-837.
- Stull, R. B., 1988. *An Introduction to Boundary Layer Meteorology*. Kluwer Academic Publishers, 666 pp.
- Stull, R. B. and E. B. Kraus, 1987. The transient model of the upper ocean. *Journal of Geophysical Research* 92, 10,745-10,755.

- Toole, J. M., H. Peters, and M. C. Gregg, 1987. Upper ocean shear and density variability at the Equator during TROPIC HEAT. *Journal of Physical Oceanography* 17, 1397-1406.
- Turner, J. S., 1973. Buoyancy Effects in Fluids. Cambridge University Press, 368 pp.
- Weller, R. A. and R. E. Davis, 1980. A vector measuring current meter. *Deep Sea Research* 27A, 565-582.
- Weller, R. A., 1981. Observations of the velocity response to wind forcing in the upper ocean. *Journal of Geophysical Research* 86, 1969-1977.
- Weller, R. A., D. L. Rudnick, N. J. Pennington, R. P. Trask, and J. R. Valdes, 1990. Measuring upper ocean variability from an array of surface moorings in the subtropical convergence zone. *Journal of Atmospheric and Oceanic Technology* 7, 68-84.
- Weller, R. A., D. L. Rudnick, C. C. Eriksen, K. L. Polzin, N. S. Oakey, J. W. Toole, R. W. Schmitt, and R. T. Pollard, 1991. Forced ocean response during the Frontal Air-Sea Interaction Experiment. *Journal of Geophysical Research* 96, 8611-8638.
- Wijesekera, H. W. and T. M. Dillon, 1991. Internal waves and mixing in the equatorial upper ocean. *Journal of Geophysical Research* 96, 7115-7125.
- Wijffels, S. and H. L. Bryden, 1991. Direct observations of the Ekman balance at 10°N in the Pacific. *Journal of Physical Oceanography*, submitted.
- Worthington, L. V., 1959. The 18° water in the Sargasso Sea. *Deep Sea Research* 5, 297-305.
- Wyrtki, K., 1981. An estimate of equatorial upwelling in the Pacific. *Journal of Physical Oceanography* 11, 1205-1214.
- Wyrtki, K., and G. Meyers, 1976. The trade wind field over the Pacific Ocean. *Journal of Applied Meteorology* 15, 698-704.
- Wyrtki, K., and B. Kilonsky, 1984. Mean water and current structure during the Hawaii-to-Tahiti shuttle experiment. *Journal of Physical Oceanography* 13, 917-935.

BIOGRAPHICAL NOTE

Rebecca Schudlich was born in Punxsutawney, PA, where "Punxsutawney Phil" pops up every Groundhog's Day to forecast the arrival of spring. This apparently sealed her early commitment to the earth sciences. She grew up in Traverse City, MI, on the shores of Lake Michigan, and attended Northwestern Michigan College from 1979-1981. She attended the University of Michigan from 1981-1985, where she received a B.S. magna cum laude in Atmospheric and Oceanic Science and an M.S. in Oceanic Science. During this time she also worked as a Physical Scientist at the NOAA Great Lakes Environmental Research Laboratory from 1982-1985 and as a Teaching Assistant at the University of Michigan in 1984. She left Michigan to enter the MIT-WHOI Joint Program in Physical Oceanography, which she attended from 1985-1991. She has participated in four oceanographic research cruises: drifter and dye patch dispersion studies on R/V Shenehon in 1984, FASINEX mooring recovery cruise on R/V Knorr in 1986, Gulf Stream SYNOP cruise on R/V Endeavor in 1988, and Transpacific 10°N cruise on R/V Moana Wave in 1989. She currently works as a postdoctoral scientist at the University of Washington in Seattle, WA, investigating the effects of physical mixing on biochemical processes in the upper ocean, and drinking lots of good coffee.

Publications

Schudlich, Rebecca R. and James F. Price, 1991.

Diurnal cycles of current, temperature, and turbulent dissipation in a model of the equatorial upper ocean. *Journal of Geophysical Research*, in press.

Price, James F., Robert A. Weller, and Rebecca R. Schudlich, 1987.

Wind-driven ocean currents and the Ekman transport. *Science* 238, 1534-1538.

Non-refereed publications

Price, James F., Robert A. Weller, and Rebecca R. Schudlich, 1987.

Some effects of heating on the wind-driven velocity in the upper ocean. *Dynamics of the Ocean Surface Mixed Layer, Proceedings of the 'Aha Huliko'a Hawaiian Winter Workshop*, Peter Muller and Diane Henderson, eds., Hawaii Institute of Geophysics Special Publication, pp. 131-139.

DOCUMENT LIBRARY

March 11, 1991

Distribution List for Technical Report Exchange

Attn: Stella Sanchez-Wade
Documents Section
Scripps Institution of Oceanography
Library, Mail Code C-075C
La Jolla, CA 92093

Hancock Library of Biology &
Oceanography
Alan Hancock Laboratory
University of Southern California
University Park
Los Angeles, CA 90089-0371

Gifts & Exchanges
Library
Bedford Institute of Oceanography
P.O. Box 1006
Dartmouth, NS, B2Y 4A2, CANADA

Office of the International
Ice Patrol
c/o Coast Guard R & D Center
Avery Point
Groton, CT 06340

NOAA/EDIS Miami Library Center
4301 Rickenbacker Causeway
Miami, FL 33149

Library
Skidaway Institute of Oceanography
P.O. Box 13687
Savannah, GA 31416

Institute of Geophysics
University of Hawaii
Library Room 252
2525 Correa Road
Honolulu, HI 96822

Marine Resources Information Center
Building E38-320
MIT
Cambridge, MA 02139

Library
Lamont-Doherty Geological
Observatory
Columbia University
Palisades, NY 10964

Library
Serials Department
Oregon State University
Corvallis, OR 97331-5503

Pell Marine Science Library
University of Rhode Island
Narragansett Bay Campus
Narragansett, RI 02882

Working Collection
Texas A&M University
Dept. of Oceanography
College Station, TX 77843

Library
Virginia Institute of Marine Science
Gloucester Point, VA 23062

Fisheries-Oceanography Library
151 Oceanography Teaching Bldg.
University of Washington
Seattle, WA 98195

Library
R.S.M.A.S.
University of Miami
4600 Rickenbacker Causeway
Miami, FL 33149

Maury Oceanographic Library
Naval Oceanographic Office
Stennis Space Center
NSTL, MS 39522-5001

Marine Sciences Collection
Mayaguez Campus Library
University of Puerto Rico
Mayaguez, Puerto Rico 00708

Library
Institute of Oceanographic Sciences
Deacon Laboratory
Wormley, Godalming
Surrey GU8 5UB
UNITED KINGDOM

The Librarian
CSIRO Marine Laboratories
G.P.O. Box 1538
Hobart, Tasmania
AUSTRALIA 7001

Library
Proudman Oceanographic Laboratory
Bidston Observatory
Birkenhead
Merseyside L43 7 RA
UNITED KINGDOM

REPORT DOCUMENTATION PAGE	1. REPORT NO. WHOI-91-29	2.	3. Recipient's Accession No.
4. Title and Subtitle Upper Ocean Dynamics during the LOTUS and TROPIC HEAT Experiments		5. Report Date September 1991	
7. Author(s) Rebecca R. Schudlich		8. Performing Organization Rept. No.	
9. Performing Organization Name and Address Woods Hole Oceanographic Institution Woods Hole, Massachusetts 02543		10. Project/Task/Work Unit No. WHOI-91-29	
		11. Contract(C) or Grant(G) No. (C)N00014-89-J-1053 (G)	
12. Sponsoring Organization Name and Address Funding was provided by the Office of Naval Research under Grant No. N00014-89-J-1053.		13. Type of Report & Period Covered Ph.D. Thesis	
		14.	
15. Supplementary Notes This thesis should be cited as: Rebecca R. Schudlich, 1991. Ph.D. Thesis MIT/WHOI, WHOI-91-29.			
16. Abstract (Limit: 200 words) <p>The vertical structure of the upper ocean in mid-latitudes and at the equator is investigated using observations from the Long Term Upper Ocean Study (LOTUS), the TROPIC HEAT experiments, and one-dimensional numerical models. When the diurnal cycle in solar heating is strong, it determines the local vertical structure of the upper ocean (in both the LOTUS and TROPIC HEAT observations). The Price et al. (1986) model and its extension to the equator simulate the upper ocean fairly well when the diurnal cycle is strong.</p> <p>During the LOTUS experiment we find good agreement with Ekman transport by using a wind-relative averaging method. The mean current e-folds over 12 m in the summer and has a strong diurnal cycle. The mean current e-folds over 25 m in the winter, with very little diurnal cycle.</p> <p>An extension of the Price et al. (1986) model to the equatorial upper ocean shows that the nighttime phase of the diurnal cycle is strongly affected by the Equatorial Undercurrent, resulting in deep mixing and large dissipation at night consistent with observations made during TROPIC HEAT. The daytime phase of the simulated diurnal cycle is unaffected by equatorial circulation and is very similar to its mid-latitude counterpart.</p>			
17. Document Analysis a. Descriptors Ekman balance equatorial upper ocean mixed layer models			
b. Identifiers/Open-Ended Terms			
c. COSATI Field/Group			
18. Availability Statement Approved for publication; distribution unlimited.		19. Security Class (This Report) UNCLASSIFIED	21. No. of Pages 158
		20. Security Class (This Page)	22. Price